UNIVERSITÀ DEGLI STUDI DI NAPOLI "FEDERICO II"

DIPARTIMENTO DI INGEGNERIA CHIMICA

*Dottorato di Ricerca in Ingegneria Chimica*
*XXIII Ciclo*

# CELL MIGRATION IN ANISOTROPIC MEDIA

**Scientific committee**

Prof. Stefano Guido
Prof. Giovanni Ianniruberto
Prof. Pietro Formisano
Prof. Luigi Maiuri
Prof. Peter Friedl

**Candidate**

Angela Vasaturo

Anno Accademico 2009-2010

*Humility, willingness and devotion make you great before as man and then as researcher.*

# TABLE OF CONTENTS

# CHAPTER 1

# GENERAL CONCEPTS OF CELL MIGRATION

## INTRODUCTION

Cell migration plays a central role in a wide variety of biological phenomena. Active cell motility is essential in physiological tissue development and homeostasis, including embryological morphogenesis, wound healing, immune surveillance, and inflammation, as well as neoplastic tumour cell dissemination and metastasis (Kunwar et al., 2006; Schneider and Haugh, 2006). During gastrulation, for example, large groups of cells migrate collectively as sheets to form the three layers that comprise the resulting embryo. Subsequently, cells migrate from various epithelial layers to target locations throughout the developing embryo where they then differentiate and form various tissues and organs (Keller, 2002) . Analogous migrations occur in the adult where, skin and intestine are renewal continuously from precursors that migrate up from the basal layer and the crypts, respectively.

Migration is also a prominent component of tissue repair and immune surveillance, in which leukocytes migrate from the circulation into areas of insult, where they mediated phagocytic and immune functions (Baggiolini and Loetscher, 2000; Campbell et al., 2003). Moreover, misregulation of cell migration can have grave consequences and contributes to several important pathological processes, including vascular disease, osteoporosis, chronic inflammatory diseases and tumor metastasis (Eccles, 2004) (Martin and Parkhurst, 2004; Sasaki and Firtel, 2006). Tumor development is accompanied by the formation of blood vessels which arise from proliferation and migration of their endothelium. In metastatic cancer some tumor cells acquire the ability to migrate out of the primary tumor to a distant organ where they form secondary tumors (Lauffenburger and Horwitz, 1996) (Yang and Weinberg, 2008). Cytoskeleton and cell-extracellular matrix (ECM) adhesions are the two major molecular machineries involved in mechano-chemical signal transduction during cell migration. Cell extensions are the prerequisite for the onset and maintenance of cell motility in normal and cancer cells, which form either spontaneously or can be induced by

chemokines and growth factors. Observation of cell extensions is therefore a useful way to monitor the onset of cell motility (Friedl and Wolf, 2003b).

### *The motility cycle of a cell*

Cell migration is a very complicated process requiring precise regulation and integration of multiple signaling pathways. It is a dynamic and cyclical process that involves a complex integration of cellular adhesion to the substratum, proteolysis and remodeling of surrounding ECM, and activation and regulation of chemical signaling by growth factors and other chemotactic cues (Friedl and Brocker, 2000). Migration of cells over a substratum requires the coordination of several cellular processes which operate in a cycle.

This cycle can be divided into five different steps (Figure 1.1):

1. Extension of the leading edge
2. Adhesion to the matrix
3. Focalized proteolisis
4. Actomyosin contraction
5. Detachment of the trailing edge

The 5-step cycle is commonly used to describe migration through 3D ECM, whereas migration over a substratum is governed by 3 or 4 steps.

**Extension of the leading edge:** A resting non-migrating cell is tightly attached to the substratum and lacks sufficient polarity to move. When a cell is exposed to a migration promoting factor, the first response is a further polarization of the cell to enable cell movements. This includes intracellular reorganization, directed transport and membrane compartmentalization assures that the cell acquires a front and a backside. This process is regulated by the actin and microtubule cytoskeleton (Goode et al., 2000) and by the formation of cell protrusions in the direction of migration. Cell protrusions can be quite diverse in morphology and dynamics. These are termed lamellipoda, filopoda, pseudopods or invadopods (Adams, 2001). Other cell extensions include ruffles (early pseudopods) or spikes (early filopods) within lamellae, as well as podosomes. These different cell protrusions all contain filamentous actin, as well as varying sets of structural and signalling

proteins (Rho family of GTPases, ERK/MAP kinases and other regulatory molecules), and lead to dynamic interactions with ECM substrates (Horwitz and Parsons, 1999); (Lock et al., 2008). Actin filaments are polarized structures with slow and fast growing ends that are the driving force of membrane protrusion. The kinetics of actin polymerisation is affected by adenosine triphosphate (ATP) hydrolysis (De La Cruz et al., 2000). This ATP hydrolysis takes place within the actin filaments. ATP-bound actin monomers bind to the plus end while ADP-bound actin monomers dissociate from the minus end. At specific sites in the cytoplasm, ADP-actin is recharged with ATP to facilitate plus end binding. This intriguing process is called “tread-milling” (Kirschner, 1980). At the leading edge of the cell, in the protruding lammelipodia a so-called actin cortex is built up. This dense actin network consists of many branched filaments. Out of a single actin filament, the Arp2/3 complex, which binds to the side of an already existing filament (or "mother filament"), nucleates the formation of a new actin filament (Machesky et al., 1994; Welch and Mullins, 2002). WASP (Wiskott-Aldrich syndrome protein) protein family members activate this Arp2/3 complex and these WASP proteins in turn are activated at the cell membrane by Rho GTPases and PIP2 (phosphatidylinositol bisphosphate) (De La Cruz et al., 2000) (Nobes and Hall, 1999). The rate of actin polymerisation is regulated by the small protein profilin, which catalyses the exchange of ADP for ATP and binds to ATP-actin monomers that serve to elongate filaments (Pollard et al., 2000). At the depolymerising end of the filaments ADP-actin monomers are disassembled, a process promoted by proteins of the ADF/cofilin family (Bamburg et al., 1999). Growing and branching filaments are terminated in their elongation by capping protein, which specifically binds to barbed ends of the filaments (Cooper and Schafer, 2000). Anti-capping proteins like Ena/VASP regulate this activity (Bear et al., 2000);(Bear et al., 2002). The local activation of Arp2/3 complex and (anti)- capping proteins induces the growth of the lammelipodium in a particular direction and thus these proteins are involved in directed cell migration. Filopodia have actin organized as parallel bundles and by forming long tiny spikes they serve to explore the matrix and microenvironment. The Rho GTPases are key regulators of both actin organization (Nobes and Hall, 1999). Rho GTPases are members of the large GTP-binding proteins family consisting of proteins with a GTP-binding globular domain. GTP can be hydrolyzed to GDP thereby inducing a conformational change and inactivation of the protein. Rho GTPases are Ras-related small GTPases and activated. and inactivated by guanine nucleotide exchange factors (GEFs) and

GTPase activating proteins (GAPs) respectively. These factors regulate the binding of GTP (active) and GDP (inactive)(Wittmann and Waterman-Storer, 2001).Important members of the Rho GTPases family are Rac, Cdc42 and RhoA.

**Adhesion to the matrix**: Within newly formed protrusions novel cell adhesions have to be established to attach the cell to the underlying ECM. These adhesions are transient and depending on the cell type, substratum and migration profile, their turnover can be very high (Webb et al., 2002). Adhesions initiate as small so-called focal complexes, which are mainly localised at the cell leading edge. These newly formed adhesions stabilize the lammelipodium and attach the protrusion to the ECM. In tightly adhering and non-motile or slowly migrating cells these focal complexes mature into focal adhesions. Depending from the cell type and ECM substrate, focal contact assembly and migration can can be regulated by different integrins (Mostafavi-Pour et al., 2003). Integrins are a family of heterodimeric transmembrane adhesion receptors that support adhesion to the ECM (or other cells) by linking matrix components outside the cell to actin filaments inside the cell (Hood and Cheresh, 2002). Next to this adhering function, integrins are known for their 'inside-out signalling' via activation by cytoplasmic signals (Geiger et al., 2001). Covalent modification of proteins by tyrosine phosphorylation is strongly implicated in the formation of adhesive structures. Upon adhesion to a substratum, a group of cytoskeletal-associated proteins are phosphorylated on tyrosines: focal adhesion kinase (FAK), paxillin and tensin are among the prominent and best characterized of these phosphoproteins that form the adhesive complexes (Lauffenburger and Horwitz, 1996).

Moreover, also members of the Rho GTPases are important in the formation of new adhesions and stabilization of existing ones (Hall, 1998). Rac and Cdc42 appear to be important in the formation of new protrusions and small focal complexes, required for adhesion at the cell periphery. Rho induces the maturation of the small focal complexes into the larger and highly organized focal adhesions (Huveneers and Danen, 2009). During the turnover and maturation of new adhesions at the front of migrating cells microtubules are reported to serve as transport route for adhesion components as growing microtubules target adhesions at leading edges of migrating cells (Small et al., 2002; Small and Kaverina, 2003).

**Focalized proteolisis:** the engagement of integrins and other adhesion receptors leads to the recruitment of surface proteases that become concentrated near substrate binding sites. In close proximity to the cell surface proteases degrade ECM components, such as collagen, fibronectin and laminins and cleave pre-matrix metalloproteinases (MMPs) to create active soluble MMPs, known for their protein cleavage activities. Soluble proteases can directly bind to integrins and similarly, membrane-type matrix metalloproteinase-1 (MT1-MMP) and MMP2 adhere to collagen fibres. MMP1 and other collagenases cleave native collagens, along with other ECM macromolecules, into smaller fragments, which, in turn, are accessible to subsequent degradation by gelatinases (MMP2 and MMP9) or serine proteases. ECM degradation occurs while the advancing cell body gains volume towards the ECM scaffold and is likely to provide the space required for cell expansion and migration, leaving behind tube-like matrix defects along the migration track (Friedl and Wolf, 2003a). This step is dependent on the cell type and the surrounding environment. Proteolytic strategies are indispensable for cells that cannot transmigrate narrow ECM gaps just by changing cell morphology and squeezing of their nuclei (Friedl and Wolf, 2009b).

**Actomyosin contraction:**. The contractile force, needed to move the cell body forward is generated by the interactions of actin filaments with Myosin II. This force at the leading edge is regulated by modulating phosphorylation of the myosin light chain (MLC). Myosin Light Chain Kinase (MLCK) phosphorylates MLC which activates myosin II. Myosin II controls the organization of actin filaments into stress fibers and contraction that are predominantly induced by Rho. Rho activates Rho kinase (ROCK), which in turn inhibits the myosin phosphates, maintaining MLCs in a contractile state (Totsukawa et al., 2004).

**Detachment of the trailing edge:** cells need to quickly dismantle the branched actin network to allow continued propagation of protrusion and movement. At the cell rear, adhesions need to be released, whereas at the front the formation of adhesion has to be controlled. Focal contact disassembly occurs through several mechanisms. Actin binding and severing proteins such as gelsolin and cofilin, cap actin filaments and cause actin filament breakage, thereby promoting filament turnover (Wear et al., 2000). Phosphatases play important roles in rear release, by limiting the assembly of cytoskeletal proteins (Zeng et al., 2003). Focal contacts are further weakened through the proteolytic cleavage of adhesion

receptors by sheddases (Moss and Lambert, 2002)and the accumulation of collagen fragments that are generated while the cell moves forward (Carragher et al., 1999). Migratory defects have been reported in cells lacking Src family kinases (Klinghoffer et al., 1999), FAK (Sieg et al., 1999) (Ilić et al., 1995)and calpain (Huttenlocher et al., 1997), all focal adhesion components. Moreover, in order to maintain a continuous retrograde flow of integrins on the cell surface, migrating cells must reload receptor at the leading edge. Two different models have been suggested to explain the recycling of these proteins. Integrins detach from the substrate and become internalized via the endocytic vesicles and transported toward the leading edge (Bretscher, 1996), or they are carried forward as a passive components of the cell cortex. (Regen and Horwitz, 1992); (Wang et al., 2008).

Although fundamental cell migration mechanisms are shared between different migrating cells, the cell type and its environment are crucial for the migration response. Some cells, like fibroblasts and astrocytes, are known as slow-moving, while other cell types, like T-cells and tumour cells, are fast-moving. In addition, different tumour cells can differ strongly in their intrinsic migratory capacity. Next to cell type, the nature of the surrounding matrix determines to great extent the migration response of cells. The composition of the ECM, availability of growth factors and cytokines, physiological circumstances like pH and $pO_2$ and, of course, intracellular constituents, all together regulate cell polarity and migration.

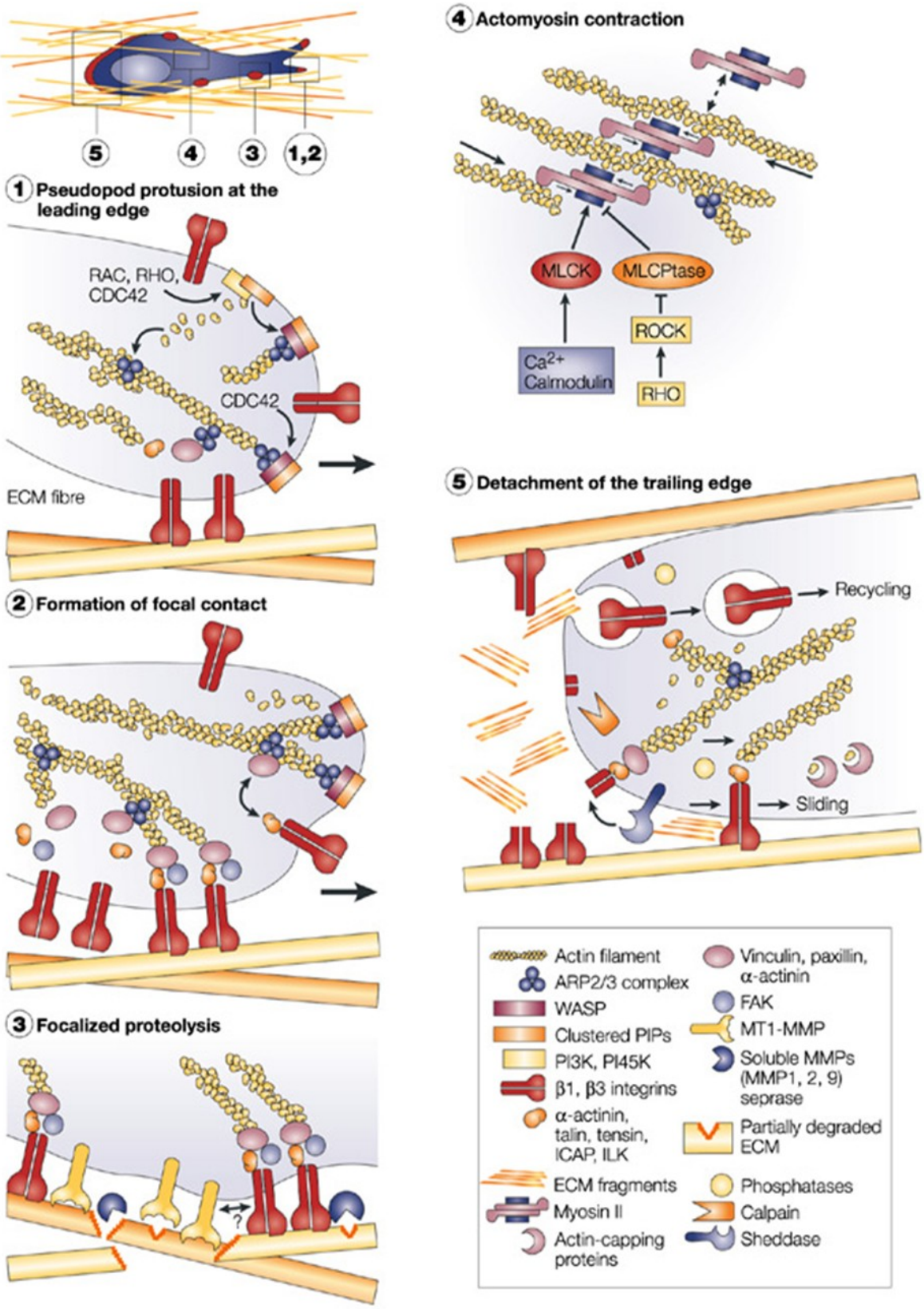


*P. Friedl and K.Wolf, Nat Rev Cancer 2003*

**Figure 1.1:Five-steps model of cell migration in 3D ECM**

# CHAPTER 2

# A NOVEL CHEMOTAXIS ASSAY IN 3-D COLLAGEN GELS BY TIME-LAPSE VIDEO MICROSCOPY

## INTRODUCTION

A wide range of basic cellular process depends on cell motility that is fundamental for all eukaryotes. The ability of cells to migrate, adhere, and change shape requires most of the time external signals, although few cells respond primarily to internal cues. One of the most interesting and important response to external stimuli is chemotaxis. Chemotaxis, the directional movement of cells according to a concentration gradient of chemicals, is implicated in physiologically relevant phenomena such as inflammatory response, homeostatic circulation, and development (Böttcher and Niehrs, 2005). It also concerns a number of disorders including infectious and allergic diseases, wound healing, angiogenesis, atherosclerosis, and tumor metastasis (Eccles, 2004) (Martin and Parkhurst, 2004; Sasaki and Firtel, 2006). However, in vivo, it is difficult to understand how soluble gradients might be continuously maintained. Under in vivo conditions, several physical events such as muscular contraction, convection of extravascular fluid, and lymph flow might perturb the graded diffusion of soluble substances, forming stable gradients. The composition of the ECM, availability of growth factors and cytokines, physiological circumstances like pH and pO2 and, of course, intracellular constituents, all together regulate cell polarity and migration. Recently, novel data on in vivo tumor cell migration during metastasis formation has revealed that the same tumor cells in vivo can migrate up to 10 times faster as compared to in vitro cell migration assays (Condeelis and Segall, 2003a; Wang et al., 2005). This strongly confirms the dependency on environmental settings of the migration response of cells. Thus, despite the ubiquity and importance of chemotaxis, it remains a difficult process to study in vitro. Several methods have been developed to measure chemotaxis in vitro. Most of them utilize systems with 2D surfaces. These 2D assays are easy to handle and provide important tools for understanding the migratory activity in response to natural or pharmacological modulators. However, since the in vivo cells environment is a 3D system, there are obvious questions regarding cell migration for which the 2D model is inadequate

even though they still represent the easiest to investigate cell migration. One of the most commonly used migration assays is the Boyden chamber/Transwell assay (Fig. 2.1)(BOYDEN, 1962).

This system is used to quantify the migration of cells exposed to different chemokine concentrations. The chamber contains two compartments separated by a porous membrane, that usually have sizes between 2 μm to 12 μm, through which cells migrate. The pore size has to be chosen small enough in relation to the size of the investigated cells so that the cells actively migrate through the pores and cannot passively pass the membrane by just dropping through them. The lower compartment is filled with a chemoattractant solution creating a gradient by natural diffusion in the upper compartment which contains the cells. The gradient which is generated allows the cells to migrate through the porous membrane into the lower compartment.

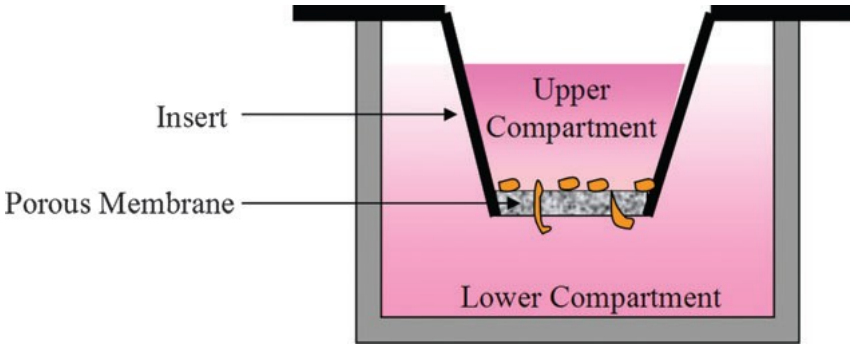


**Figure 2.1: Boyden chamber**

However, chemotaxis and chemokinesis (undirected increase of cell speed) cannot be discriminated in this assay because an equilibrium of the chemotactic factor to be investigated is quickly formed. In case that the response is chemokinetic, an increased number of cells migrating through the filter should be observed regardless whether the substance is applied to the upper or lower compartment or to both compartments. In the event that the response is chemotactic, the number of transmigrating cells should be higher when the substance is applied in the lower compartment, compared to the same concentration of the substance applied to the upper compartment or to both compartments in parallel. However, no substance has been described, which influences the directionality of migration without an increase of migratory activity. Thus, a chemokinetic effect can occur

without a chemotactic effect but chemotaxis does not occur independently from chemokinesis (Zigmond and Hirsch, 1973). The practical advantage of the Boyden chamber assay are that the filter inserts with different pore sizes are commercially available and that the assay can be used to quickly screen chemotactic effect of many compounds. On the other hand, the Boyden chamber shows many limitations due to the fact that it is a system that rely on uncontrolled chemo-attractant gradients to induce migration. In fact, the chemokine becomes homogeneously diffused in the upper chamber and the cells will no longer migrate through the pores. Another limitation of Boyden chamber assays is that they are primarily end-point assays and cannot be used for live cell imaging. Consequently, speed of cell migration cannot be determinate.

The agarose (Köhidai, 1995) or Dunn chamber assays (Zicha et al., 1991) are other standard chemotaxis assays which have been used to show the importance of chemokine gradients by evaluating leukocyte motility dependant on the concentration of specific chemokines. However, they all have the same disadvantage: the cells are incubated in static conditions and dynamic parameter of cell migration cannot be evaluated. However, the in vivo environment is far more complex in comparison to conventional cell assay chambers.

An ideal *in vitro* assay of cell chemotaxis should be performed in a tissue-like collagen or fibrin gel, allow for direct cell tracking and imaging of the concentration gradient of the chemotactic factor within the gel, and be relatively simple to set up with significant reproducibility.

The work carried out in this thesis present a novel chemotaxis assay in 3-D collagen gels in a direct-viewing chamber. Chemotaxis studies require a way to deliver chemicals to cells in a controlled gradient because cells need to be able to sense an increase in concentration of chemokine to direct their motion. In this chemotaxis assay a chemoattractant concentration gradient in the collagen gel sample seeded with cells is generated by diffusion trough a porous membrane. The diffusion process is monitored by fluorescence microscopy of FITC labelled dextran. Cell motion under the action of the chemoattractant gradient is followed by time-lapse video microscopy. Cell tracking is performed off-line by image analysis and the results are expressed in terms of a chemotactic index and velocity. The assay has been tested by using human neutrophils as a model.

Neutrophils are the first line of defense against microbial pathogens in the innate immune response and their migration is essential for the immune system organization (Baggiolini

and Loetscher, 2000; Campbell et al., 2003). Misdirected or over-activated neutrophils can cause disorders such as chronic inflammation (Woolhouse et al., 2002). Thus, neutrophils need to be precisely directed to specific sites to perform their immune functions properly. The migration of leukocytes from the vasculature into tissue requires a multistep cascade of adhesive and migratory events which are mediated by a number of different molecules including adhesion molecules (selectins, integrins and adhesion receptors of the immunoglobulin superfamily), and chemoattractants (Fig. 2.2) (Moser et al., 2004). These steps are the initial selectin-mediated rolling, the chemokine-induced activation and the integrin-dependent firm adhesion and subsequent transendothelial migration (Rao et al., 2007). Chemokines, a family of endogenous chemotactic factors made up of small basic peptides (8–14 kDa)(Zlotnik and Yoshie, 2000), are responsible for the directed migration of leukocytes from the bloodstream into tissue (Baggiolini and Loetscher, 2000; Frevert et al., 1995; Tsai et al., 2000). Here, we used Interleukin-8 (IL-8), an important neutrophils chemotactic factor (Baggiolini and Loetscher, 2000; Baggiolini et al., 1989; Olson and Ley, 2002), member of the family of chemokines, to generate gradient across three-dimensional (3D) collagen gels.

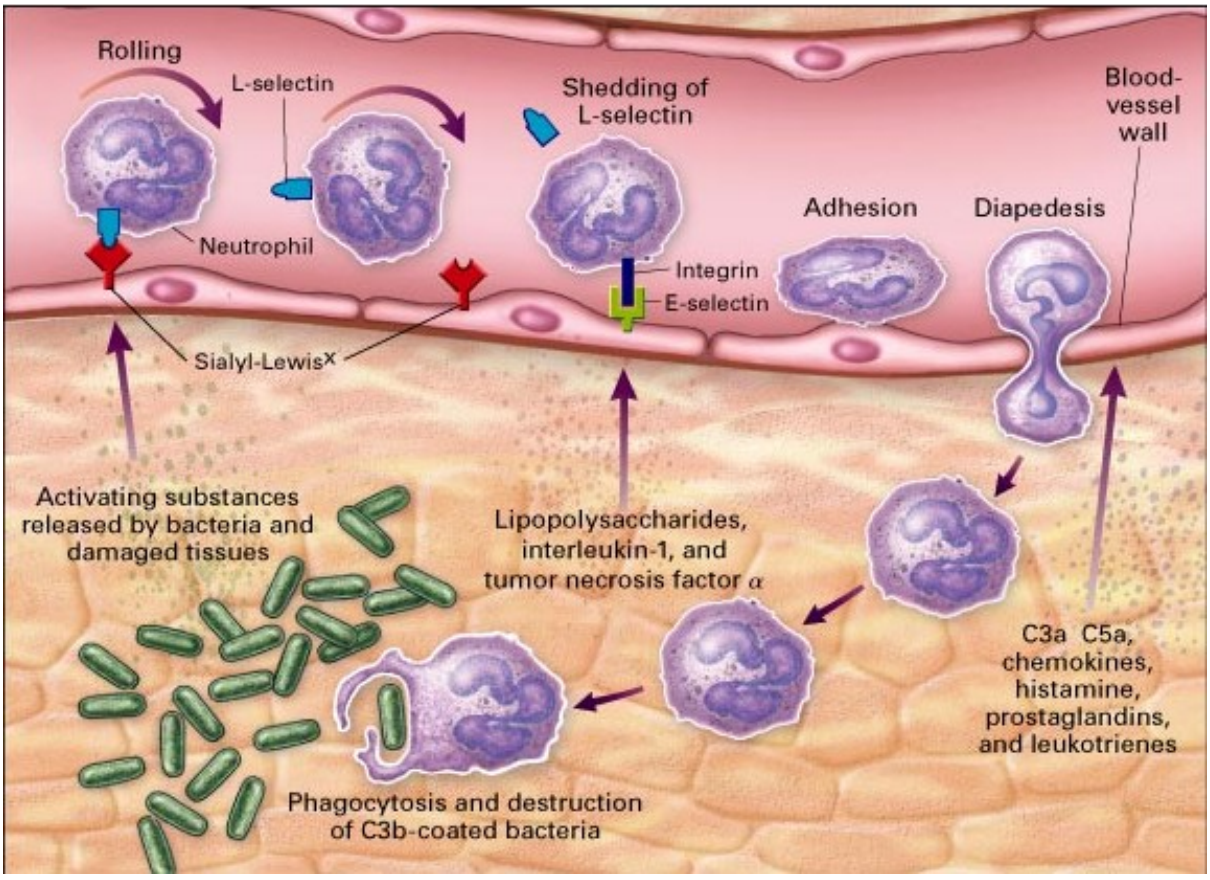


**Figure 2.2: Mechanism of leukocytes recruitment from the blood vessels**

## MATERIALS AND METHODS

### *Neutrophils isolation*

Peripheral blood (10 ml) was taken from healty human donors into BD Vacutainers containing $K_3$EDTA. Neutrophils were freshly isolated by dextran sedimentation and centrifugation on Ficoll-Hypaque. The pellet of a density- gradient centrifugation containing neutrophil granulocytes and erythrocytes was diluted 1:1.3 with a high-molecular-weight dextran solution. After 2h erythrocytes had settled down and the neutrophil granulocytes containing supernatant was separated from the pellet. If necessary, red blood cells in the neutrophil-rich fraction were lysed with hypotonic saline. The neutrophils were washed twice with phosphate buffered saline (PBS) and then resuspended in RPMI 1640 containing 10% heat-treated fetal bovin serum (FBS). The obtained purified neutrophil granulocytes were used immediately after isolation.

### *Preparation of chemotaxis assays*

A 2.2 mg/mL collagen gel solution was prepared under sterile conditions by mixing cells suspended in RPMI with 10% FBS RPMI 1X in such a way that the cell concentration is $10^5$ cells/ml, 0.1 M NaOH (9%), RPMI 10X (7%) and type I rat tail collagen (stock 9.33 mg/mL, BD Biosciences). All components required to make collagen gels were placed on ice except for the cell suspension. Thus, the mixture was incubated in a humidified incubator at 37 in 5% CO2 where collagen polymerization is allowed to occur (Fig. 2.3) and the polymerization was completed after 40 min. The collagen solution was placed in one of the compartments of the chamber, which has been previously sterilized in an autoclave.

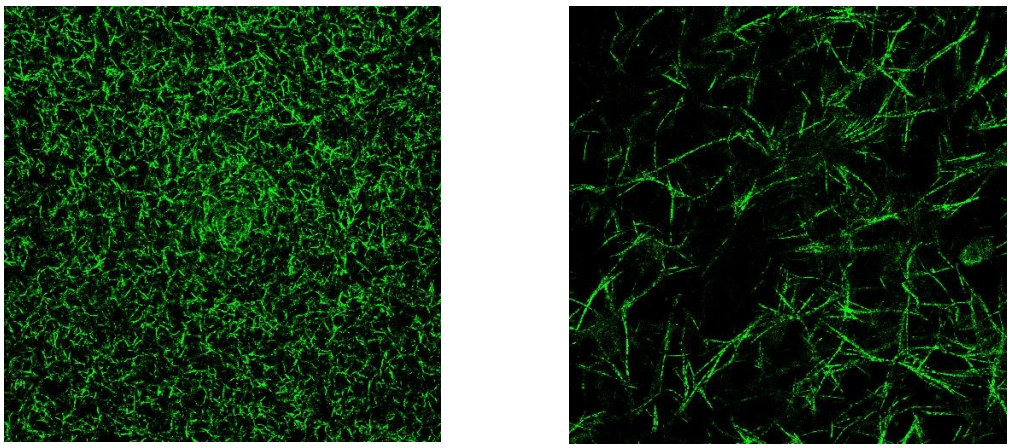

**Figure 2.3: Confocal reflection images of type I rat tail collagen matrices at high magnification(63X and 100X)**

### *Chemotaxis Chamber*

The chamber was designed with the requirements of maintaining both cell viability and good optical quality over the time scale of 24 h. The chamber, shown in Figure 2.4, consists of a single aluminum block glued on top of a microscope slide by using a silicone adhesive. A porous membrane, sandwiched between two rectangular open frames, separates two compartment, one used for the cell seeded collagen gel, and the other as the reservoir of the chemoattractant solutions

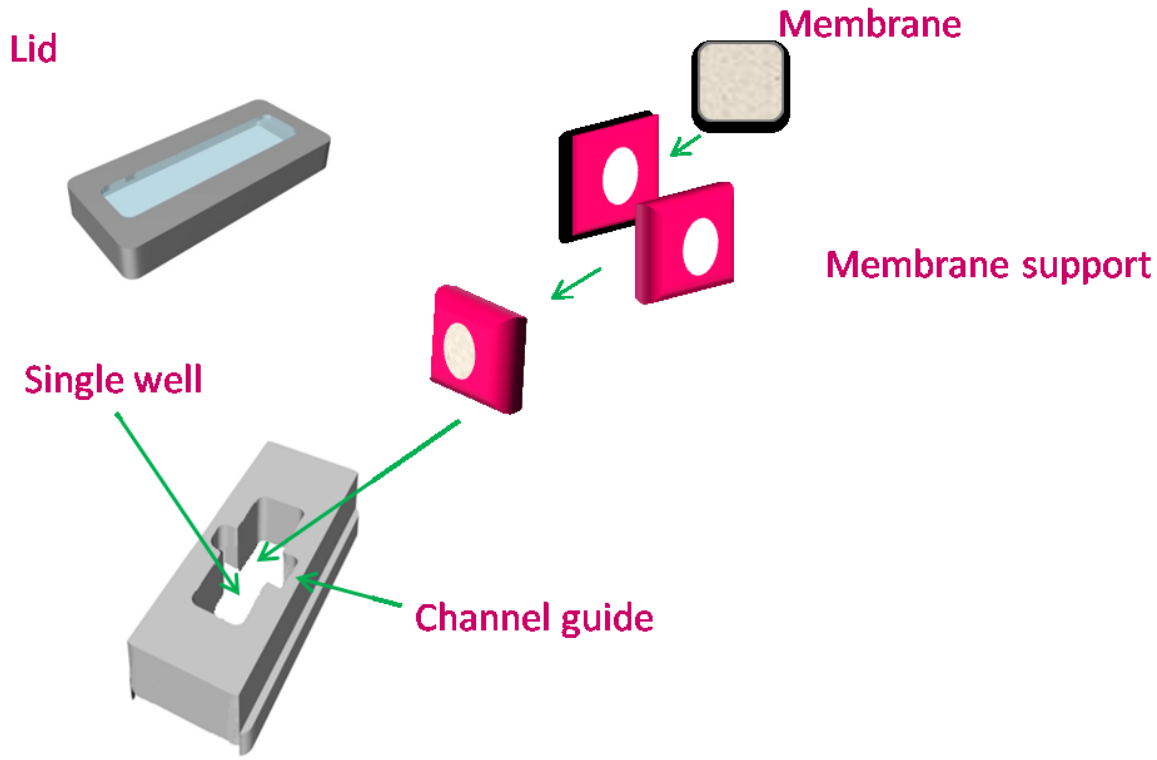


**Figure 2.4 : Chemotaxis chamber**

### *Time lapse experimental apparatus*

The time-lapse microscopy technique allows continuously observing and recording phenomena that can last up to several days. By means of motorized sample positioning, multiple fields of view can be imaged in an iterative fashion, in order to ensure reproducibility and statistical significance of the collected data. Time-lapse live cell imaging requires the right environmental conditions (i.e temperature, humidity and $CO_2$ concentration) under the microscope stage. This was achieved in this work by using a microscope cage incubator (Okolab, Italy), which enclose the whole microscope and allows

to maintain the cells in a 5% $CO_2$ atmosphere at 37°C. To avoid humidity-induced damage to the mechanical and electrical parts of the microscope, the samples were placed inside a small chamber on the microscope stage where a suitable microenvironment for live cell imaging was created by feeding a pre-heated humidified air stream with the desired CO2 concentration. Time-lapse video microscopy was performed by using a Zeiss Axiovert 200 inverted microscope with a 10× long working distance objective. Z-stacks of images along the sample depth were acquired at several x-y positions in an iterative fashion by using a time-lapse software (Okolab), which allows the user to select the fields of view to be imaged at a given time interval. The time-lapse software controls the operation of an x-y motorized stage (Ludl, USA), a motorized focus stage (Ludl, USA) and a video camera (Hamamatsu, Japan). The setup of the time-lapse microscopy workstation is shown schematically in Figure 2.5.

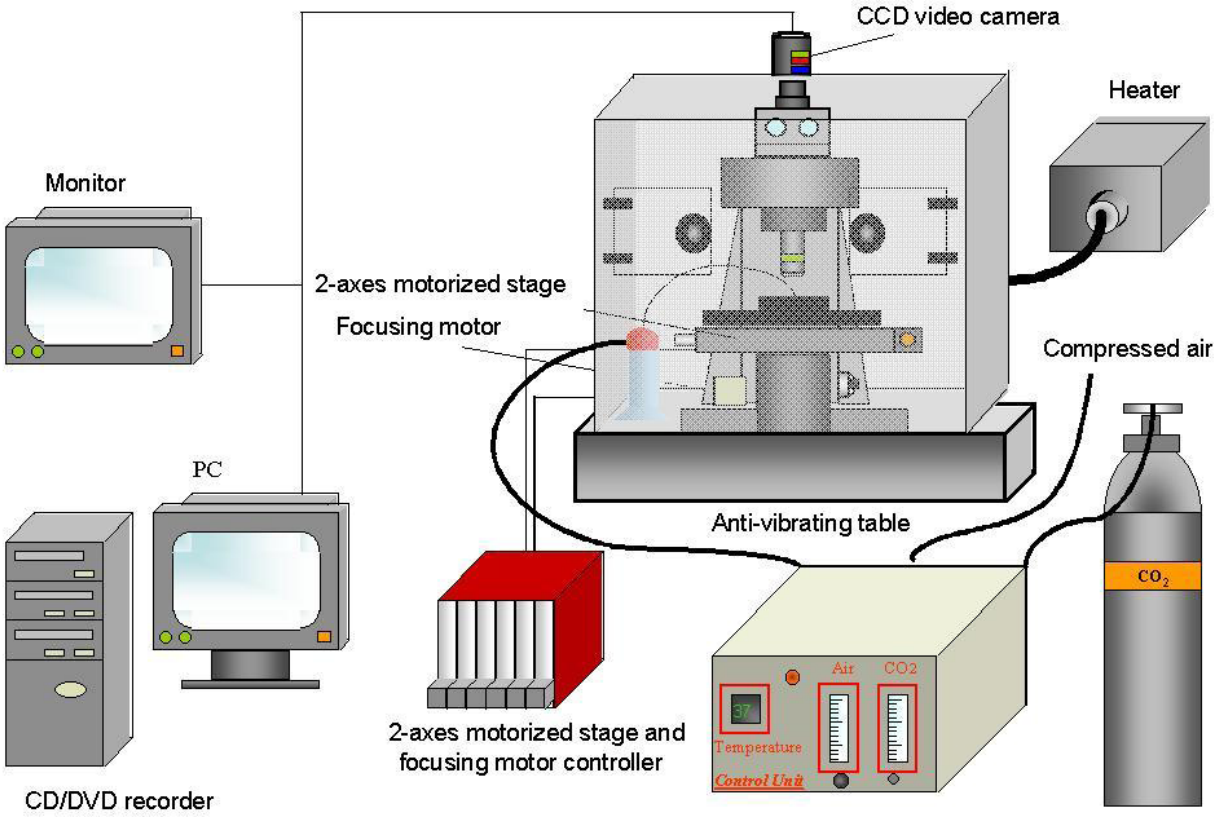


**Figure 2.5: Time Lapse experimental apparatus**

## CF concentration profile measurements

In order to quantify the chemoattractant gradient a preliminary characterization was made using a fluorescently labeled dextran (FITC-dextran), having a molecular weight comparable to that of the chemoattractants investigated, so that a similar diffusion behavior can be assumed. Observing the collagen gel in epifluorescence microscopy, the mean grey level, which is proportional to fluorescensce intensity, was measured as a function of time and position inside the chamber compartment, in order to characterize the propagation of FITC-dextran front in the collagen gel. The fluorescence intensity data can be easily converted in FITC-dextran concentration quantification by means of a proper calibration. To perform the calibration collagen gels with FITC dextran concentrations in the range 0,2 μM - 5 μM were prepared. The solutions were then loaded in a multiwell plate, which was incubated for 40 minutes to allow collagen gelification. Fluorescence images were acquired within each well by using the same settings of light power and contrast. The mean gray level, as calculated from the image histogram, shows to be a linear function of FITC-dextran concentration, as reported in Figure 2.6.

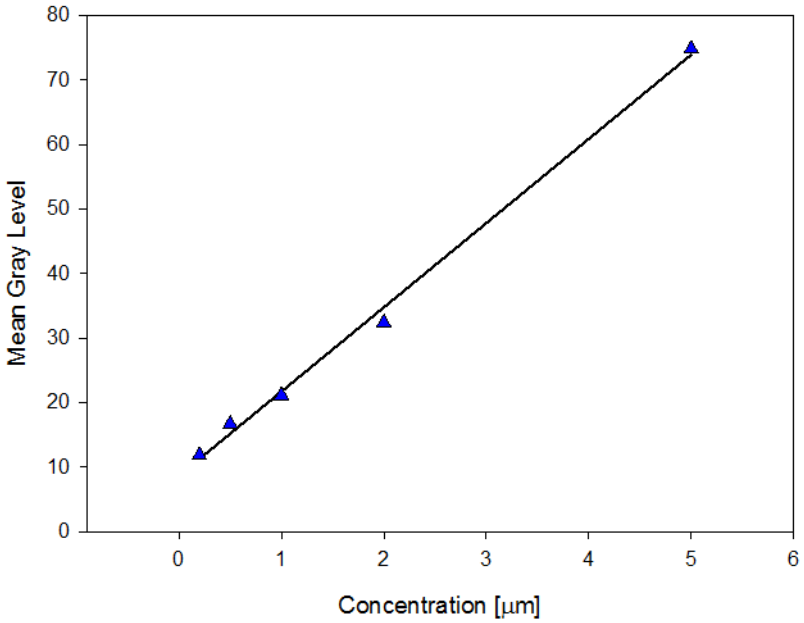


**Figure 2.6: Calibration curve of mean gray level vs FITC-dextran concentration**

In the calibration experiment, time lapse images were acquired at 4 different distances from the membrane.

Figure 2.7 A shows a typical image where the FITC–dextran fluorescence intensity profile is evident. In Figure 2.7 B the image surface plot is reported.

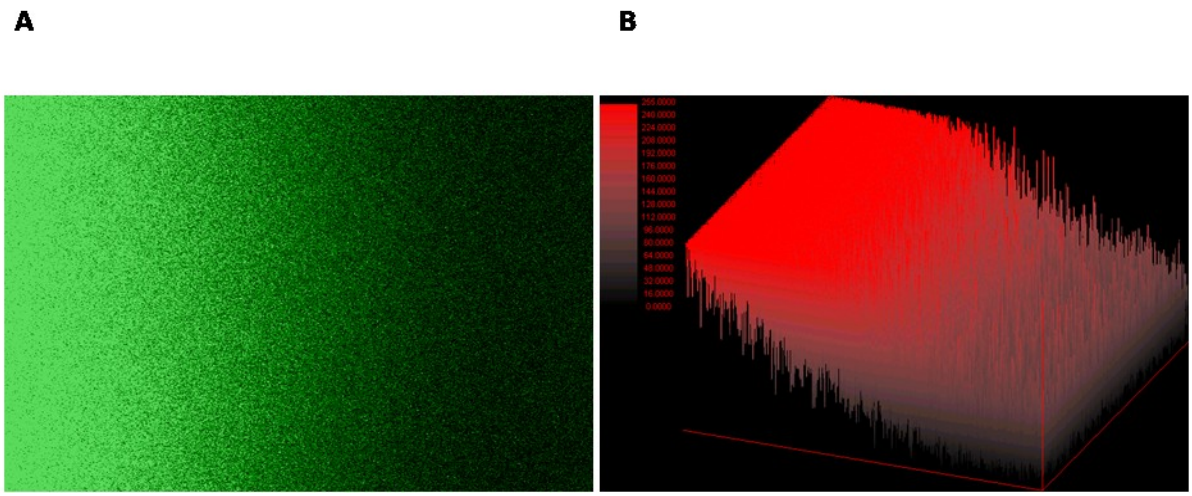


**Figure 2.7: A) Fluorescence image of FITC-dextran during diffusion calibration B) Surface plot of image**

For each acquisition point the evolution of FITC-dextran concentration as function of time was calculated by measuring the fluorescence intensity (Fig. 2.8).

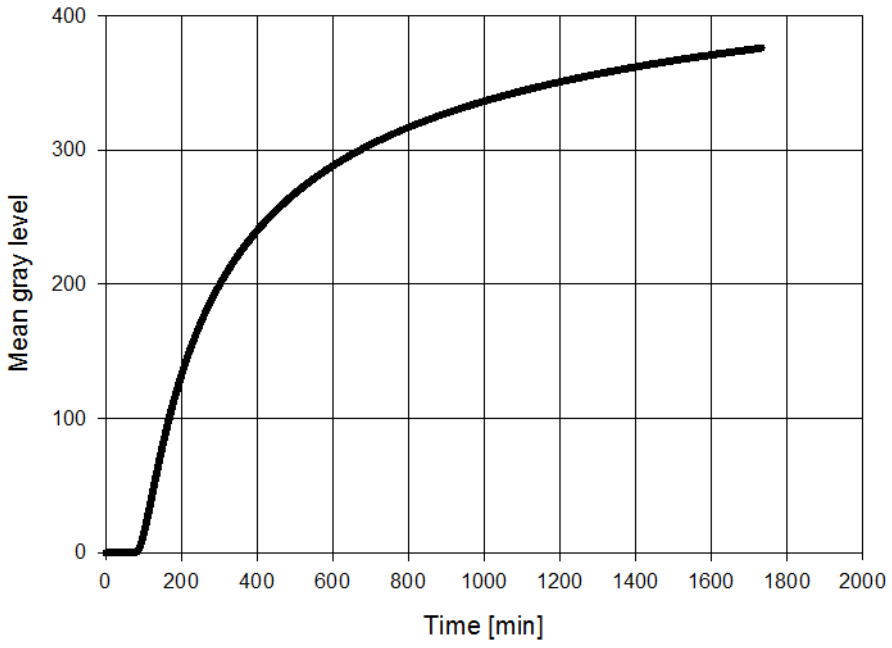


**Figure 2.8: Concentration profile of FITC–dextran at 2 mm distance from the membrane.**

By assuming classic Fickian diffusion in a semiinfinite medium, the diffusion coefficient D was obtained by fitting Eq. (1), where $C_0$ is the initial concentration in the reservoir, x the distance from the membrane. The value obtained is equal to 1.3 $e^{-6}$ $cm^2/s$.

$$C = \frac{C_0}{2}\left[1 + erf\left(\frac{x}{\sqrt{4Dt}}\right)\right] \quad \text{Eq. (1)}$$

In Figure 2.9 the FITC-Dextran concentration is reported both as function of time and space, according to Eq (1). The gray plane cuts the plot at the distance of 2 mm from the membrane, the curve projection at 2 mm has been reported above in fig 2.8.

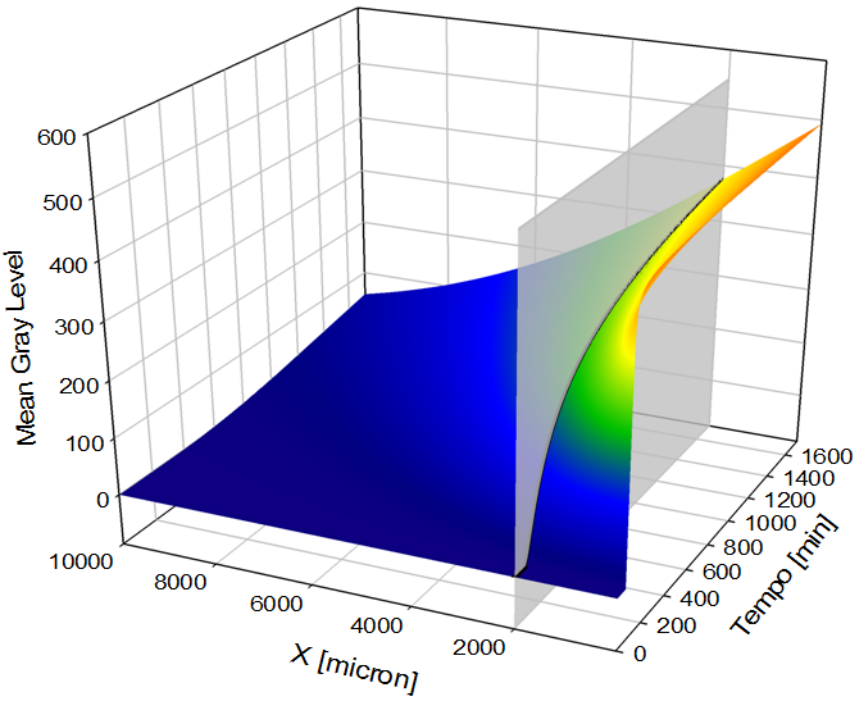


**Figure 2.9: 3D concentration profile of FITC–dextran as a function of time and distance from the chemotactic source.**

## RESULTS

### *Qualitative analysis of cell motility: cell trajectory reconstruction*

In order to validate our chemotaxis assay, several experiments were conducted on human neutrophils freshly isolated from different healthy donors. Neutrophils cell motility was studied by time-lapse imaging and analyzed using a semi-automated Cell Tracking software. This assay allows us to observe and analyze the behavior of cells in the absence and presence of external pro-migratory chemotactic factors. In each experiment neutrophils were observed prior and after the addition of 50μg/ml IL-8. The samples were imaged every minute for 110 minutes and for each time point 70 cells were individually tracked by overlaying each cell contour manually. Here we show representative results obtained from two different donors (donor A and donor B). The response of neutrophils to IL-8 was first analyzed qualitatively through cell trajectories reconstruction. Since collagen fibrils can become aligned near the surface as the gel forms or within the gel as it compacts due to traction exerted by entrapped cells, the possible contributions of contact guidance to directional cell migration and orientation needs to be considered. Restricting measurements to regions of the gel that are at least 1 mm away from the surface mitigated any surface-induced alignment effects. In addition, using low cell concentrations prevented any significant gel compaction during the observation period. In the control where no chemoattractant was added, cell were moving in a random orientation in the xy plane which is uniformly distributed in space (i.e., no preferential direction of motion can be distinguished) (Fig. 2.10 A). This confirms the absence of any matric-mediated contact guidance effects. In the presence of IL-8 concentration gradient, cell trajectories reconstruction was, instead, directed towards the chemoattractant source (Fig. 2.10 B). Each cell trajectory starts in the same origin, coinciding with the intersection of the axis.

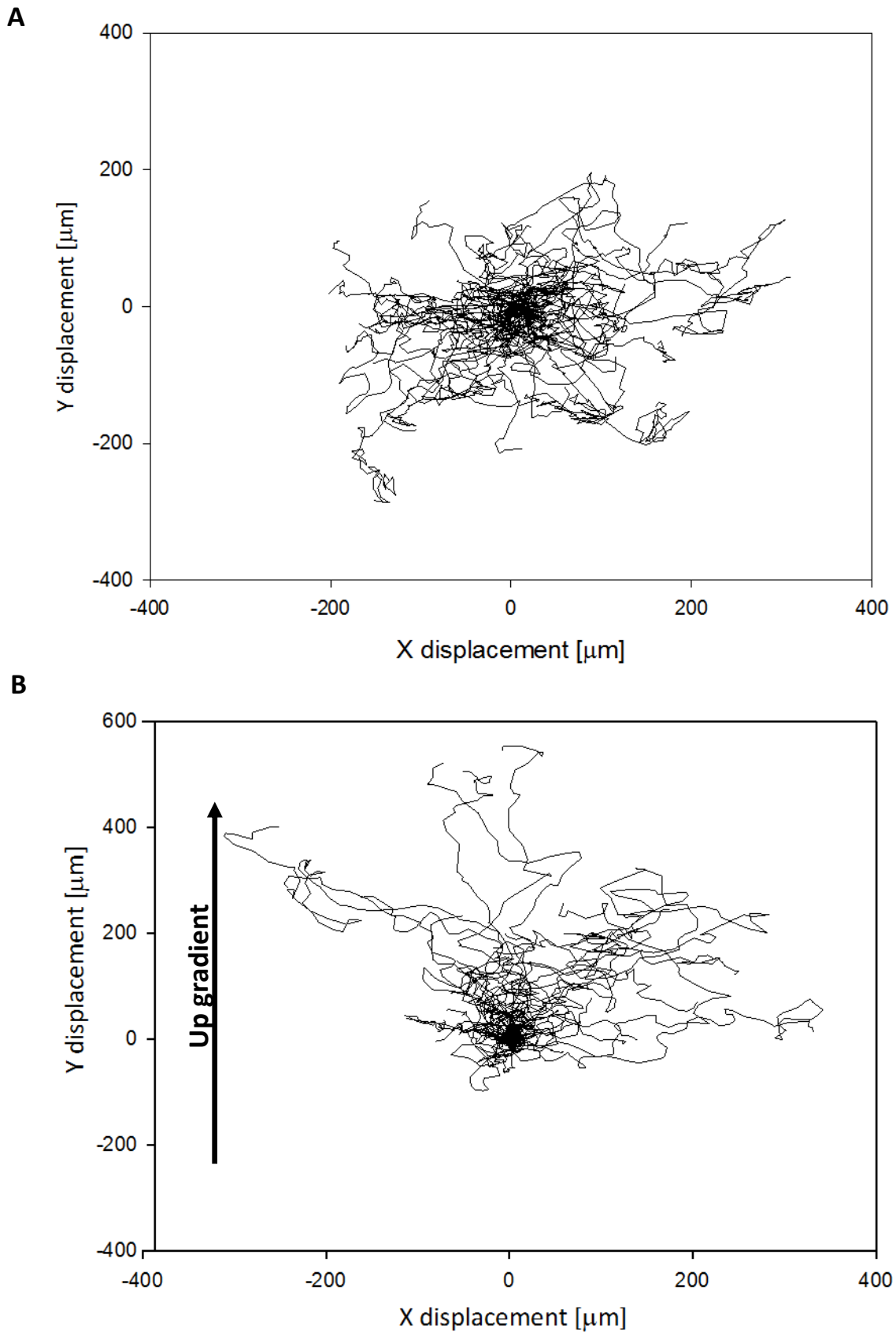


**Figure 2.10: Trajectories of neutrophils: A) in absence of chemoattractant, B) in presence of chemoattractant**

## *Quantitative analysis of cell motility: evaluation of chemotaxis index, cell velocity and cellular motile fraction*

The coordinates of the contour points and of the cell center mass, obtained by semi-automated cell tracking, were automatically recorded in files that were subsequently used as input files for a script developed in-house in the programming platform Matlab. This software was used to characterize quantitatively the induction of chemotaxis in terms of changes in dynamic parameters, i.e. the locomotory active fraction of a cell population, the velocity of migration, and orientation bias of cells quantified by the chemotactic index (CI). The chemotactic index is used to quantitatively assess directional cell movement. It ranges from 0 (random steps) to 1 (trajectory fully oriented towards the source of chemoattractant). For observation times that are sufficiently long (greater than the cell persistent time), the chemotactic index for a single cell I*m* is defined as the ratio between the net movement in the direction of the gradient (Y*t*) and the total curvilinear length of cell trajectory (L*t*) (Moghe et al., 1995):

$$I_m = Y_t / L_t$$

Where $Y_t = y_k - y_1$

$$L_k = [(x_2-x_1)^2 + (y_2-y_1)^2 + (x_3-x_2)^2 + (y_3-y_2)^2 + \ldots + (x_k - x_{k-1})^2 + (y_k - y_{k-1})^2]^{1/2}$$

for $t = k\Delta t$

The value of I is determined by averaging the I*m* values weighted on the trajectories of each cell:

$$\mathrm{I} = \frac{\sum_{m=1}^{M} \mathrm{I}m\mathrm{t}m}{\sum_{m=1}^{M} \mathrm{t}m}$$

where $t_m$ is the trajectory of cell *m*.

For each experiment, the chemotaxis index was calculated in regular interval of 5 minutes. In the first 30 minutes cells were followed in the absence of the chemotactic factor. The chemotactic index of the cells from donor A (Fig. 2.11 A) and B (Fig 2.11 B) are plotted as a function of time. Neutrophils from donors A and B showed different behavior without chemotactic gradient. In fact, CI for donor A fluctuated around 0 and for donor B around 0,25. However, both samples showed a pronounced chemotactic response after about 25 minutes from the addition of IL-8. In particular, the observed value of CI was equal to 0.25 in the donor A and 0.5 in the donor B.

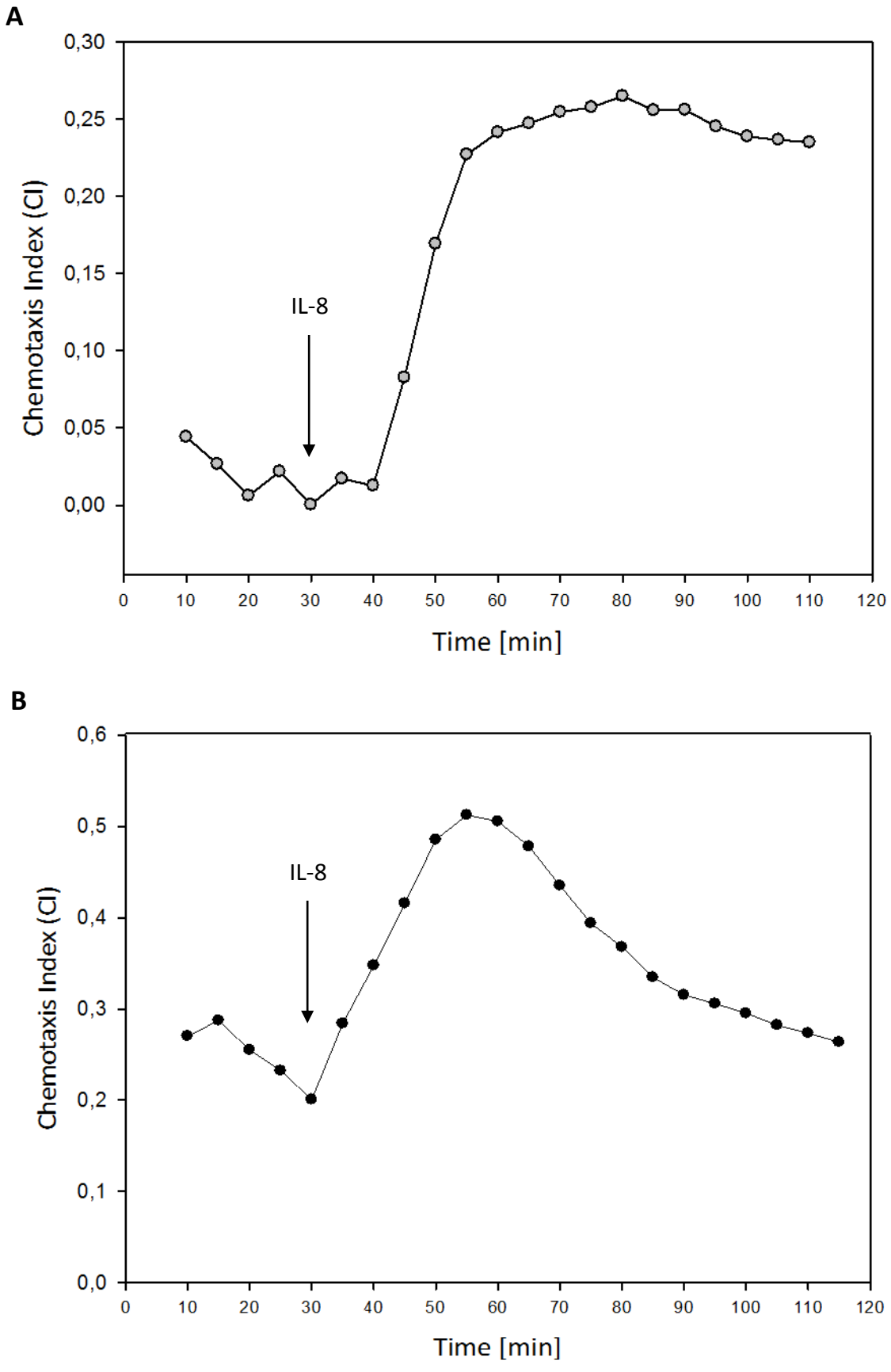


**Figure 2.11: Chemotaxis index as a function of the time for neutrophils A) from donor A, B) from donor B**

In order to characterize the effect of chemokine gradient on neutrophils in our chemotaxis chamber, the average velocity of cells was calculated for each time point. As showed for the CI, in basal condition, cells from donor A displayed  a lower average velocity then cells from donor B, 0.65 μm/min (Fig. 2.12 A) and 1.7 μm/min (Fig. 2.12 B) respectively. This value increased after the addition of IL-8 up to 3.5 μm/min in donor A (Fig. 2.12 A) and 3 μm/min in donor B (Fig. 2.12 B), according to the increment of the CI. The graphs below show a break in the time axis due to the procedure of the addition of the IL-8.

**A**

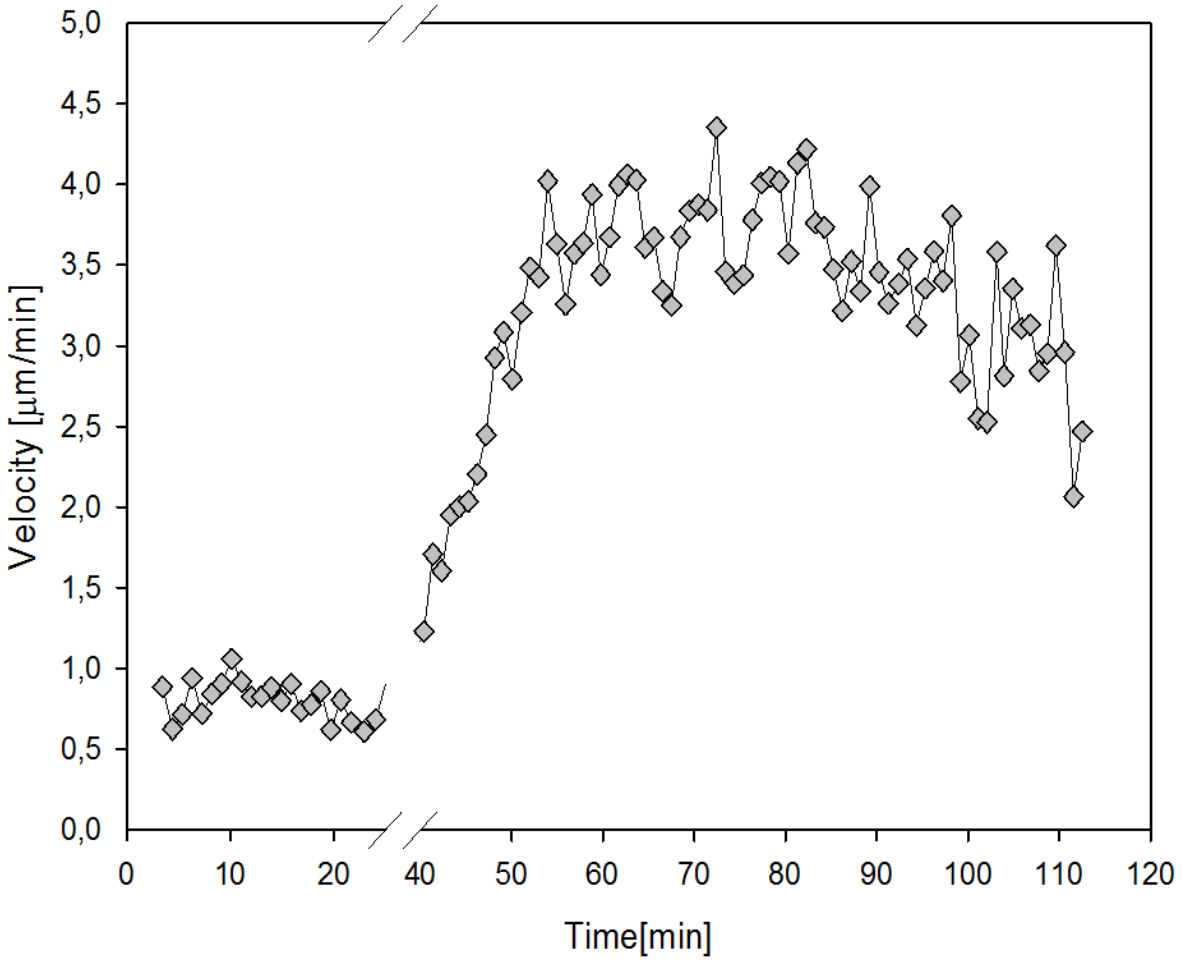

**B**

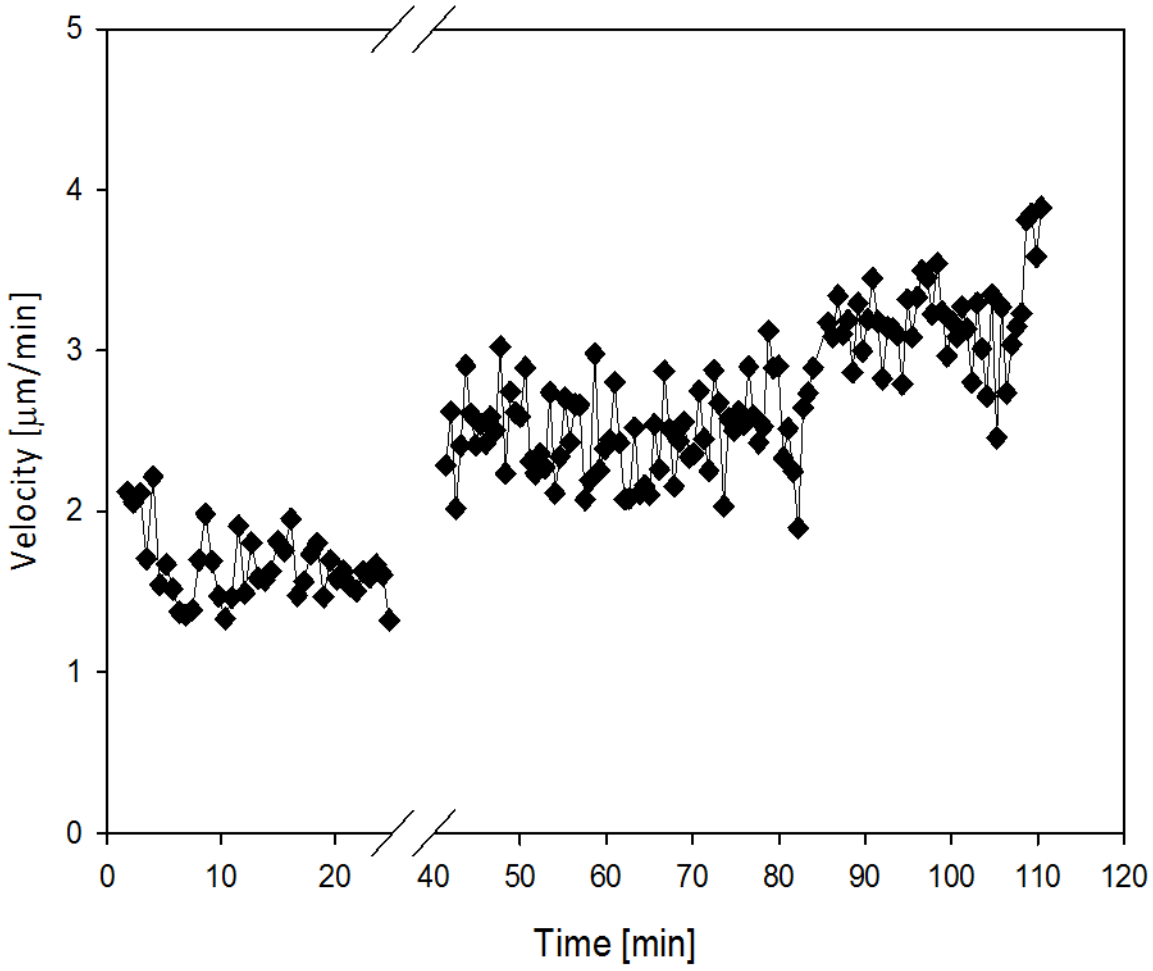


**Figure 2.12: Average velocity of cells as a function of the time for neutrophils from A) donor A, B) donor B**

Visual inspection of the time-lapse videos showed that only a fraction of the cells did actually move during the experiment. The figure below shows a xy plane of the collagen gen within neutrophils at time 0 (Fig. 2.13 A) and at time 110 minutes (Fig. 2.13 B). The white and the black circles indicate the position of cells at time 0 (Fig.2.13 A) and at time 110 minutes (Fig. 2.13 B) respectively. The white arrows in fig. XA indicate the start position of motile cells while in fig. XB their trajectories and end position (black arrows) are shown.

**A**

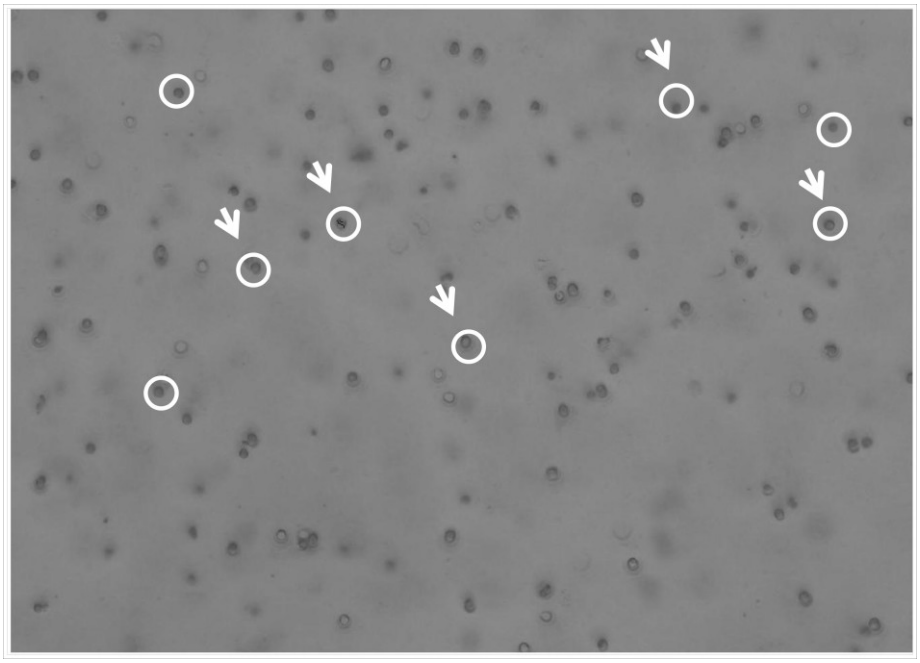

**B**

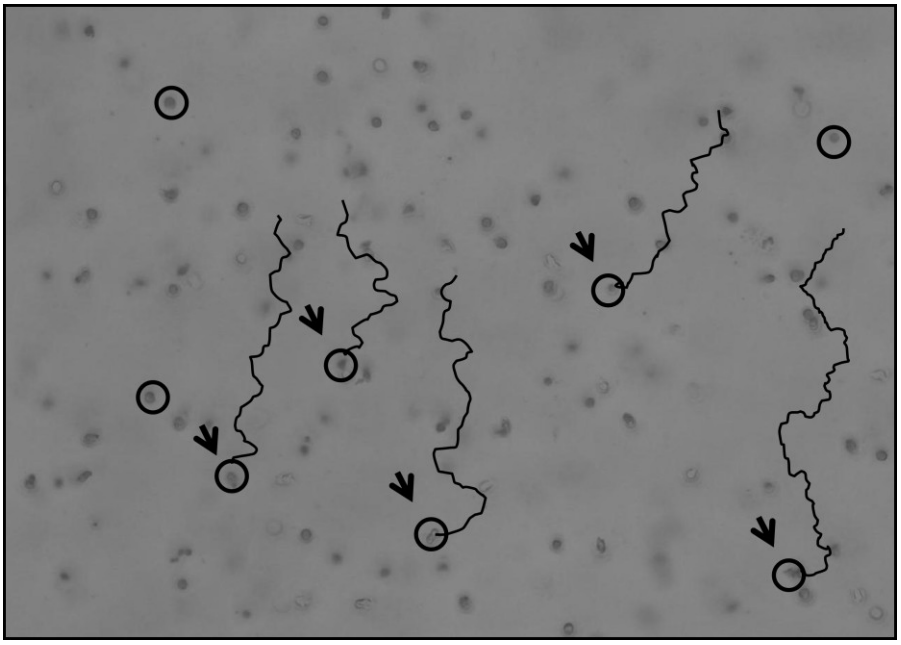

**Figure 2.13: Bright field images of collagen gel within neutrophils A) at time 0 and B) at time 110 minutes of the experiment**

A cell was considered motile if its total displacement exceeded its own diameter. This criterion was used to exclude values representing minor cellular displacement that might be caused by either the repositioning of the microscope motorized stage or by external perturbation of the system. Cellular motile fraction was assessed for regular interval of 10 minutes in presence and in absence of IL-8. Although a different percentage of motile cells was clearly visible in unstimulated conditions, the stimulation of the cells by IL-8 induced an increase in the number of motile cells in both donors (Fig. 2.14 A-B), according to the chemotaxis index and the cell average velocity. These results highlight a striking correlation between the increase in the percentage of motile cells, velocity and the increase of the chemotaxis index.

**A**

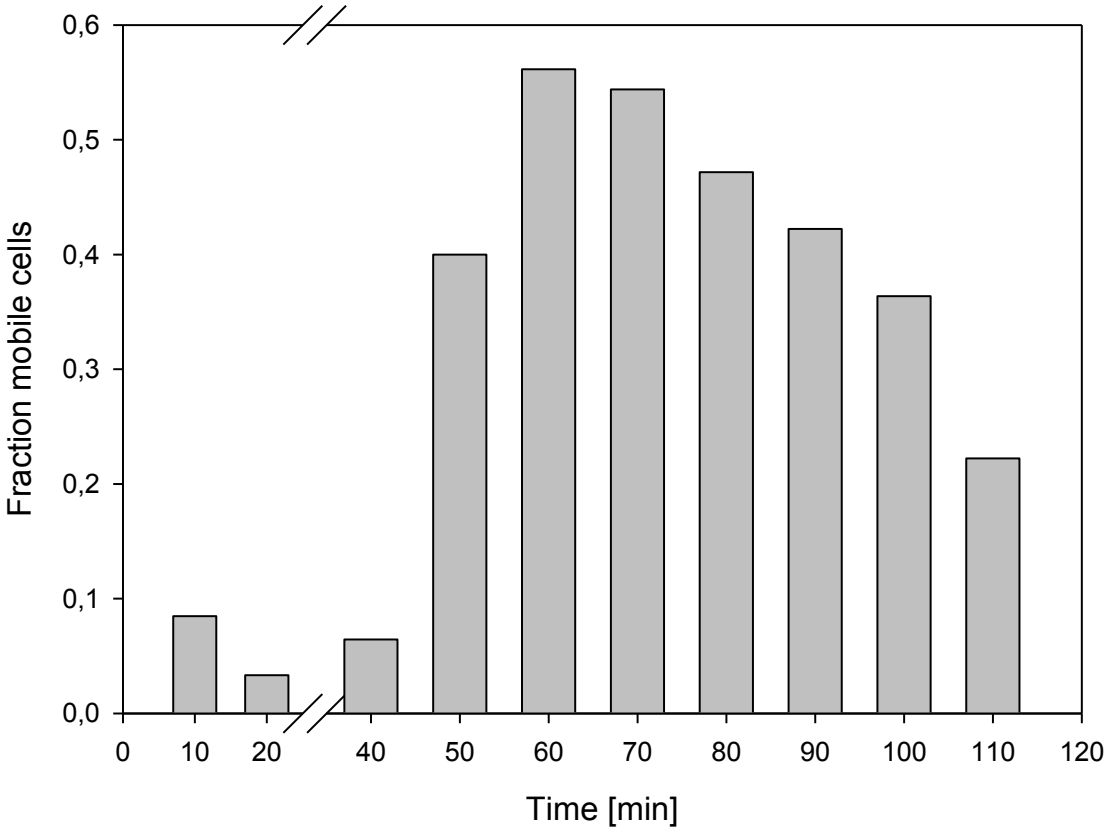

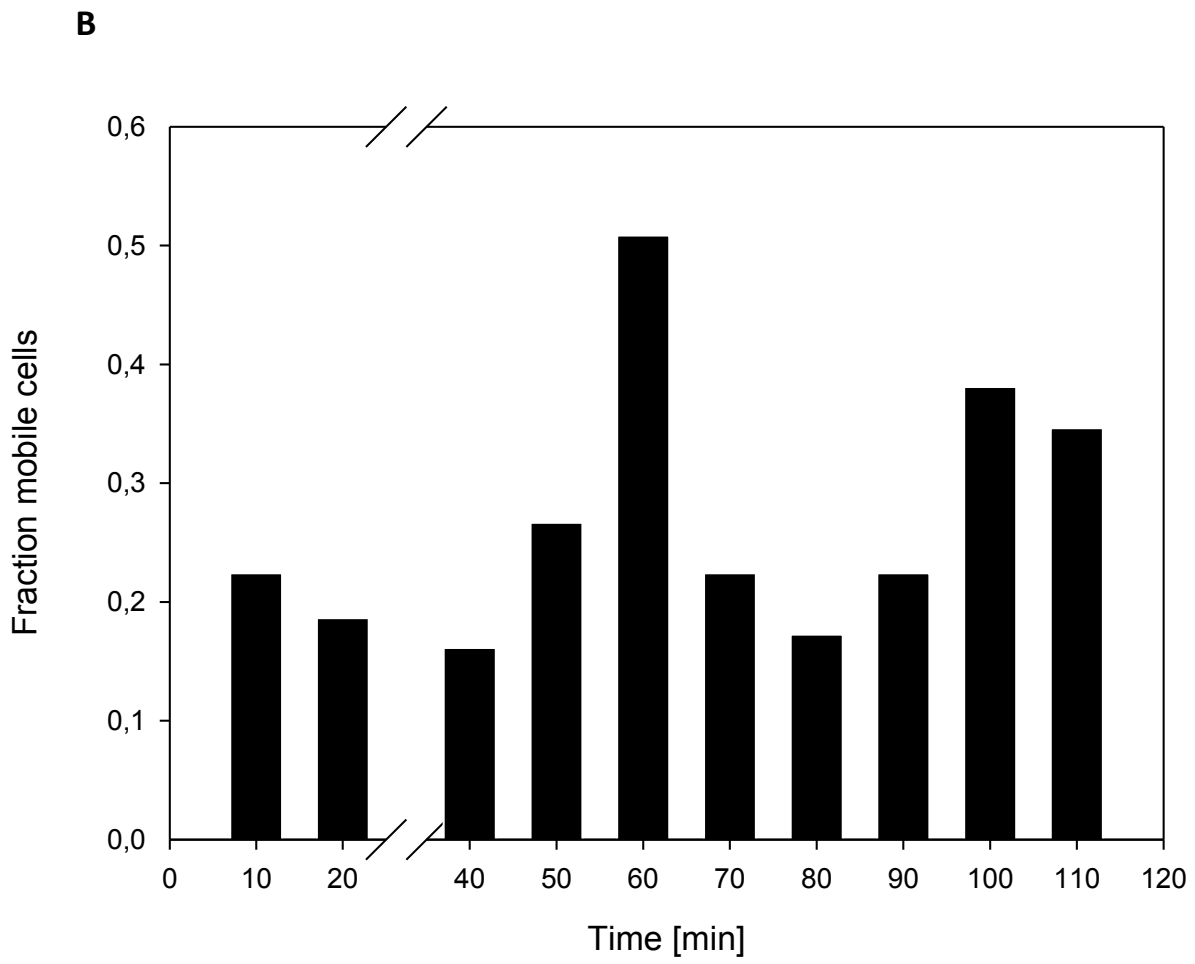


**Figure 2.14: Motile fraction of neutrophils as a function of the time from A) donor A, B) donor B**

Moreover, in confirmation of what was observed in the cellular motile fraction, the distribution of the donors' A neutrophils velocity prior to IL-8 (pre IL-8) showed a very high percentage of non-motile cells (the speed motion was observed in a range between 0 and 1 μm/min for more the 80% of cells) (Fig. 2.15 A). Post IL-8 stimulation (Post IL-8) only ~ 20% of cells maintained a velocity ranging between 0 and 1 μm/min, while ~ 60% of cells increased the speed motion in a range between 2 and 7 μm/min (Fig.2.15 B). The same effect of IL-8 stimulation was observed in cells isolated from the donor B (data not shown).

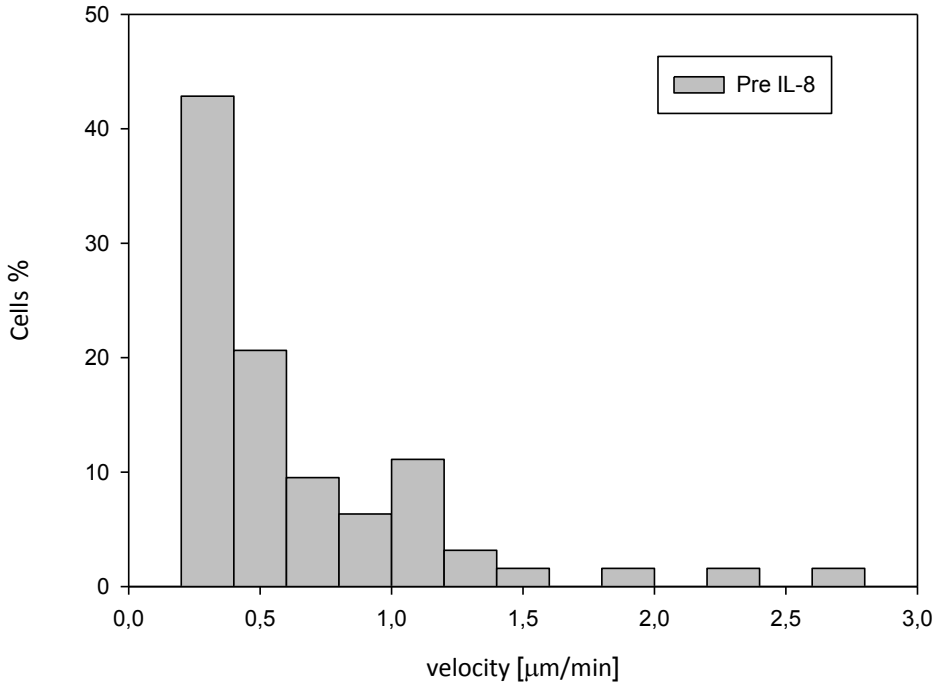


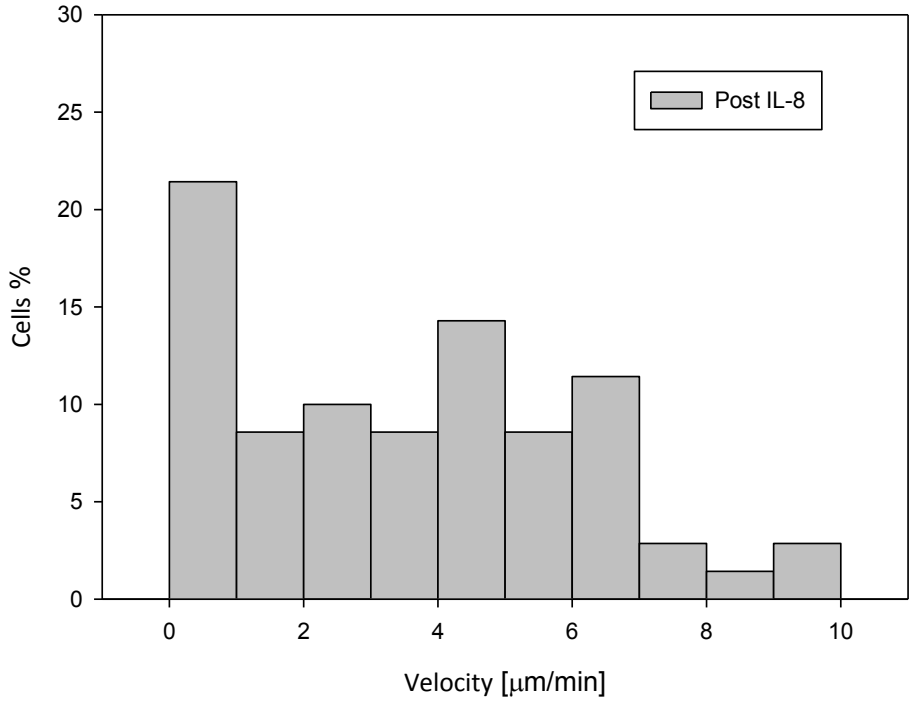


**Figure 2.15: Average velocity distribution of cells vs time A) before, B) after IL-8.**

## DISCUSSION

The main purpose of this study is to describe an in vitro chemotaxis assay in a tissue-equivalent collagen gel by using Time-Lapse microscopy. The cell behavior was observed in a physiologically relevant environment and in dynamic conditions, unlike other chemotaxis assays from literature (BOYDEN, 1962; Zigmond and Hirsch, 1973). To study chemoattractant diffusion a fluorescently labeled dextran was used (FITC-dextran). The FITC-dextran selected for the experiments has a molecular weight comparable to that of the chemoattractants investigated, so that a similar diffusion behavior can be assumed. Cell motion under the action of the chemoattractant gradient was followed by time-lapse video microscopy. Human neutrophils, freshly isolated from peripheral blood of different volunteers, under the effect of the pro-chemotactic factor Interleukin-8 (IL-8) (Baggiolini and Loetscher, 2000; Baggiolini et al., 1989; Olson and Ley, 2002)**,** were used as a model to test the assay. The response of neutrophils to IL-8 was first analyzed qualitatively through cellular trajectory reconstruction. Since collagen fibrils can become aligned near the surface as the gel forms or within the gel as it compacts due to traction exerted by entrapped cells, the possible contributions of contact guidance needed to be considered. Contact guidance in 3D is the phenomena by which the matrix provides directional cues to the cells and directs the motility response via anisotropy in the microenvironment (Dallon et al., 1999; Dickinson et al., 1994; Guido and Tranquillo, 1993). For instance, in fibroblasts it has been shown that contact guidance cues from collagen alignment promote 3D cell migration along the axis of collagen alignment (Dickinson et al., 1994; Guido and Tranquillo, 1993). In our chemotaxis chamber assay, in absence of IL-8, the motion of cells in the xy plane showed a random orientation uniformly distributed in space, supporting the absence of any contact guidance effects. Instead, in the presence of IL-8 concentration gradient, cell trajectories were directed towards the chemoattractant source. Then, cell behavior was quantitatively characterized by calculating some key parameter of the cell migration: chemotactic index, cellular average velocity and motile fraction of the cells. Neutrophils from two different donors displayed different behaviors both prior to the addition of IL-8 and after IL-8 stimulation. In particular, the cells from donor B showed higher value in all the evaluated parameters compared to the cells from donor A.

In absence of IL-8, the average velocity of neutrophils from donor A resulted to be 0.65 μm/min. Furthermore, only ~5% of the cells did actually move and the chemotaxis index fluctuated around 0. On the other hand, cells from donor B showed average velocity equal to 1.5 μm/min. The chemotaxis index value was calculated around 0.25 and the percentage of motile cells was found to be ~20%. However, the cell trajectories reconstruction indicated a random orientation in both samples. The differences in speed and in the cells motile fraction might be related to different IL-8 circulating level in the two volunteers. In fact, IL-8 production, that contribute to neutrophils activation and the development of acute inflammation (Harada et al., 1994), can be rapidly induced by several factor including bacterial and viruses infections (Hoffmann et al., 2002; Roebuck, 1999). Concerning the chemotactic index, it showed a lower value in the neutrophils from donor A, likely due to a smaller fraction of motile cells. Indeed, the motile cellular fraction and the chemotactic index as a function of the time showed a comparable trend. In conclusion, our chemotaxis chamber represent a good model for studying chemotactic effects of IL-8 on polimorphonuclear lymphocytes in three-dimensional collagen matrices. Moreover, this assay might be useful to investigate the chemotactic effects of different compounds on several cell lines and the role of chemotaxis in pathological samples.

# CHAPTER 3

# CHRONIC AIRWAY INFLAMMATION IN CYSTIC FIBROSIS (CF): A MODEL OF DISEASE TO IDENTIFY TARGET OF MODULATION OF CELL RECRUITMENT

## INTRODUCTION

The cell motility is the base of numerous biological processes, from morphogenesis to inflammation. One of the mechanisms that cells use to move in a particular direction is to respond to gradients of chemicals, which they can detect through cell surface receptors. If the movement involves direction sensing followed by directed migration up or down the chemical gradient, this process is known as chemotaxis (Affolter and Weijer, 2005). Although the physio-pathological relevance of cell motility processes, the techniques currently available for their characterization take data of hard quantitative interpretation. The 2D study of cell motility phenomena is usually performed by fluorescence microscopy technique on fixed samples, where the examined cells are observed in instants of time that precede and follow the addition of a certain factor. This cannot give a dynamic quantification of the phenomena, but only a "static" one, limited to two time steps, missing the progression of motility event. The advent of technology as time-lapse microscopy has allowed to overcome these limits, being able to follow cell motility from time to time and obtain quantification of the random or directional (chemotaxis) cell movement (Su et al., 2007) and it represents the nearest approach to in vivo assays. Cell migration is a very complex phenomenon that regulates the inflammatory response as well as several processes of cell biology and development. Moreover, deregulation of cell migration can have grave consequences and contributes to several important pathological processes, including vascular disease, osteoporosis, chronic inflammatory diseases and tumor metastasis (Lauffenburger and Horwitz, 1996; Ridley et al., 2003). Chronic inflammation is an ideal condition for the study of cell migration and its deregulation. In this condition several cell populations are recruited in response to the enhanced local release of chemo-attractant molecules (chemokines) that favors the infiltration of circulating leukocytes

within a disease-target tissue. Inflammation is a physiological process of response to tissue injury and it is achieved by the increased movement of plasma and leukocytes (especially granulocytes) from the blood into the injured tissues. However, the dysregulation of the proper control of inflammation, induces a massive infiltration of leukocytes (neutrophils, monocytes, lymphocytes) within the target tissue as it occurs in gut, airways, skin, joints leading to chronic inflammatory response and tissue damage. Thus, neutrophils infiltration is a hallmark in rheumatoid arthritis, vasculitis, inflammatory bowel diseases and chronic lung diseases (Eyles et al., 2006). Cell migration is influenced by many factors as chemokine production, 3D moving, chemical gradient and interaction with neighboring cells within the tissue. This may generate several problems in the interpretation and quantitative analysis of data and deserve careful evaluation. In order to understand the mechanisms of migration and to identify appropriate target of modulation of cell recruitment in pathological condition, we used a model of disease and focused on chronic airway inflammation in Cystic Fibrosis (CF). Cystic Fibrosis (CF), the commonest life-threatening inherited disease in Caucasians, is due to mutations in the CF in the CF trans membrane conductance regulator (CFTR) gene, which encodes a cAMP-regulated chloride channel expressed at the apical membrane of epithelial cells in the airways, pancreas, testis, and other tissues. The most common CFTR mutation producing CF is deletion of phenylalanine at residue 508 (F508del) in its amino acid sequence (Ratjen and Döring, 2003; Thelin and Boucher, 2007). The misfolded F508del-CFTR protein is degraded and fails to reach the cell membrane, leading to defective chloride cannel function (Gelman and Kopito, 2003; Kopito, 1999; Reddy et al., 1996; Ward et al., 1995). Although CF is a systemic disease, the main cause of death is due to chronic airway inflammation and persistent and untreatable pulmonary infections, with Pseudomonas aeruginosa colonizing most of the patients (Scheid et al., 2001; Smith et al., 1996; Thelin and Boucher, 2007). Defects of the CFTR are associated with a marked increase of proinflammatory cytokines, such as TNF-α, IL-6, IL-1β, IL-17 (Gelman and Kopito, 2003; Kopito, 1999; Osika et al., 1999). The production of tumor necrosis factor (TNF)-a, IL-1b, IL-6, and IL-8 and other pro-inflammatory cytokines by airway epithelial cells and lung macrophages along with the accumulation and activation of neutrophils in the CF airways may underlie the early pathogenesis of CF lung disease (Dean et al., 1993) (Balough et al., 1995). The inflammatory cytokine responses, particularly that of the potent neutrophil chemoattractant and activator IL-8, which recruits large numbers of neutrophils into the

airways, are excessive in bronchoalveolar lavage fluid from patients with CF compared with control subjects (Hubeau et al., 2001; Tirouvanziam et al., 2000) (Bals et al., 1999; Bonfield et al., 1995). Several studies have shown an increased pro-inflammatory activity in the CF tissues, regardless of bacterial infections, as inflammation is similarly observed in CFTR-defective cell lines kept in sterile conditions. Despite recent studies have indicated that CF airway epithelial cells can spontaneously initiate the inflammatory cascade, the molecular mechanisms involved in this increased inflammatory response is still not clear. CFTR-defective bronchial epithelial cell lines, IB3-1 human CF bronchial epithelial, (carrying F508del/W1282X CFTR mutation) and isogenic stably rescued C38 (Smith et al., 1996) have been used to understand the molecular link between a defected CFTR and the excessive inflammatory responses typical of CF airways. It has been shown that nasal polyp mucosa from CF patients as well as human CFTR-defective cell lines constitutively up-regulate tissue transglutaminase (TG2) (Maiuri et al., 2008). TG2 belongs to a family of mammalian enzymes that post-translationally modify proteins in a calcium-dependent manner (Malorni et al., 2008) leading to the formation of covalent e(g-glutamyl)lysine linkage. It is localized inside the cell in free cytosolic, mitochondrial, and nuclear forms, in the extracellular environment and in association with the cell surface (Griffin et al., 2002). TG2 is apparently involved in disparate biological processes including apoptosis (Fésüs and Szondy, 2005), cell adhesion and migration (Griffin et al., 2002), ECM homeostasis, angiogenesis and wound healing (Haroon et al., 1999). The increased TG2 activity drives inflammation through down-regulation of the antiinflammatory peroxisome proliferator- activated receptor (PPAR)g, a negative regulator of inflammatory gene expression (Daynes and Jones, 2002). CF airways high levels of reactive oxygen species (ROS) lead to an increase of TG2 activity, TG2-mediated PPARγ cross-linking, ubiquitination, and proteasome degradation, thus driving inflammation (Maiuri et al., 2008). Blocking TG2 through specific gene-silencing or TG2 inhibitors increases PPARg protein and reverses inflammation (Maiuri et al., 2008). TG2 is therefore a master regulator of inflammation in CF airways and mediates the production of inflammatory cytokines and chemokines via targeting key regulatory pathways of inflammation. To underpin the mechanisms leading to inflammation and secretion of cytokines and chemokines, we investigated the mechanisms of TG upregulation and its impact on inflammation within the pro-oxidative environment that characterizes CF epithelial cells. TG2 is regulated by retinoids, steroid hormones, peptide growth factors and

cytokines that also lead to a time-dependent decrease in TG2 ubiquitination (Lorand and Graham, 2003). This indicates that posttranslational control mechanisms may regulate TG2 tissue levels in CF airways. We focused on small ubiquitin like-modifier (SUMO) post-translational modification since this has been defined as a central way of regulating key cellular functions and stability of proteins (Geiss-Friedlander and Melchior, 2007; Meulmeester and Melchior, 2008). SUMOylation has been defined as a key player of the post-translational network to regulate key cellular functions including transcription, nuclear translocation, stress response and chromatin structure as well as of diversifying localization and even stability of the modified proteins (Geiss-Friedlander and Melchior, 2007; Meulmeester and Melchior, 2008). Sumoylation is accomplished via an enzymatic cascade involving, among the others, E3 ligases, that catalyze the transfer of SUMO from the conjugating enzyme UBC9 to a substrate (Meulmeester and Melchior, 2008). E3 ligases have gained a central role in the SUMO machinery, since they regulate sumoylation in response to different stresses (Meulmeester and Melchior, 2008).

## MATERIALS AND METHODS

### *Cell lines and cultures*

Human CF bronchial epithelial cell line IB3-1, carrying F508del/W1282X CFTR mutation, and isogenic stably rescued C38 cell lines (LGC Standards) were cultured as recommended by American Type Culture Collection. IB3-1 cell line was incubated for 24 h with cystamine (400 μM; Sigma-Aldrich) followed or not by rosiglitazone for 6 h (10 μM; Alexis Biochemicals).

### *RNA interference and Adenoviral vector*

IB3-1 cells were transfected with 50 nM human SUMO-1 or scrambled small interfering RNA (siRNA) duplex using Lipofectamine RNAiMAX at 37°C for 72 h. The SUMO-1 duplex siRNA was a pool of three sequences. siRNA-mediated knockdown of PIASy was performed using specific siRNA oligos, as previously described (Mabb et al., 2006). TG2 gene silencing was performed as previously reported (Maiuri et al., 2008). Human manganese superoxide dismutase (MnSOD) cDNA was cloned into the shuttle vector pAd5CMVK-NpA (Du et al., 2006). MnSOD adenovirus was a gift from Michael Brownlee (Albert Einstein College of Medicine, New York, NY). IB3-1, cell lines was infected with MnSOD or control adenovirus for 2 h, as previously described (Du et al., 2006).

### *Cell fractionation*

IB3-1 cells were collected in cold buffer A (20 mM Tris-HCl (pH 7.4), 2 mM EDTA, 20 mM 2-ME, 1x PMSF, 1 μg/ml inhibitor protease cocktail), homogenized in Potter-Elvehjem pestle and glass tube (Sigma-Aldrich), and centrifuged at 2000 rpm for 15 min at 4°C to obtain nuclear pellets. Supernatants were collected as cytoplasmic fractions. Nuclear pellets were washed with buffer A and resuspended in buffer B (2 mM $Na_3VO_4$, 400 mM NaCl, 1 mM $MgCl_2$, 1 mM EGTA, HEPES 10 mM (pH 7.9), 1 mM DTT, 1x PMSF, 1 μg/ml inhibitor protease cocktail) and incubated on ice for 50 min with occasional mixing to extract nuclear proteins. Nuclear extracts were cleared by centrifugation (7000 rpm, 15 min, 4°C), and supernatants were collected as nuclear fraction. Then, cytoplasmic and nuclear whole-cell fractions were analyzed by immunoblotting.

## *Immunoblot*

The blots were incubated with anti-phospho-p42/p44 MAP kinases (rabbit polyclonal IgG, 1/500; Cell Signaling Technology), TG2 (clone CUB7402, mouse monoclonal IgG1, 1/500; NeoMarkers), ubiquitin (clone FL-76 sc9133, rabbit polyclonal IgG, 1/500; Santa Cruz Biotechnology), SUMO-1 (clone FL-101 sc9060, 1/500; Santa Cruz Biotechnology), phopsho-p65(Ser$^{536}$) (rabbit polyclonal, 1/500; Cell Signaling Technology), PIASy (clone H75 sc50437, rabbit polyclonal IgG, 1/1000; Santa Cruz Biotechnology), I$\kappa$B$\alpha$ (clone H4 sc1643, mouse monoclonal IgG1, 1/1000; Santa Cruz Biotechnology), β-actin (clone 13E5, rabbit polyclonal IgG, 1/2000; Cell Signaling Technology), and $\alpha$β-tubulin (rabbit polyclonal IgG, 1/2000; Cell Signaling Technology). The primary Abs were counterstained by a HRP-conjugated anti-IgG Ab (Amersham Biosciences) for 60 min at room temperature. Proteins were visualized by chemiluminescence (ECL Plus; Amersham Biosciences) and exposed to X-OMAT film (Eastman Kodak). The amounts of proteins were determined by a Bio-Rad protein assay to ensure equal protein loading before Western blot analysis. Fifty micrograms of cell lysate was loaded in each lane.

## *Immunoprecipitation*

Treated and untreated cells were harvested, lysed, and 500 µg of cell lysate was immunoprecipitated by overnight incubation at 4°C on a mixer with an appropriate dilution of specific Ab (anti-TG2 CUB 7402 mAb, anti-PIASy, anti-PPAR$\gamma$, anti-I$\kappa$B$\alpha$) in cold lysis buffer. The samples were then incubated with protein G-Sepharose at 4°C for 2 h with constant mixing. After washing, the immunoprecipitated proteins were electrophoresed through 10% polyacrylamide gels (Bio-Rad), transferred onto blotting membranes (PolyScreen polyvinylidene difluoride; NEN), and analyzed.

## *Mice*

Young adult female CF mice homozygous for the F508del mutation in the 129/FVB outbred background (Legssyer et al., 2006) and their wild-type littermates were housed in static isolator cages at the animal care specific pathogen-free facility of the University of Louvain following recommendations of the Federation of European Laboratory Animal Science Associations (Nicklas et al., 2002). To prevent intestinal obstruction CF mice were weaned to

a liquid diet (Peptamen; Nestlé Nutrition). Peptamen was replaced daily. The genotype of each animal was checked at 21 days of age, as previously described (Legssyer et al., 2006). CF (*n* = 7) and normal homozygous wild-type mice (*n* = 7), 10 to 14 wk of age, were treated i.p. (Karpuj et al., 2002) for 7 days with a daily dose of 100 µl of 0.01 M cystamine or PBS solution. Mice were then killed by i.p. injection of 20 mg of sodium pentobarbital (Abbott Laboratories).

## *Confocal microscopy*

**Mice lung tissue.** Seven-micrometer frozen lung tissue sections from each mice were fixed in acetone for 10 min. The sections were incubated for 2 h at room temperature with the following Abs: anti-phospho-p42/p44 MAP kinases (1/200; Cell Signaling Technology), PPAR $\gamma$ (clone H100 sc-7196, rabbit polyclonal IgG, 1/100; Santa Cruz Biotechnology), TG2 (clone H237 sc20261, rabbit polyclonal IgG, 1/100; Santa Cruz Biotechnology). This was followed by incubation with Alexa 488 donkey anti-rabbit (used for detection of phospho-p42–44, PPAR$\gamma$, and TG2 protein, 1/200; Invitrogen). Data were analyzed under fluorescence examination by confocal microscopy as previously described (Maiuri et al., 2008).

## *Elisa*

Human or murine TNF-$\alpha$ secretion was measured using the BD OptEIA TNF-$\alpha$ ELISA kit II (BD Biosciences). Measurements were performed at least in triplicate. Values were normalized to $10^6$ cells; results were expressed as means ± SEM.

## RESULTS

### *PIASy-mediated TG2 SUMOylation increases TG2 protein levels in CF airway epithelial cells*

To investigate whether posttranslational modifications could result in the persistence of high levels of TG2 protein, the protein extract from IB3-1 (CF epithelial cell lines carrying F508-del/W1282X CFTR mutations) and C38 cells (the isogenic stably rescued) were analyzed by Western blots and revealed that SUMO-1 protein level was increased in IB3-1 cells as compared with C38 cell lines (Fig. 3.1 A). Furthermore, when TG2 immunoprecipitates from IB3-1 cells were probed with the anti-TG2 Ab, two TG2 bands were detected, with the upper band corresponding to the SUMOylated TG2 (Fig. 3.1 B). Moreover, TG2 protein levels were higher in IB3-1 than in C38 cell lysates (Fig. 3.1 C).

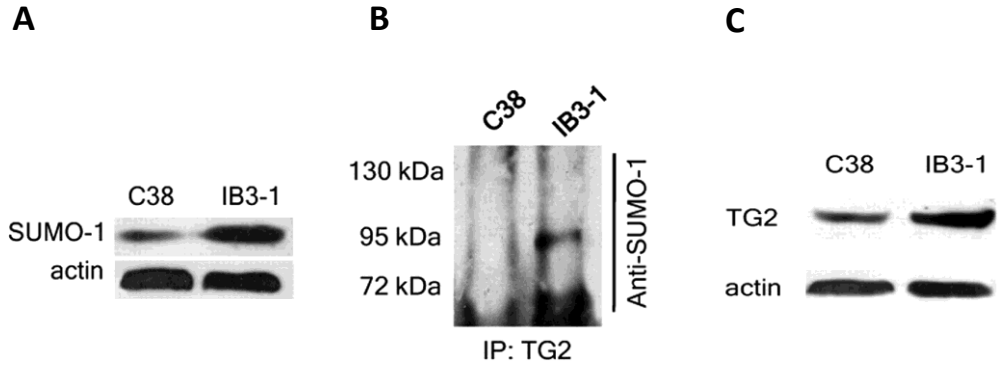


**Figure 3.1: A) Immunoblot analysis of SUMO-1 expression B) SUMO-TG2 immunoprecipitation and C) Immunoblot analysis of TG2 expression in CF IB3-1 and C38 cells.**

Since Protein Inhibitor of Activated STAT (PIAS)y, a member of the PIAS family (Mabb et al., 2006), has recently been defined as the first SUMO ligase for NF-kB essential modulator (NEMO) (Mabb et al., 2006) and PIASy-NEMO interaction is mediated by Reactive Oxygen Species (ROS) (Mabb et al., 2006), we also investigated whether PIASy-TG2 interaction could mediate ROS-driven post-translational modifications of TG2. In the experiments the IB3 cell lysates were immunoprecipitated with PIASy antibody and probed with TG2 antibody; the results evidenced the corresponding band to molecular weight of TG2, to confirm the interaction TG2-PIASy (it is performed also the reciprocal IP) (fig 3.2 A) . Since PIASy SUMO-1

E3-ligase activity is influenced by ROS (Mabb et al., 2006), IB3 cells were treated or not with virus infection of human manganese superoxide dismutase (MnSOD) to regulate the pro-oxidative environment of cell. Human manganese superoxide dismutase (MnSOD) cDNA was cloned into the shuttle vector pAd5CMVK-NpA (Du et al., 2006). MnSOD adenovirus was a gift from Michael Brownlee (Albert Einstein College of Medicine, New York, NY). The cell lines were infected with MnSOD or control adenovirus for 2 h. The protein extract was resolved by SDS-Page and probed with SUMO, TG2, PIASy antibodies evidencing the reduction of level with MnSOD (Fig.3.2 C). The overexpression of human MnSOD (Du et al., 2006) controlled PIASy-TG2 coimmunoprecipitation (Fig. 3.2 A) as well as SUMO-TG2 coimmunoprecipitation (Fig. 3.2 B) thus reducing TG2 protein levels (Fig. 3.2 C). Furthermore, MnSOD overexpression reduced PIASy and SUMO-1 protein levels (Fig. 3.2 C).

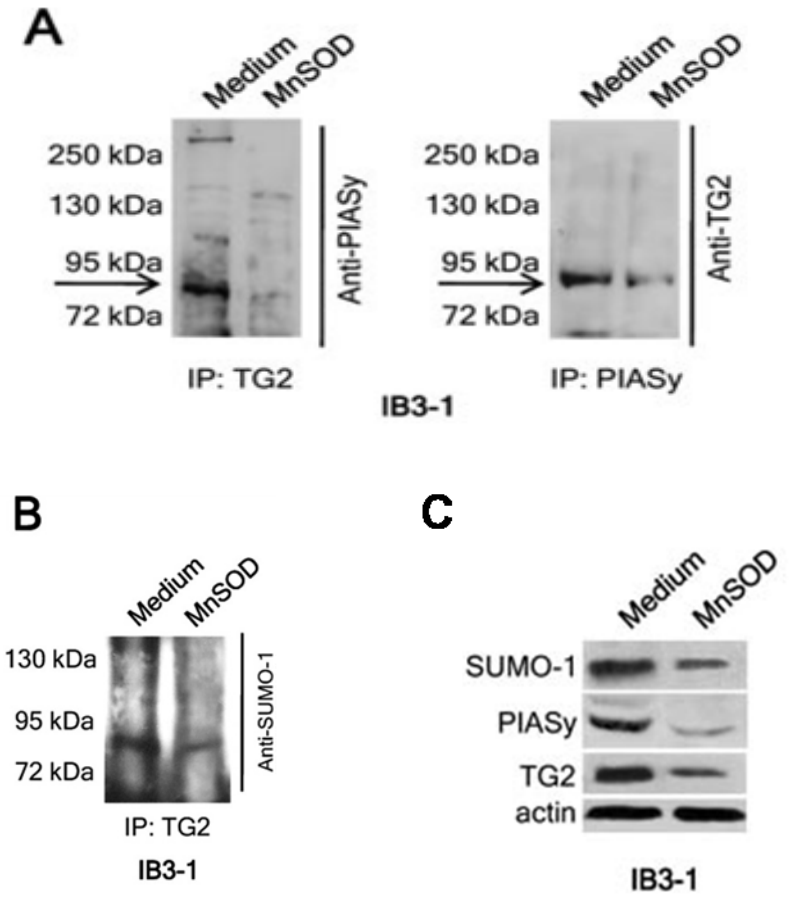


**Fugure 3.2: A) Effect of the overexpression of human MnSOD on A) PIASy-TG2 coimmunoprecipitation, B) SUMO-TG2 coimmunoprecipitation and C) TG2, PIASγ and SUMO-1 protein expression.**

The data of experiments indicate that in CF airway epithelia the pro-oxidative intracellular milieu leads to PIASy-mediated TG2 sumoylation. SUMOylation of TG2 decreased TG2 ubiquitination since these two main posttranslational changes may compete each other for the same lysine residues on the aminoacid sequence. We performed experiments of SUMO gene silencing by SUMO-1 or PIASy specific siRNAs introduced into cell by using Lipofectamine RNAiMax according to the manufacturer's instructions for 72h at 37°C. IP studies revealed an increase of TG2 ubiquitination upon proteasome inhibition by MG132 (Fig.3.3 A, B), thus allowing TG2 to be targeted to proteasome for degradation. This induced decreases of TG2 protein (Fig. 3.3 C) Therefore, oxidative stress increases PIASy protein levels and favours TG2 SUMOylation that leads to the persistence of high TG2 tissue levels by downregulating TG2 ubiquitination and proteasome degradation.

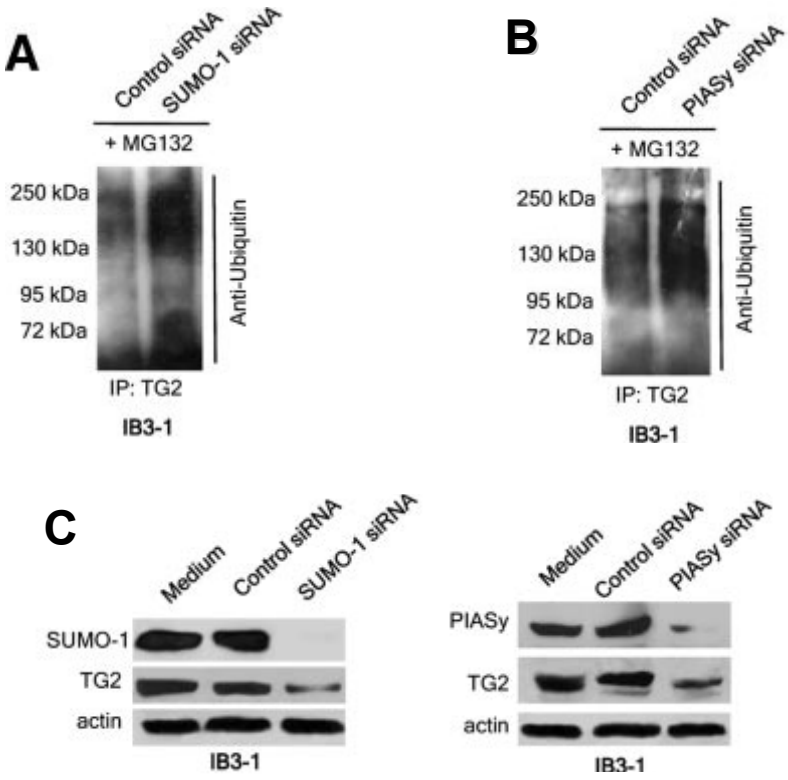


**Figure 3.3: Effect of A) SUMO or B) PIASy gene silencing on TG2 ubiquitination upon proteasome inhibition by MG132. C) Immunoblot analysis of TG2 protein upon SUMO-1 or PIASy gene silencing respectively.**

## *SUMO-1 or PIASy gene silencing controls inflammation in CF airway epithelial cells*

TG2 SUMOylation might provide the missing link between cellular stress and inflammation. We investigated whether the control of TG2 SUMOylation might modulate TG2-driven inflammation previously described in CF epithelia (Maiuri et al., 2008). The figure 7 demonstrated that gene silencing of either PIASy or SUMO by specific siRNAs induced a significant decrease of p42– 44 phosphorylation in IB3-1 cells.

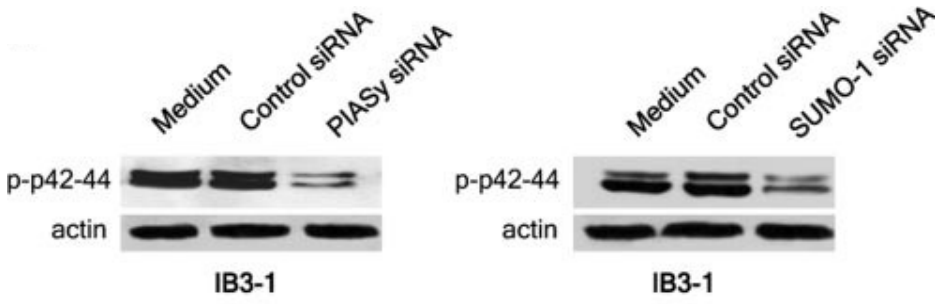


**Figure 3.4: Effect of SUMO-1 or PIASy gene silencing on p42– 44 phosphorylation**

## *TG2 inhibition modulates PPARg and IkBa SUMOylation in CF airway epithelia*

TG2 SUMOylation may have great relevance in driving CF inflammatory phenotype and release of pro-inflammatory cytokines and chemoattractants. PPARγ which may be targeted by TG2 to crosslinking and proteasome degradation (Maiuri et al., 2008), may also be targeted by SUMO-1 and undergo sumoylation in response to a PPARg agonists, such as Rosiglitazone (Maiuri et al., 2008; Pascual et al., 2005). Sumoylated PPARg interacts with the nuclear-receptor co-repressor (N-CoR)-histone deacetylase 3 (HDAC3) complex and thereby blocks its ubiquitination, thus maintaining a repressor condition (Pascual et al., 2005). This study shows that sustained TG2 activation inhibits PPARg SUMOylation and its interaction with the N-CoR (Pascual et al., 2005), thus favoring inflammation. Moreover TG2 induces crosslinking and degradation of Ik-Bα, a known TG2 substrate (Kim et al., 2006) and a negative regulator of NF-kB activation, inhibits Ik-Bα SUMOylation and favors NF-kB activation (Fig. 3.5). The data shows that blocking TG2 through specific gene silencing or

specific inhibitors, such as cystamine, (Fig. 3.5 A) increased PPARγ sumoylation in response to rosiglitazone (agonist of PPARγ) in IB3 cell line. Moreover siRNA of TG2 or cystamine induced increase of Ik-Bα sumoylation (fig. 3.5 B) and its protein level (fig. 3.5 C, left). Finally reduced p-65 NF-kB was detected in nuclear extracts of IB3-1 cells after TG2 inhibition (Fig 3.5 C right).

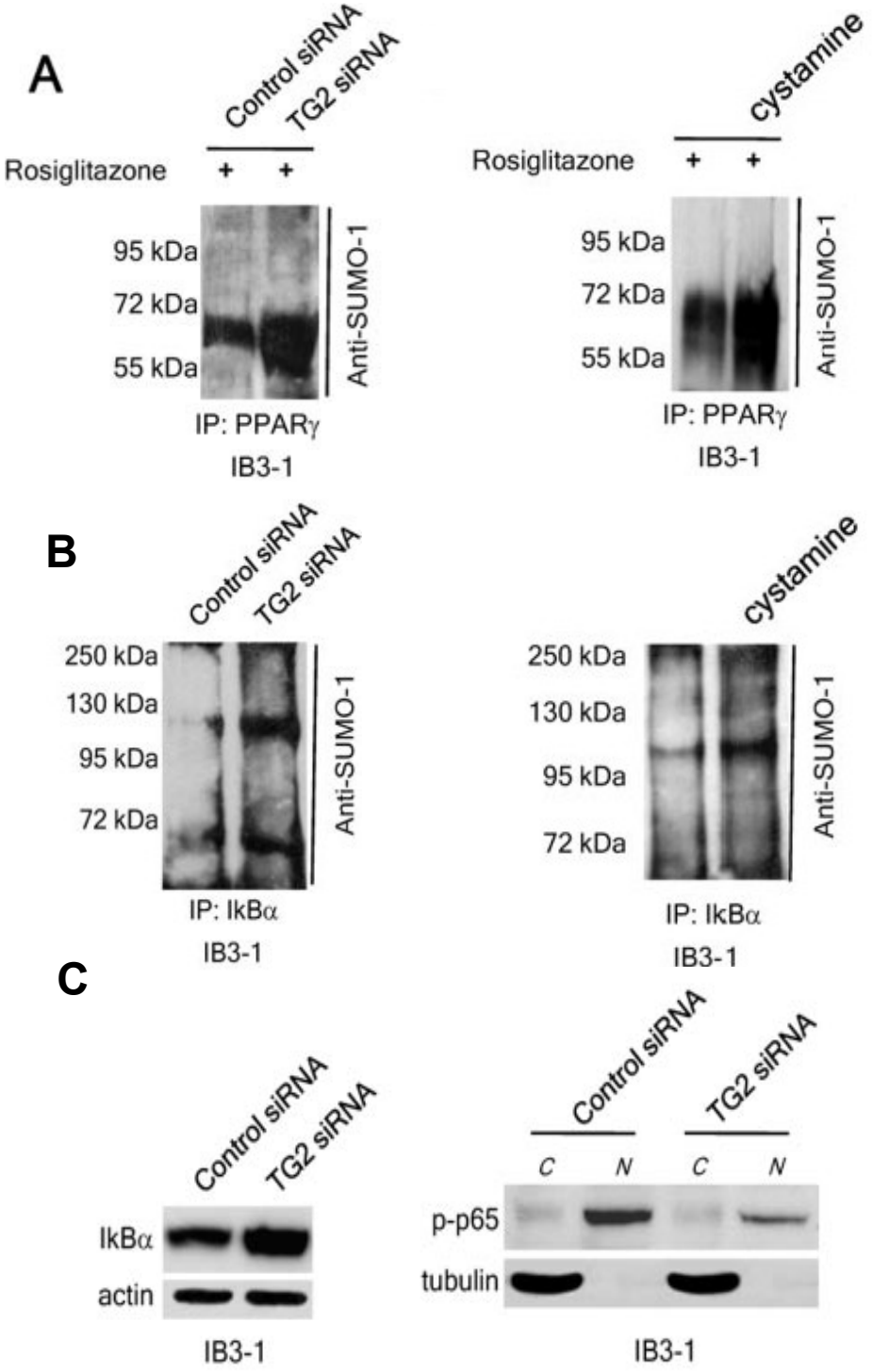


**Figure 3.5 Effect of TG2 inhibition on A) PPARγ SUMOylation, B) Ik-Bα SUMOylation, C) Ik-Bα protein level (left) and p-65 NF-kB nuclear translocation (right)**

This cascade of events leads to reduced secretion of inflammatory cytokines as TNF-a (Fig. 3.6) and of the neutrophils chemoattractant IL-8 (data not shown).

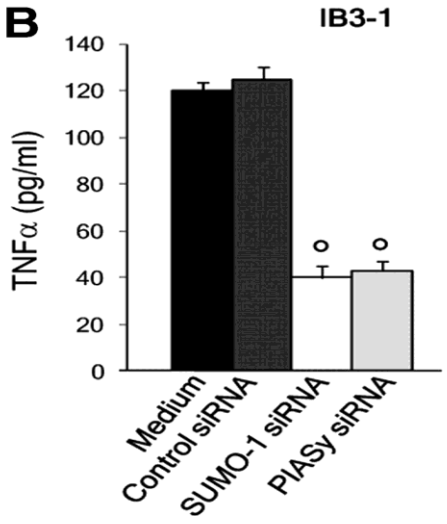


**Figure 3.7:Effect of SUMO-1 or PIASy gene silencing on TNF-α protein expression**

## *TG2 inhibition controls inflammation in F508del-CFTR homozygous mice*

To test the effects of TG2 inhibition in vivo, we treated CF mutant mice homozygous for F508del-CFTR mutation (Legssyer et al., 2006) and their control littermates (Legssyer et al., 2006) with cystamine, previously reported to inhibit TG2 and ameliorate disease manifestations in a mouse model of Huntington's disease (Karpuj et al., 2002). We treated CF and wild-type mice with a daily injection of cystamine (i.p. injection of 100 μl of 0.01 M in PBS for 7 days) or PBS (i.p. injection of 100 μl of PBS for 7 days). After treatment with PBS the expression and distribution of the tested markers remained unaltered as compared with the pattern observed in untreated CF mice. Before treatment, as well as after treatment with PBS, all seven tested CF mice showed increase of TG2 activity (Fig. 3.8 A), phosphorylation of p42–44 (Fig. 3.8 A) and of TNF-α protein (Fig. 3.8 B) as compared with control littermates. In all CF mice, the treatment with cystamine controlled TG2 activity, increases PPARγ levels and its nuclear localization and reduced p42–44 phosphorylation (Fig. 3.8 A) and TNF-α protein levels (Fig. 3.8 B), thus restoring the pattern observed in their control littermates. Cystamine did not induce any changes in wild-type mice.

**A**

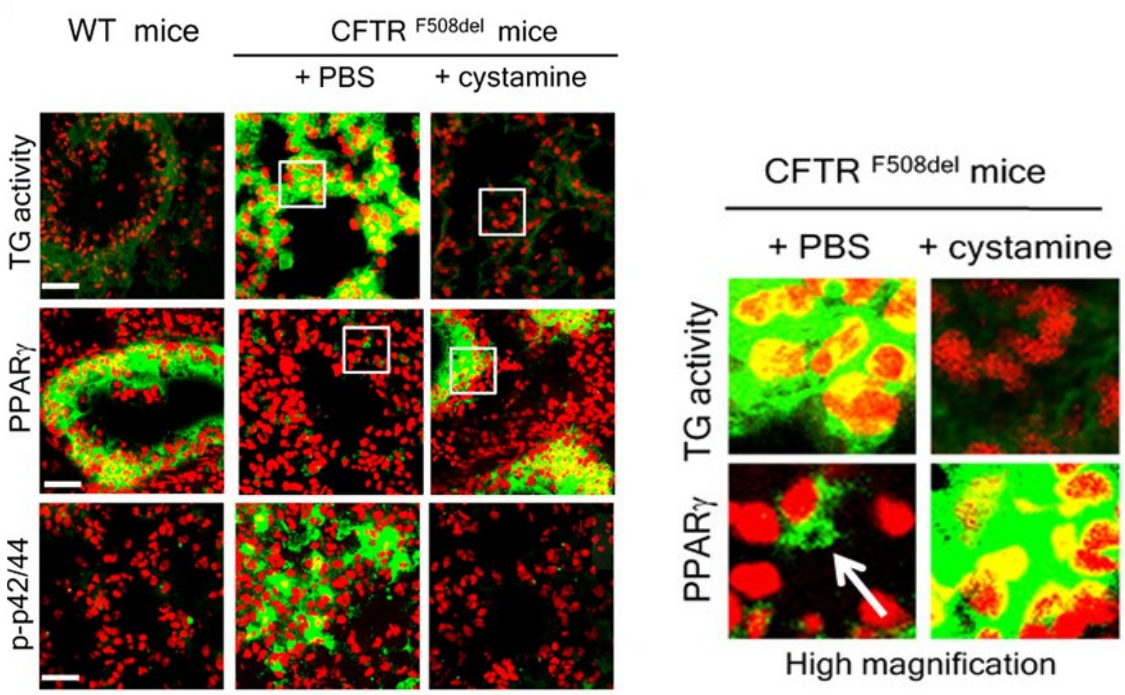


**B**

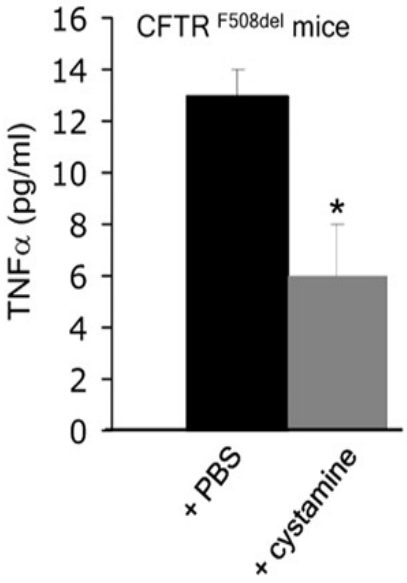


**Figure 3.8: Effect of cystamine on A) TG2 activity, PPARγ levels localization, p42–44 phosphorylation and B) TNF-α protein in F508del-CFTR mice**

## DISCUSSION

The cellular response to stress involves a finely tuned posttranslational network that provides proteins with functional ability at the right time and place, and its perturbations have been shown to contribute to the aetiology of various human diseases (Tempé et al., 2008). SUMOylation has been defined as a key player of the posttranslational network to regulate key cellular functions, including transcription, nuclear translocation, stress response, and chromatin structure, as well as of diversifying localization and even stability of the modified proteins (Tempé et al., 2008) (Meulmeester and Melchior, 2008) (Geiss-Friedlander and Melchior, 2007). SUMOylation is accomplished via an enzymatic cascade involving, among others, E3 ligases, that catalyze the transfer of SUMO from the conjugating enzyme UBC9 to a substrate (Meulmeester and Melchior, 2008). E3 ligases have gained a central role in the SUMO machinery, since they regulate SUMOylation in response to different stresses (Meulmeester and Melchior, 2008). In CF airway epithelia the increased levels of ROS lead to TG2 SUMOylation via interaction of TG2 with PIASy, an E3 ligase already reported to mediate NEMO SUMOylation upon genotoxic stress through ROS generation (Mabb et al., 2006). Oxidative stress increases PIASy protein levels and favors TG2 SUMOylation that leads to the persistence of high TG2 tissue levels by down-regulating TG2 ubiquitination and proteasome degradation. TG2 SUMOylation may therefore switch off the posttranslational regulatory mechanisms in response to the oxidative stress. Most proteins involved in the pathogenesis of chronic human diseases, as huntingtin, ataxin-1, tau, and $\alpha$-synuclein, were reported to be SUMO (Steffan et al., 2004) as well as TG2 substrates (Junn et al., 2003). PPAR$\gamma$, which may be targeted by TG2 to cross-linking and proteasome degradation (Maiuri et al., 2008), may also be targeted by SUMO-1 and undergo SUMOylation in response to a PPAR$\gamma$ agonists, such as rosiglitazone (Maiuri et al., 2008; Pascual et al., 2005). Moreover TG2-mediated cross-linking and degradation of IkB$\alpha$, a known TG2 substrate (Kim et al., 2006), inhibits IkB$\alpha$ SUMOylation and favors NF-kB activation. Therefore, TG2 may function as a link between oxidative stress and inflammation by driving the decision as to whether a protein should undergo SUMO-mediated regulation or degradation. TG2 is suggested to be an attractive target to restore cellular homeostasis and dampen chronic inflammation in CF airways. The regulation of the high levels of TG2 protein or the inhibition of sustained TG2 enzyme activation may represent a new attractive

approach to control disease evolution in CF patients. To evaluate whether we can translate our in vitro findings into an appropriate animal model and confirm their biological relevance in vivo we have studied CF mutant mice homozygous for F508del-CFTR (Legssyer et al., 2006). We have demonstrated TG2-SUMO colocalization and increased TG2 activity in lung tissues from F508del-CFTR homozygous mice. These mice displayed inflammation in the lungs. We treated these CF mice with daily i.p. injections of cystamine, already used in a mouse model of Huntington's disease (Karpuj et al., 2002). Cystamine is known to inactivate TG2 through a disulfide-exchange reaction and is a substrate for TG2 (Karpuj et al., 2002). Daily injections of cystamine inhibit TG2 activation, increase PPAR$\gamma$ protein expression, and control inflammation. All together these results highlight TG2 as an unforeseen unifying link between genetic defect and inflammation. They indicate that CFTR genetic defect drives a cascade of events starting with TG2 SUMOylation and increase levels of TG2 activity that in turn trigger inflammation and cytokine secretion via PPARg downregulation. The modulation of TG2 SUMOylation or the control of TG2 enzyme activity may represent a useful tool in the identification of proper modulators of NF-kB activation and the production of inflammatory cytokines and chemoattractant factors. Therefore, TG2 might be a candidate target for the design of a pathogenic-based therapy in CF and TG2 inhibition might represent a new attractive option to control the evolution of chronic inflammatory diseases, neurodegenerative diseases, and even cancer.

# CHAPTER 4

# WOUND HEALING IN DIABETES: ROLE OF PHOSPHOPROTEIN ENRICHED IN DIABETES/PHOSPHOPROTEIN ENRICHED IN ASTROCYTES-15 (PED/PEA-15)

## INTRODUCTION

Cell adhesion, migration and contraction play significant roles in creating contractile force of wound margins and in contributing to wound closure. Thus, misregulation in one of these cell functions may have severe consequences, and impair wound healing process (Gary Sibbald and Woo, 2008). Altered wound healing is a significant cause of morbidity and mortality for a large portion of the adult population worldwide (Association, 2003; Edmonds, 2004). One of the most common conditions associated with impaired wound healing is diabetes mellitus. About 15% of patients with diabetes present ulcers at lower extremities, quite difficult to heal (Trousdale et al., 2009). Multiple factors contribute to deficient healing in a subset of diabetic patients (Braiman-Wiksman et al., 2007). They include an altered host response, diminished anti-bacterial defences, prolonged inflammation, altered protease activity, a tendency for vascular abnormalities, the generation of an inadequate number of cells to accomplish rapid and robust healing, decreased growth factor production, a failure to form a sufficient amount of extracellular matrix, and alterations in apoptosis that may interfere with healing by decreasing the number of cells that participate in new tissue formation (Galkowska et al., 2006; Peppa et al., 2009; Schultz and Wysocki, 2009; Siqueira et al., 2010; Velander et al., 2008; Wall et al., 2008). In particular, fibroblasts play a pivotal role in tissue repair. Fibroblasts play a key role in wound healing process. Infact, they produce, secrete and remodel ECM and act as signal cells secreting the growth factors important for cell-cell communication during the repair process (Falanga, 2005; Giacco et al., 2006). Any impediment to fibroblast functions prevents normal wound closure and results in chronic non-healing wounds (Lerman et al., 2003). Noteworthy, alterations of fibroblast functions have been reported in individuals with type 2 diabetes (Lerman et al., 2003).

The Phosphoprotein Enriched in Diabetes/ Phosphoprotein Enriched in Astrocytes-15 (PED/PEA-15) is a 15 kDa cytosolic protein widely expressed in different tissues and highly conserved among mammals, whose gene maps on human chromosome 1q21-22 (Estellés et al., 1996). Overexpression of the PED/PEA-15 gene is a common defect in type 2 diabetes (Condorelli et al., 1998a, b; Condorelli et al., 2001; Valentino et al., 2006). During a study using a differential display technique to identify genes whose expression was altered in type 2 diabetes, it has been demonstrated that both PED/PEA-15 mRNA and protein levels were overexpressed in fibroblasts from type 2 diabetics compared with non-diabetic individuals. Also skeletal muscle and adipose tissues, two major sites of insulin resistance in type 2 diabetes, showed the same behaviour (Condorelli et al., 1998a). Furthermore, a recent study showed that PED/PEA-15 overexpression represents a common abnormality in both type 2 Diabetes Mellitus and their First Degree Relatives (Valentino et al., 2006).

Cells overexpressing PED/PEA-15 showed an impaired insulin-dependent glucose uptake. Transgenic mice overexpressing PED/PEA-15 exhibit mildly elevated random-fed blood glucose levels and become hyperglycemic after glucose loading, indicating that increased expression of this gene is sufficient to impair glucose tolerance. Moreover, transgenic mice become diabetic after administration of high-fat diets, indicating that, in vivo, the overexpression of PED/PEA-15 in conjunction with environmental modifiers may lead to diabetes (Vigliotta et al., 2004)Thus, these findings identify PED/PEA-15 as a novel gene controlling insulin action contributing, under appropriate environmental conditions, to genetic susceptibility to type 2 diabetes in humans.

PED/PEA-15 gene product is a ubiquitously expressed protein, which has been implicated in the control of cell survival and growth and glucose metabolism (Fiory et al., 2009). PED/PEA-15 lacks enzymatic function and mainly serves as a molecular adaptor. Indeed, it has been identified as an interactor for several signalling molecules including phospholipase D1 (Zhang et al., 2000), RSK2 (Vaidyanathan and Ramos, 2003) and extracellular signal regulated kinase 1/2 (ERK1/2) (Condorelli et al., 2002; Eckert et al., 2008; Glading et al., 2007; Roth et al., 2007). In particular, PED/PEA-15 binding to ERK1/2 prevents its nuclear translocation and determines cytosolic accumulation, thereby modifying its targeting to specific subsets of substrates (Formstecher et al., 2001). We show that the increase of PED/PEA-15 expression results in a reduced fibroblasts motility and this may contribute to defect of wound healing in TgPED mice.

## MATERIALS AND METHODS

### *Materials*

Tribromoethanol (Avertin®) was from Sigma-Aldrich (St. Louis, Mo). Media, sera, and antibiotics for cell culture were purchased from Invitrogen Ltd. (Paisley, United Kingdom). Rabbit polyclonal Paxillin antibodies were from Zymed Laboratories (Invitrogen Corporation, Calif.). Rabbit polyclonal fibronectin antibodies were from Chemicon (Millipore Corporation). Western blotting, ECL reagents were from Amersham (Arlington Heights, Ill). Electrophoresis reagents were from BioRad. Rabbit polyclonal β-actin antibodies and mytomicin C were from Sigma-Aldrich (St. Louis, Mo.)

### *Cell culture and Western Blot*

Skin fibroblasts were obtained by punch biopsy, the cultures established and grown as previously described (31), and used for experimental procedures between 3 and 10 passages. For Western blotting, the cells were solubilized in lysis buffer (50mM HEPES pH 7.5, 150mM NaCl, 4mM EDTA, 10mM Na4PO7, 2mM Na3VO4, 100mM NaF, 10% glycerol, 1% Triton X-100, 1mM phenylmethylsulfonyl fluoride, 100 μg of aprotinin/ml, 1mM leupeptin) for 60 min at 4°C. Lysates were clarified at 5,000 x g for 15 min. Solubilized proteins were then separated by SDS-PAGE and transferred onto 0.45-μm-pore-size Immobilon-P membranes (Millipore, Bedford, Mass.). Upon incubation with the primary and secondary antibodies, immunoreactive bands were detected by ECL according to the manufacturer's instructions.

### *Scratch assay*

Fibroblasts were seeded at a density of $8\times10^5$ cells per well into the 6-well microplates, wounded by manually scratching with a pipette tip, washed twice with phosphate-buffered saline (PBS) and incubated at 37°C, with or without mitomycin C (10 μg/ml; Sigma-Aldrich, St. Louis, Mo.). Wound gap was photographed at 0 and 24 h at the same location. Images of areas were collected with a Canon Powershot digital camera coupled to the microscope and percentage of closure was calculated with NIH IMAGE J. These experiments were repeated at least three times.

### *Time-Lapse Microscopy*

Time-lapse microscopy (TLM) experiments were performed by using a video optical microscopy workstation which has been already described elsewhere (Dickinson RB, 1993). The images are captured by a cooled monochromatic CCD video camera. The samples were imaged every 10 min with a long working described above were carried out in the TLM experiments and cells motion was analyzed offline as described in the following.

### *Cell Tracking*

Image analysis of the scratch assay was performed by using a semi-automated Cell Tracking software. For each time step, about 40 cells on the wound edges were individually followed by manual overlaying each cell contour, and the coordinates of the contour points and of the cell centre of mass are stored on hard disk. To assist the operator in cell identification, the color-coded contour of each cell at the previous time step is also shown in the image overlay. From the centre of mass coordinates the trajectory of each cell was reconstructed for the whole experiment. Furthermore, average motility parameters of the cell population, such as velocity, were calculated as a function of time. The analysis of cell motility was based on the persistent random walk theory (Dickinson et al., 1994) (Matthes and Gruler, 1988), where it is assumed that cell motion is characterized by a diffusion coefficient (also referred to as the random motility coefficient) D ($\mu m^2$/min) and a persistent time P (min). According to the theory, the mean square displacements are given by the equation

$$< d^2(t) >= 4D\left[t - P\left(1 - e^{-t/P}\right)\right] \quad (1)$$

where <d2(t)> ($\mu m^2$) is the mean square displacement of the tracked cell sample at time t. The trend predicted by Eq. 1 is linear at t >>P (i.e., <d2(t)>≈4Dt), with a slope proportional to the diffusion coefficient. The mean square displacements are calculated from the following relation

$$< d^2(k) >= \sum_{i=1}^{N} \sum_{j=1}^{M-k} \left[ \left(x_i(j+k) - x_i(j)\right)^2 + \left(y_i(j+k) - y_i(j)\right)^2 \right] \quad (2)$$

where k is the current time expressed in units of the time interval $\Delta t$ between two consecutive image acquisitions, the double summation is on the index *i* representing cell

number (up to the total cell number N) and on index j representing the number of intervals (the total number being M-k), x and y are the centre of mass coordinates obtained by cell tracking. The mean square displacements are calculated from non-overlapping intervals (Dickinson et al., 1994). Eq. (1) was fit to the experimental data of mean square displacements (calculated from Eq. (2)) as a function of time with D and P as the only adjustable parameters.

## *Cytoplasmic spreading*

Fibroblasts were seeded at a density of $1\times10^4$ cells per well into the 12-well microplates coated with fibronectin (1 µg/well) or heat-denatured BSA, as a negative control. Then after 3 h, cells were gently washed with PBS and fixed in 4% formaldehyde for 15 min. After staining with 0.1% crystal violet, the cells were examined by microscopy. Five randomly chosen visual fields, representing approximately 15% of the dish surface area, were photographed and the number of cells was counted (at least 1000 cells). The cells were scored as either non-spreading or spreading, depending on whether the cell had obtained cytoplasm extensions.

## *Confocal microscopy*

Subconfluent cells on glass coverslips were fixed for 20 min with 4% paraformaldehyde (Sigma) in PBS containing 0.9mM calcium and 0.5mM magnesium (PBS CM) at room temperature, washed twice in 50mM NH4Cl in PBS CM and twice in PBS CM. Cells were permeabilized for 5 min in 0.5% Triton-X 100 (Bio-Rad) in PBS CM, washed twice, for 10 min, in 0.2% gelatin (Sigma) in PBS CM and then incubated for 1 h with the primary antibodies diluted in 0.5% BSA (Sigma) in PBS. After three washes with 0.2% gelatine, cells were incubated for 20 min with the appropriate rhodamine- or fluorescein-tagged goat anti-mouse or anti-rabbit secondary antibody (Jackson ImmunoResearch, West Grove,PA), diluted 1:50 in 0.5% BSA in PBS. After final washes with PBS, the coverslips were mounted on a microscope slide using a 50% solution of glycerol in PBS and examined with a Zeiss LSM 510 version 2.8 SP1 Confocal System.

### *In vivo wound healing and histological analysis*

TgPED and Wt control mice have been generated and characterized as described previously (Vigliotta et al., 2004). We used 16 eight month olds, sex and aged matched, TgPED and Wt mice littermates for each time point of the study. The animals were anesthetized with a single intraperitoneal injection of tribromoethanol (Avertin® 250 mg/kg body weight). The hair on the back of each mouse was cut and 2 full-thickness wounds (4 mm in from each edge, 2 cm in length) were made with scalpel (Braiman-Wiksman et al., 2007). Wounds from all animals were harvested at 3, 4 and 6 days after injury and used for histological analysis. Samples were fixed in 10% neutral buffered formalin and subsequently processed, blocked and sectioned perpendicularly to the wound surface in 5 µm consecutive sections. The slides obtained from the block were stained with haematoxylin-eosin (H&E) for morphometric analysis, with PicroSirius Red/Fast Green for differential staining of collagen during matrix production phase, and with anti-FGF-2 (sc-79, Santa Cruz Biotechnology) at 1:500 dilution for immunohistochemical-based quantification of fibroblast content. All stained samples were examined under digital and light microscope by at least two trained pathologists in blind. Fibroblast content and collagen fibers production/organization were evaluated using a semi-quantitative three point of range value. For the extracellular matrix production we attributed score 0 for absence of collagen production, score 1 and 2 for 10-40% and 40%-80% collagen fibers content compared to adjacent normal tissue respectively, and finally score 3 for wound matrix indistinguishable from adjacent normal tissue. To evaluate activated fibroblasts amount we attributed score 0 for no increase, score 1, 2 or 3 for little, moderate or high increase of fibroblasts activated content compared to adjacent tissue, respectively.

## RESULTS

### *PED/PEA-15 effect on scratch wound assay*

Wound closure was studied in cellular skin fibroblasts isolated from mice overexpressing PED/PEA-15 (TgPED) and control (Wt) mice. As expected, PED/PEA-15 protein abundance was about 10-fold higher in the fibroblasts of TgPED mice (Fig. 4.1). Confluent monolayers were scratched and images were taken at 0 and 24 hours after wounding (Fig. 4.2).

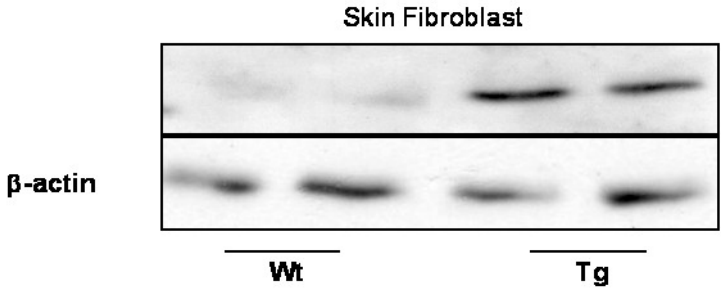


**Figure 4.1: PED/PEA 15 protein expression in skin fibroblasts isolated from TgPED and control (Wt) mice.**

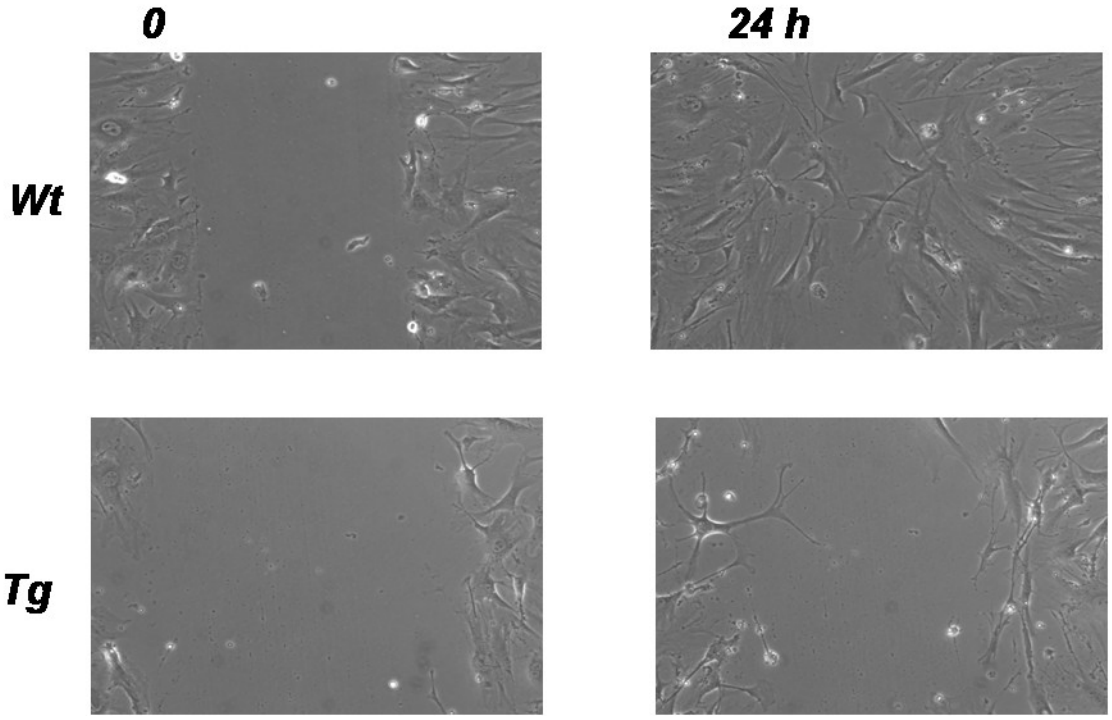


**Figure 4.2: Fibroblasts from TgPED mice and their Wt controls in the scratch assay at the beginning (0) and after 24h time-lapse experiment (24 h)**

The wound closure was significantly decreased in TgPED fibroblasts compared to controls (Fig. 4.3). To determine whether the effect of PED/PEA-15 was due to alteration of cell proliferation, scratch assays were also performed in the presence of 10 μg/ml mitomycin C, an irreversible inhibitor of mitosis. Pretreatment with mitomycin C decreased the wound closure rate in fibroblasts of both genotypes. However, the extent of closure of TgPED fibroblasts was still reduced compared to controls (Fig. 4.3). Moreover, no difference between Wt and TgPED fibroblasts was detected in thymidine incorporation experiments, suggesting that PED/PEA-15 effect on wound closure was not due to changes in cell proliferation.

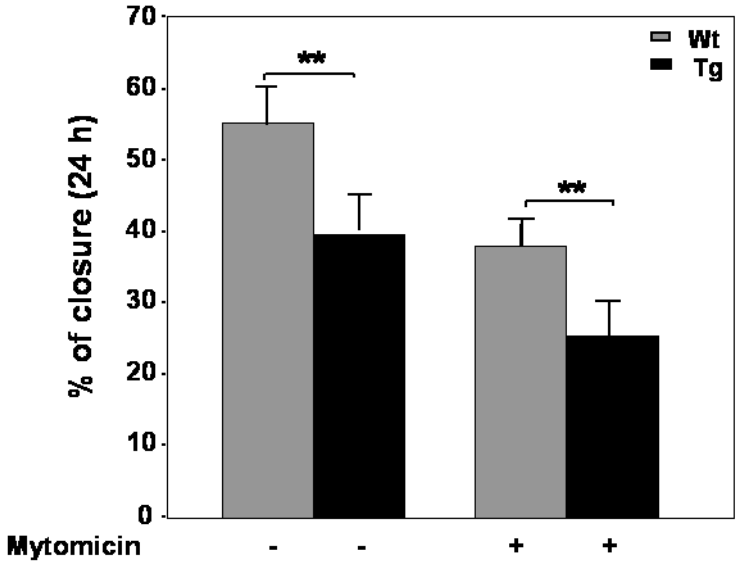


**Figure 4.3: Wound healing evaluation in cultured fibroblasts from TgPED and Wt mice in the absence or in the presence of Mitomycin C**

## *Direct evaluation of fibroblast motility by time-lapse microscopy (TLM)*

Fibroblast motility was then assessed by quantitative analysis of images acquired in TLM experiments following the scratch and images were recorded in TLM with a time interval of 10 min for 24 h. Wound closure was visually almost complete in 24 h for Wt cells, whereas TgPED fibroblasts were lagging behind. In agreement with the striking difference in wound closure rate, TgPED fibroblasts exhibited a significant lower average velocity,

(Table 1). Moreover, cell trajectories were reconstructed by the cell tracking image analysis. In both Wt (Fig. 4.4 A) and TgPED (Fig. 4.4 B) fibroblasts, the trajectories showed a random orientation being uniformly distributed in space (i.e., no preferential direction of motion can be distinguished). However, more extended cell trajectories were detected in Wt compared to TgPED fibroblasts (Fig. 4.4 A,B). The mean square displacements $<d^2(t)>$ of the two populations were calculated from the cell centers of mass at each time (see Eq. 2 in Material and Methods). The $<d^2(t)>$ values, which are representative of cell migration by random diffusion, were about 2-fold higher in Wt fibroblasts. Accordingly, the values of *D* (diffusion coefficient) and *P* (persistence time) were about 2-fold higher in Wt compared to TgPED fibroblasts (Table 1).

**A**

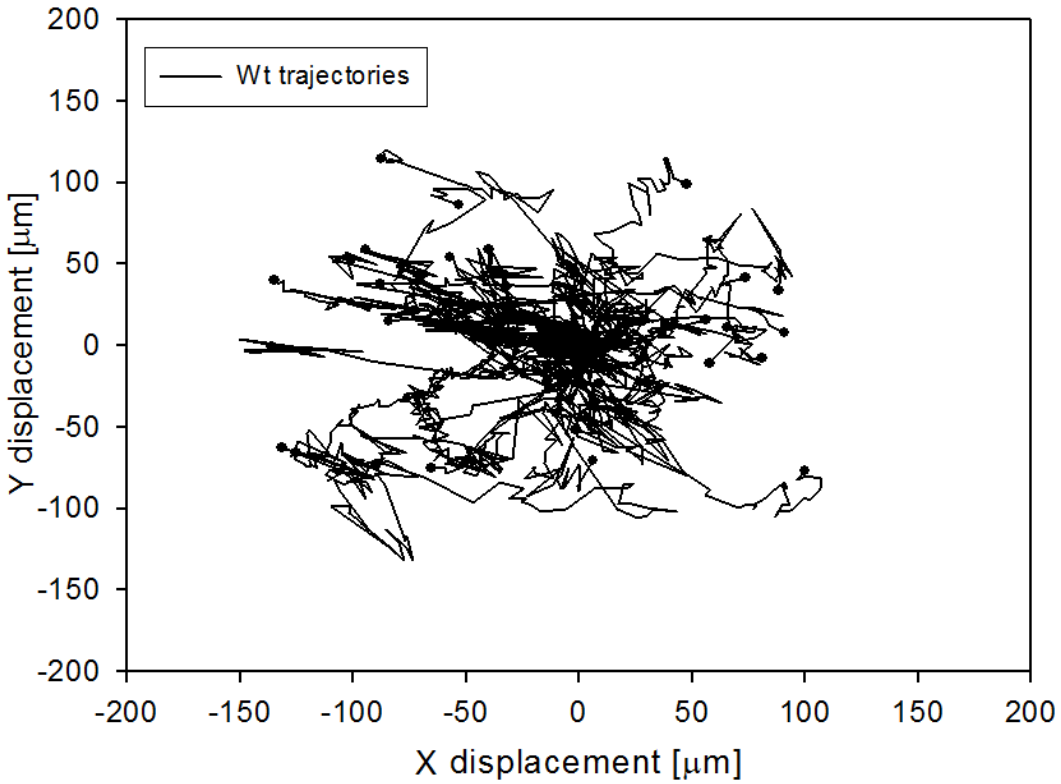

**B**

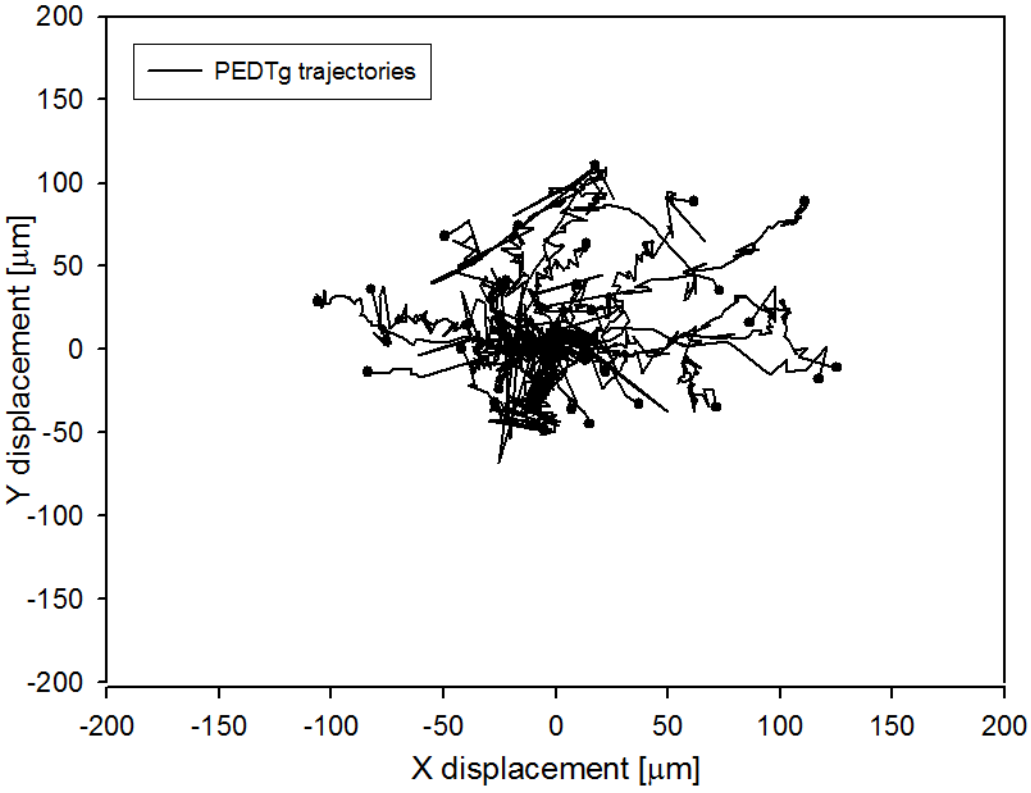


**Figure 4.4: Trajectories of fibroblasts isolated from A) Wt mice, B) PEDTg mice**

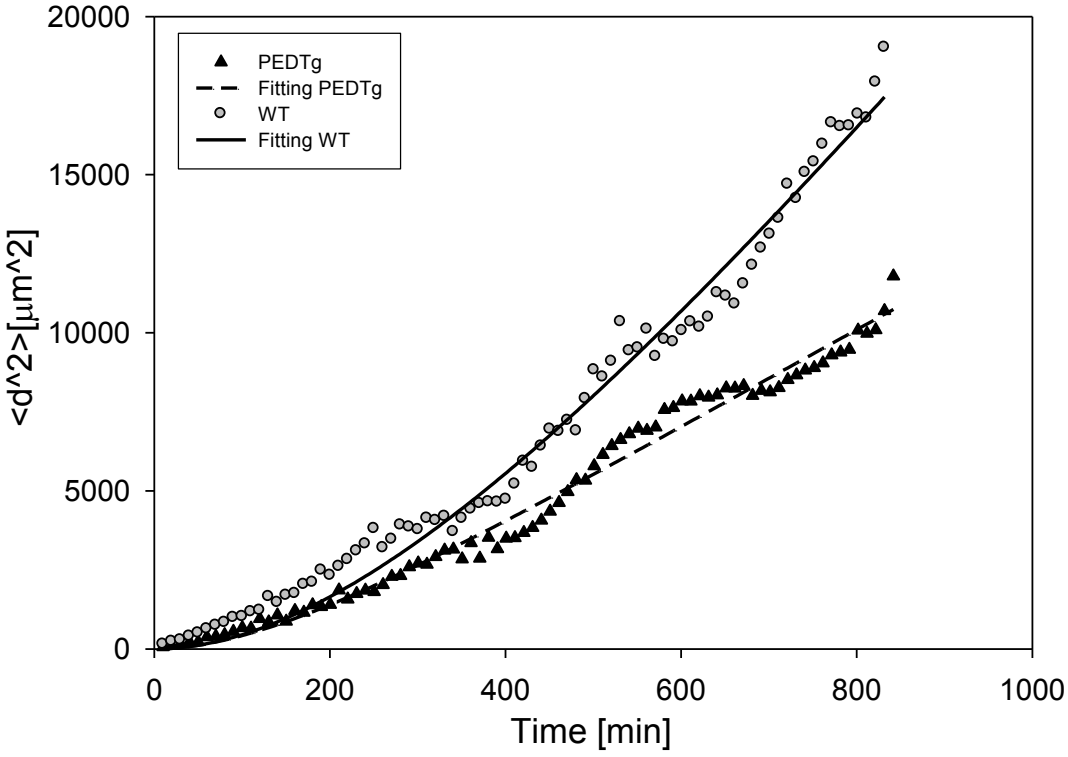


**Figure 4.5: Comparison of mean square displacements of Wt and PEDTg fibroblasts**

| Genotype | Velocity (μm/min) | D ($\mu m^2$/min) | P (min) |
|---|---|---|---|
| Wt | 0.9±0.08 | 8.3±2.7 | 332±75 |
| PED-Tg | 0.5±0.09 | 3.9±1.2 | 143±25 |

**Table 1: Assessment of motility parameters in fibroblasts from Wt and PEDTg mice.**

## *PED/PEA-15 effect on cell adhesion, spreading and cytoskeleton organization*

Fibroblast motility is dependent on cell ability to adhere to substrates and to transfer into the cytoplasm the signal that induces cytoskeleton reorganization (Arnaout et al., 2007; Chou et al., 2003; Ridley et al., 2003). TgPED fibroblasts showed no significant difference in adhesion compared to the controls (data not shown). We have then evaluated cytoplasmic spreading by staining with crystal violet. After 3 h plating on fibronectin, about 60% of Wt cells exhibited a spread cytoplasm, by contrast, the number of spread cells was about 30% for TgPED (Fig. 4.6 A). To analyze actin cytoskeleton organization and focal adhesion plaques, Wt and TgPED fibroblasts were stained with rhodamin-conjugated phalloidin or with specific anti-paxillin antibodies, respectively. Clearly, the results showed that TgPED fibroblasts displayed a marked decrease of stress fibres and focal adhesion plaques compared to controls (Fig. 4.6 B).

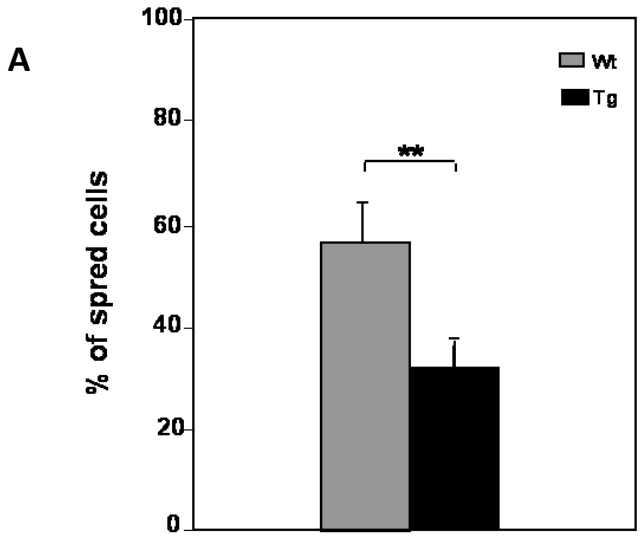

**B**

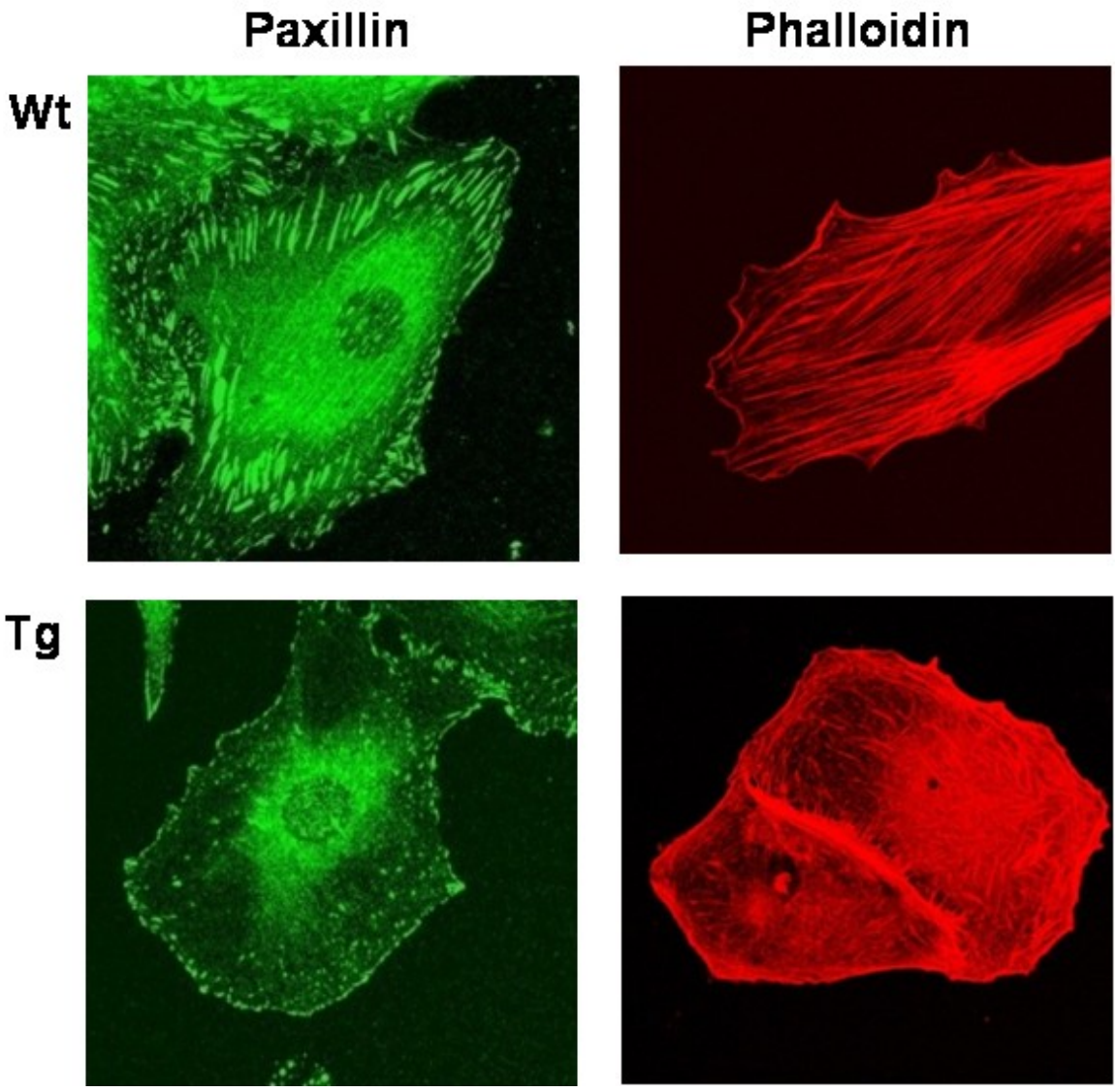


**Figure 4.6: A) Cytoplasmic spreading and B) cytoskeleton organization in Wt and TgPED fibroblasts.**

### *PED/PEA-15 depletion increased fibroblasts spreading and wound closure*

To further address the role of PED/PEA-15 in the regulation of cellular motility, we used fibroblasts from *ped/pea-15*–null mice. These animals have been previously characterized and reported (Miele et al., 2007) and feature no PED/PEA-15 expression in skin fibroblasts (data not shown). Importantly, after 3 h plating on fibronectin, cytoplasmic spreading was increased by about 30% compared to control cells (Fig. 4.7 A). Likewise, the wound closure

ability to recolonize the wounded area was also increased in *ped/pea-15*–null fibroblasts (Fig. 4.7 B). Furthermore, wound closure was almost complete already after 12 h in *ped/pea-15*–null fibroblasts, while it occurred after 24 h in control mice (Fig. 4.8).

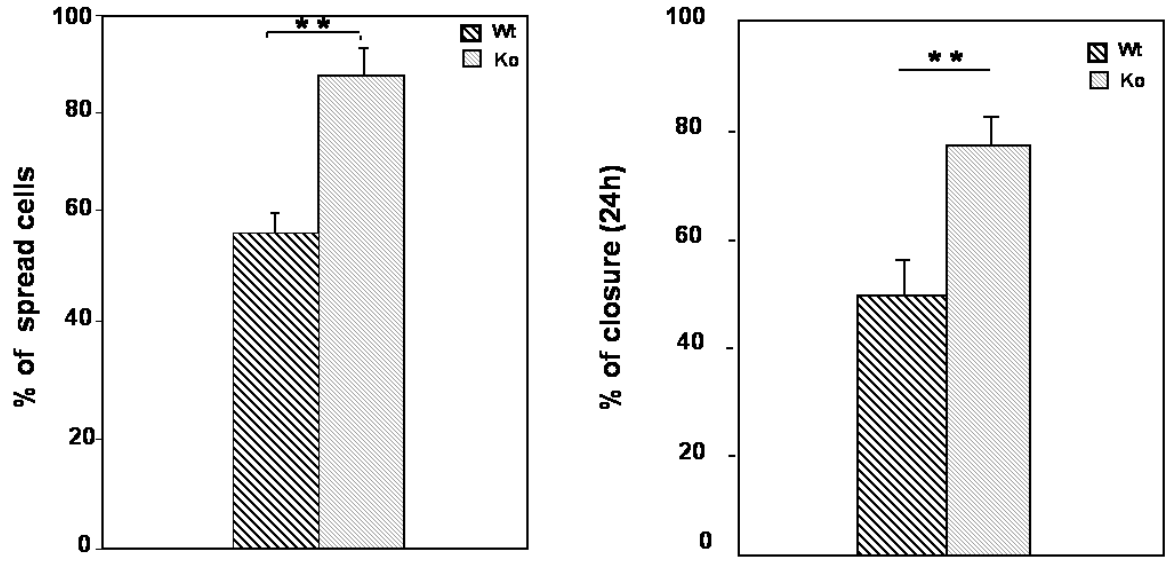


**Figure 4.7: Quantification of A) cytoplasmic spreading and B) in vitro wound healing in *ped/pea-15 null* fibroblasts**

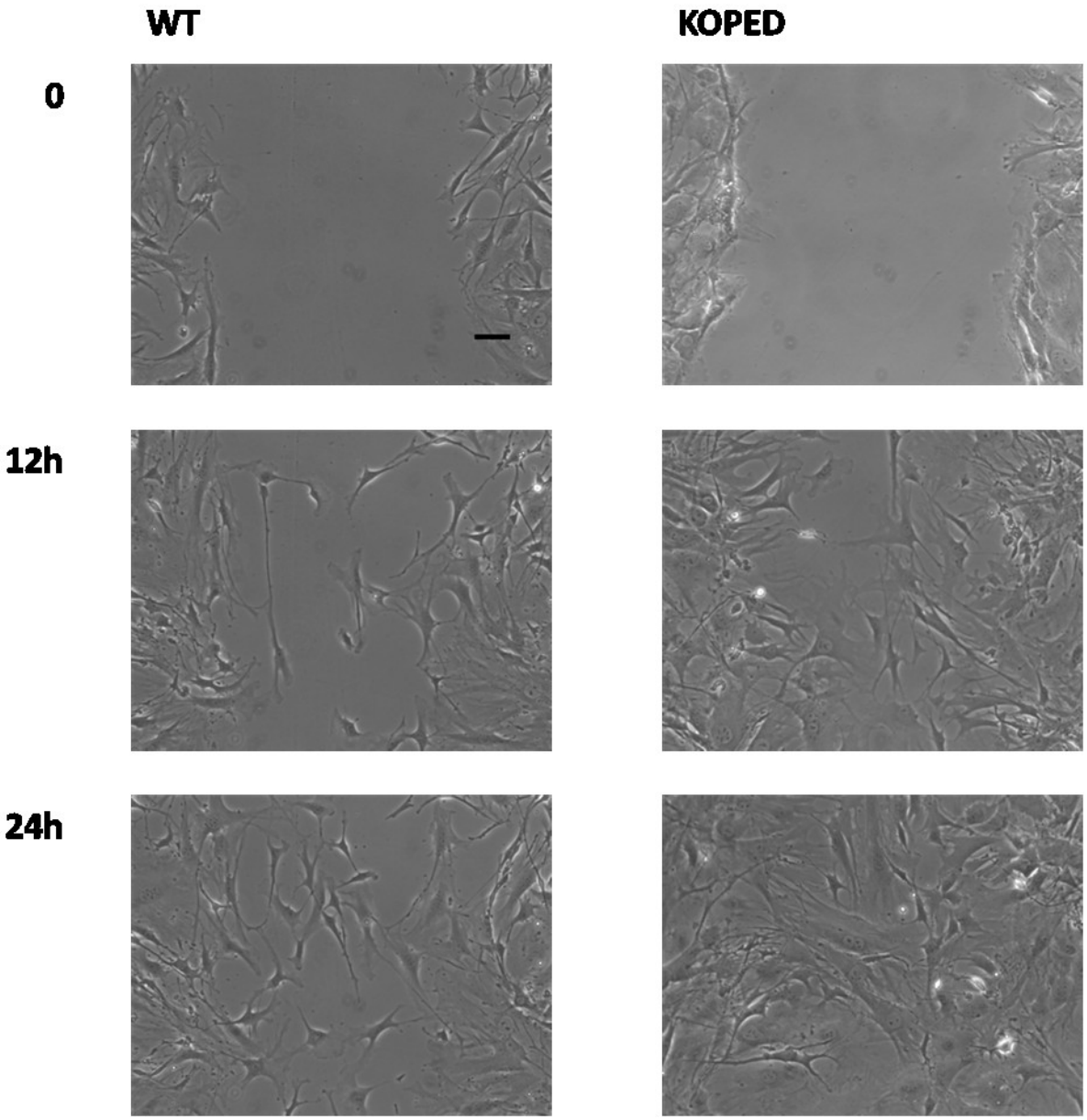


**Figure 4.8: Fibroblasts from KOPED mice and their Wt controls in the scratch assay at the beginning (0) and after 12h (16h) and 24 h time-lapse experiment (24 h)**

## *PED/PEA-15 effect on wound healing in vivo*

In order to assess whether PED/PEA-15 may also affect fibroblast motility *in vivo*, we examined wound healing in TgPED and in Wt mice. Interestingly, histological exam of the wounded skin at 72 h and 96 h after a dorsal incision, revealed a significantly reduced number of activated fibroblasts and a comparable reduction of collagen fibres production in the TgPED specimens compared to those observed in the Wt (Table 2 and 3), while no significant difference was observed in the adjacent normal skin. Moreover, the distance

between the wound edges was 3- and 2-fold higher, respectively, in TgPED compared to Wt mice (data not shown). Also, after 6 days, a complete closure of the wound was observed in all Wt while not in TgPED mice.

| Genotype | Activated fibroblasts content | Collagen fibres production |
|---|---|---|
| Wt | 1.3±0.5 | 1.2±1 |
| PED-Tg | 0.4±0.4<br>(p>0,01) | 0.4±0.75<br>(p>0,01) |

**Table 2: Assessment of wound healing parameters in Wt and PEDTg mice after 3 days**

| Genotype | Activated fibroblasts content | Collagen fibres production |
|---|---|---|
| Wt | 1.6±1 | 1.4±0.7 |
| PED-Tg | 0.9±1<br>(p>0,01) | 0.6±0.9<br>(p>0,001) |

**Table 3: Assessment of wound healing parameters in Wt and PEDTg mice after 4 days**

## DISCUSSION

Cell migration is an essential process important not only during development, but also in wound repair. Interestingly, tissue repair results largely inefficient in patients with diabetes mellitus (Baum and Arpey, 2005; Terranova, 1991). Nevertheless, the molecular mechanisms involved in wound closure alterations in diabetes are not well understood. Ped/pea-15 overexpression represents a common feature in skeletal muscle and adipose tissues from individuals with type 2 diabetes (Condorelli et al., 2001; Valentino et al., 2006). Moreover transgenic mice overexpressing *ped/pea-15* (TgPED) to levels comparable to those occurring in type 2 diabetes patients, present mildly elevated random-fed blood glucose levels and become diabetic when the body weight increases through administration of high-fat diets. Moreover, they are much more insulin resistant than their Wt littermates (Vigliotta et al., 2004). TgPED mice are markedly hyperinsulinemic in the basal state and also show reduced insulin response to a glucose challenge, indicating that the overexpression of *ped/pea-15* impairs both insulin action and insulin secretion (Vigliotta et al., 2004). This work shows that overexpression of *ped/pea-15* affects wound closure rate in cultured primary fibroblasts from TgPED mice. TgPED fibroblasts displayed reduced average velocities compared to Wt and their trajectories were much shorter than those of Wt fibroblasts. Cell interaction with the ECM components is crucial for adhesion and migration and is mediated by various receptors, including integrins (Raftopoulou and Hall, 2004). These proteins provide a transmembrane link between the ECM and the cytoskeleton, activating intracellular signalling processes (Raftopoulou and Hall, 2004). By analysing cell adhesion we found no difference betwen TgPED and Wt fibroblasts (data not shown). At variance, TgPED fibroblast spreading, focal adhesion plaques and actin stress fibres formation were reduced. Thus, wound closure, spreading and cytoskeleton organization are deregulated in fibroblasts overexpressing PED/PEA-15. Interestingly, fibroblasts isolated from *ped/pea-15*–null mice show an increased ability to recolonize wounded area after a scratch and an increased spreading compared to control cells. These results strongly support a role of PED/PEA-15 in the regulation of cell motility. Moreover, the control exerted by PED/PEA-15 on cell migration is not restricted to fibroblasts, as it was already shown that PED/PEA-15 controls astrocytes motility (Renault-Mihara et al., 2006). Finally, the histological analysis of TgPED wounded skin showed a remarkable reduction in activated fibroblasts and in collagen fibre

content. TgPED mice present also a significant delay in skin repair. These data suggest that PED/PEA-15 is able to impair fibroblast functions, also *in vivo*. Considering the different known cellular function of PED/PEA-15 in a chronic disorder such as diabetes (Condorelli et al., 2001; Valentino et al., 2006; Vigliotta et al., 2004), the observation that PED/PEA-15 regulates cellular motility may have a significant impact on future investigation of its role in diabetic complications.

# CHAPTER 5

# TWO-PHOTON LASER GENERATED MICROTRACKS IN 3D COLLAGEN LATTICES: PRINCIPLES OF MMP-DEPENDENT AND -INDEPENDENT COLLECTIVE CANCER CELL INVASION

## INTRODUCTION

Cell migration in vivo is a complex process defined by determinants of both the cell and the tissue environment on or through which the cell migrates. In interstitial migration through 3D ECM, important physical ECM determinants of cell movement include the degree of ECM alignment, the width of pores present therein, and the ECM stiffness (Egeblad M, in press; Erler and Weaver, 2009; Friedl and Wolf, 2010). Thereby, the ECM provides both, a physical scaffold for cell adhesion and migratory guidance but also a physical barrier which, if sufficiently dense, hinders or prevents cell movement (Hotary et al., 2003; Wolf et al., 2007). In vivo interstitial ECM is heterogeneous in composition, density and organization. It comprises regions of high density with tightly packed collagen fibres and loose regions composed of random collagen fibres resulting in variable gap diameters and clefts (Condeelis and Segall, 2003b; Provenzano et al., 2008b; Wolf et al., 2009). Both the degree of alignment and density of 3D ECM directly impacts molecular mechanisms of cell migration, particularly the engagement of integrins and the requirement for pericellular proteolysis (Friedl and Wolf, 2010; Ruiter et al., 2002). ECM density and the space provided by pores therein determine the physical space available for moving individual cells or cell groups (Friedl and Wolf, 2010), and determines the speed and persistence of migration (Ghajar *et al.*, 2008). In vivo loose and randomly organized connective tissue favours single cell dissemination of amoeboid breast cancer cells (Brown *et al.*, 2003; Kedrin *et al.*, 2008); conversely regions of highly aligned collagen bundles in the deep mouse dermis support cell collective invasion in fibrosarcoma xenografts (Alexander *et al.*, 2008). In vitro, collective invasion into dense collagen lattices requires localized cell-mediated pericellular proteolysis and ECM realignment resulting in elongated gaps and tracks of least resistance (Wolf *et al.*, 2007). The major cell surface collagenase controlling type I collagen degradation is MT1-MMP/MMP14 (Sabeh *et al.*, 2004) and consequently rate-limiting for collective invasion into

3D collagen lattices in vitro (Wolf *et al.*, 2007). However, when and under which ECM conditions pericellular proteolysis is required for cancer cell invasion is controversial, based on divergent results from different labs using different collagen matrix substrates in vitro (Hotary *et al.*, 2003; Provenzano *et al.*, 2008b; Wolf *et al.*, 2003) and in vivo (Wyckoff *et al.*, 2006). Thus, the physical determinants of the ECM structure to either support, mechanically impede or arrest cell migration in vitro and in vivo remain to be determined. Different in vitro collagen-based cell invasion models consisting of 3D collagen lattices after re-assembly of monomeric collagen mimic the structure of connective tissue in vivo to varying degree (Wolf *et al.*, 2009). In most cases, in vitro reconstituted fibrillar collagen provides porosity as well as barrier function, similar to loose connective tissue in vivo, but they lack well-controlled spatial characteristics because smaller and larger pores form as part of a stochastic polymerization process which fails to recreate defined in vivo-like trails (Egeblad et al., 2010; Provenzano et al., 2008a; Wolf et al., 2009). Consequently, to create well-defined physical models for cell migration through collagen-based 3D environments, random fibrillar matrix polymerization needs to be combined with procedures to generate predefined tracks that mimic particular patterns of connective tissue organization. We here show how two-photon excited laser microsurgery can be used to generate physical tracks in 3D collagen matrices of defined width and length. The resulting micro- and macropatterned lattices were used to address the conditions for MMP-dependent and -independent collective migration of invasive cancer cells.

## MATERIALS AND METHODS

### *Cell culture and reagents*

Dual-colour mouse mammary tumour cells (MMT) that express cytoplasmic DsRed2 and nuclear EGFP coupled to histone 2B (Tsuji *et al.*, 2006) were maintained in RPMI 1640 growth medium (Invitrogen) supplemented with 10% FCS (Sigma), penicillin and streptomycin (each 50 U/ml) (PromoCell) in a humidified incubator at 37 °C in 5% $CO_2$. The function of MMPs was inhibited with the broad-spectrum inhibitor GM6001 (final concentration: 20 µM) (Chemicon).

### *3D spheroid culture*

Cells from subconfluent cultures were detached with 2mM EDTA, and multicellular spheroids were generated using the hanging-drop method (Korff and Augustin, 1998). In brief, cells were re-suspended in RPMI 1640 growth medium supplemented with 10% methylcellulose, and incubated in 25 µl droplets overnight. After cell aggregation, spheroids were washed in PBS and incorporated into 3D type I collagen lattices consisting of non-pepsinized rat-tail collagen (final concentration: 6 mg/ml; BD Biosciences) which correspond to dense ECM regions of in vivo interstitial matrix (Wolf *et al.*, 2009).

### *Two-photon laser microsurgery*

Generation of microtracks ablated from fibrillar collagen within 3D collagen lattices was performed using two-photon excitation at 830 nm with a Ti:Sapphire laser (Chemeleon XR, Coherent) on an upright microscope stage (LaVision BioTec) using a 20x NA 0.95 water-immersion objective ( Olympus) and a focal power of 400 mW. Regions of interest of 150 µm in length and variable widths and depths were positioned directly adjacent to the edge of multicellular spheroids before the onset of invasion. Following microtrack generation spheroid-containing lattices were maintained at 37°C and monitored for growth and invasion activity for up to 48 h. At the end-point, cultures were fixed (4% paraformaldehyde, room temperature, 30 min) and reconstructed by confocal microscopy (Olympus FV100), using confocal reflection for visualizing collagen fibres.

### *Time-lapse microscopy and image analysis*

Migration of MMT cells into collagen-ablated microtracks was monitored for 48 h using time-lapse two-photon microscopy. Images were acquired every 15 min at 830 nm excitation wavelength allowing the simultaneous visualization of DsRed2, EGFP and second harmonic generation (SHG), as described (Friedl *et al.*, 2007). Z-stacks were obtained with a step-size of 5 µm. Image processing and 3D reconstruction was obtained using the ImageJ (1.40v; W. Rasband, NIH) or ImSpector 3.4 (LaVision BioTec) software.

## RISULTS

### *Two-photon laser microsurgery to generate microtracks in 3D collagen lattices*

To mimic naturally occurring clefts and tracks within connective tissue in vivo, microtracks forming trails of least resistance within 3D collagen matrices were generated by two-photon laser ablation and used for studying cell migration along barrier-free interfaces. Regions of interest were defined and ablated using a power density of 400 mW, resulting in rectangular 3D tracks devoid of collagen structures (Fig. 1A, B). Scanning at higher laser intensities resulted in cell damage and poorly defined edges of the microtracks, consistent with out-of focus energy absorbtion and overshoot-vaporization. Lower laser power was not sufficient to reliably ablate the collagen fibres and form defined microchanels (data not shown). To vary geometry, microtracks were created with constant length (150 µm) but varying widths and depths (3 to 30 µm in both x and z directions) (Fig. 1C). The channels showed precise medium-collagen interfaces and were largely free of inner debris or partially degraded collagen fibres (Fig. 1B), thus representing a highly defined model of 3D tracks with a physiological substrate as a border to support cell adhesion and guided migration.

**A** **B**

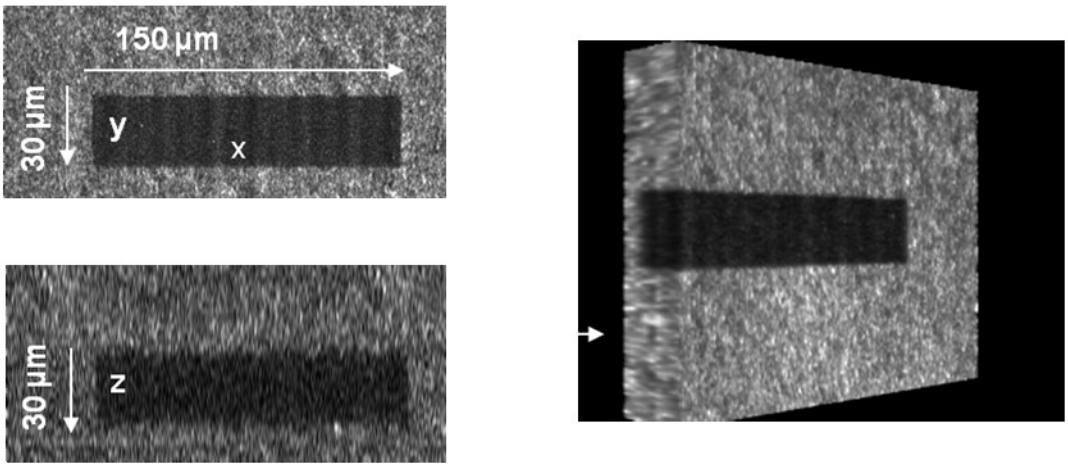

C

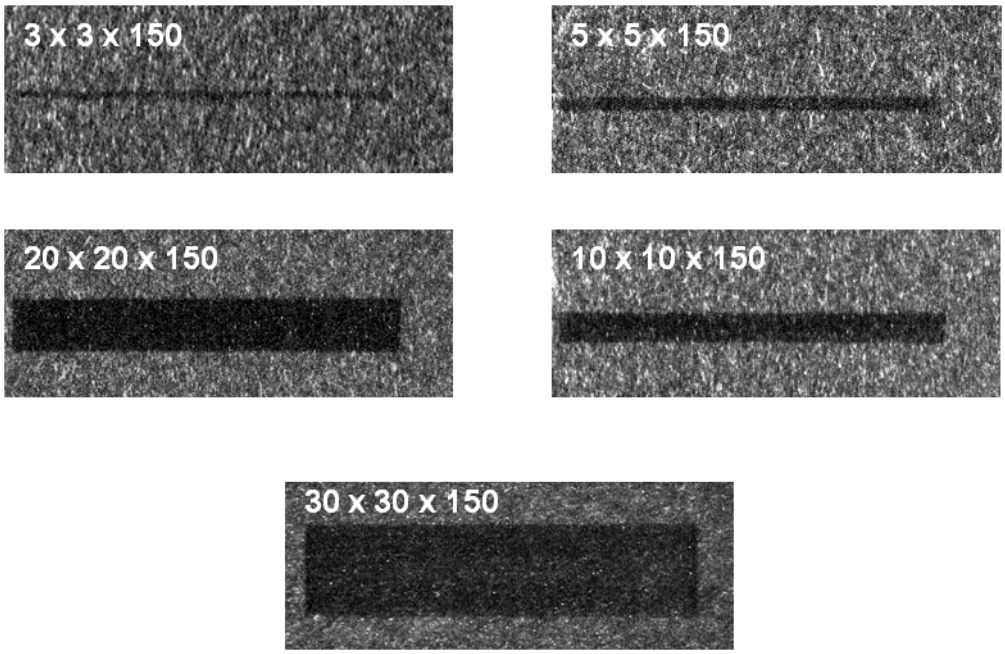


**Figure 1: Microtracks in collagen lattices A) in x and z direction and B) its 3D reconstruction. C) Microtracks with varying widths and depths.**

## *Cancer cells migrate collectively into collagen-ablated microtracks*

The physical structure of ECM has been shown to influence greatly the efficiency of cancer cell invasion (Harley *et al.*, 2008) and requirements for pericellular proteolysis (Friedl and Wolf, 2010; Gaggioli et al., 2007; Wolf et al., 2007). Using dense collagen substrate in combination with the highly space-controlled microtracks as physiological substrate, we tested whether collective cell migration into collagen-ablated microtracks within 3D collagen matrix requires MMP-dependent pericellular proteolysis. Multicellular spheroids of invasive MMT cells expressing cytoplasmic DsRed2 and nuclear H2B/EGFP were embedded within 3D collagen lattices , and subsequently two-photon excited ablation of tracks was performed adjacent to the spheroid-collagen matrix interface (Fig. 2A). In untreated control cultures, MMT cells invaded spontaneously as multicellular strands into the collagen matrix along preformed microtracks (Fig. 2A, numbers) as well as secondary invasion zones de-novo generated by the cells themselves (Fig. 2A, arrowheads), similar to invasive HT-1080 fibrosarcoma cells (Friedl and Wolf, 2008; Wolf et al., 2007). In track-free collagen lattices, all invasion activity was ablated by the broad-spectrum MMP inhibitor GM6001 (20 µM) whereas growth of spheroids remained undiminished (Fig. 2B, C), consistent with the abrogation of MMP-dependent *de novo* track generation but uncompromised cell viability in

the presence of GM6001. Thus, for penetrating dense collagen matrix which provides stringent physical resistance, MMT cells require MMP function for collective invasion, as described (Friedl and Wolf, 2008). However, in the presence of microtracks at a track calibre that exceeds the single-cell diameter (15 to 20 µm), MMT cells maintained vigorous collective invasion despite the presence of GM6001 but lacked the capability to form secondary de novo tracks (Fig. 2B). Subsequent to the first cell, multiple cells followed in an MMP-independent manner thereafter using the track edge for migratory guidance until the lumen of the microtrack was filled completely (Fig. 2D). Thus, collective invasion along barrier-free interfaces with space that corresponds to or exceeds the cell diameter does not require proteolytic degradation of ECM structures.

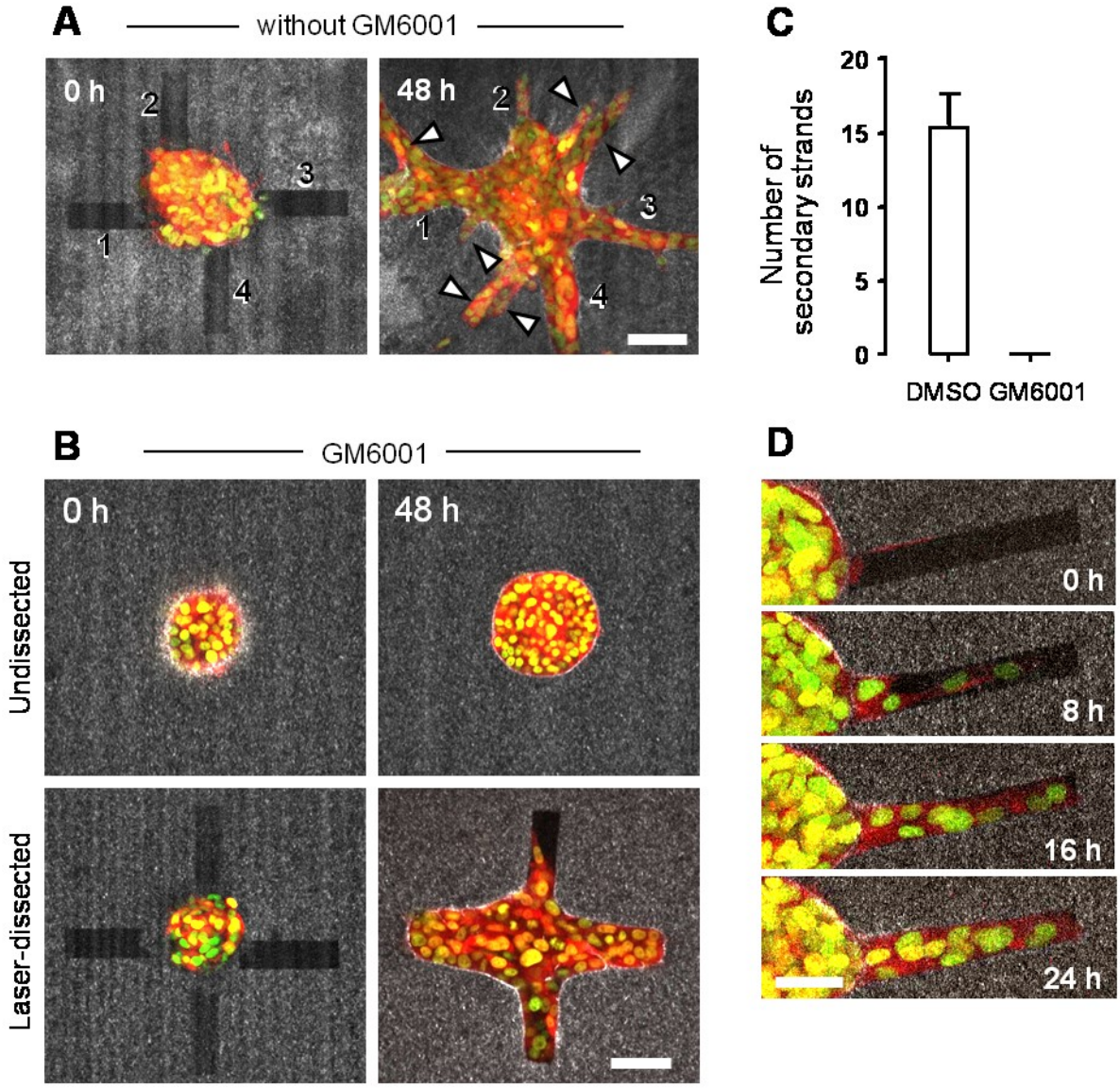


**Figure 2: Collective cell migration along preformed microtracks in collagen matrix and effect of MMP inhibition on invasion activity**

### *MMP-independent collective migration into narrow microtracks*

In vivo invasion of cancer cells occurs within ECM of varying structure and pore size (Egeblad et al., 2010; Provenzano et al., 2008a; Wolf et al., 2009). To test the track dimensions permissive for collective invasion and to further approach the minimum gap size supporting non-proteolytic invasion, the dimensions of microtracks were reduced to the technical minimum of a single-line scan which resulted in tracks measuring approximately 3 x 3 µm (Fig. 3A) thus exceeding the lateral point spread function by factor 4 and the vertical by factor 2 (Andresen *et al.*, 2009). Despite their cell diameter of 15 to 20 µm and the presence of GM6001, MMT cells were able to migrate into microtracks of all tested dimensions (Fig. 3A, B). As mechanism in all conditions, collagen-ablated microtracks were laterally enlarged by invading cell strands, probably by physical pressure on collagen by moving cell strands, so that resulting tracks matched the diameter of single cells or multicellular strands (Fig. 3A, B). In 3 µm microtracks, the morphology of cells and cytoplasm adopted a cylinder-like shape and cells arranged as single cell chain-like files, consistent with substantial cell deformation and squeezing in the absence of pericellular proteolysis to accommodate the available space (Fig. 3A, insets). Thus, collective invasion is an adaptive process the protease-requirements of which are defined by the geometry of pre-existing tracks of least resistance, ECM elasticity allowing track widening by cell-mediated pressure, and the deformability of the cell body.

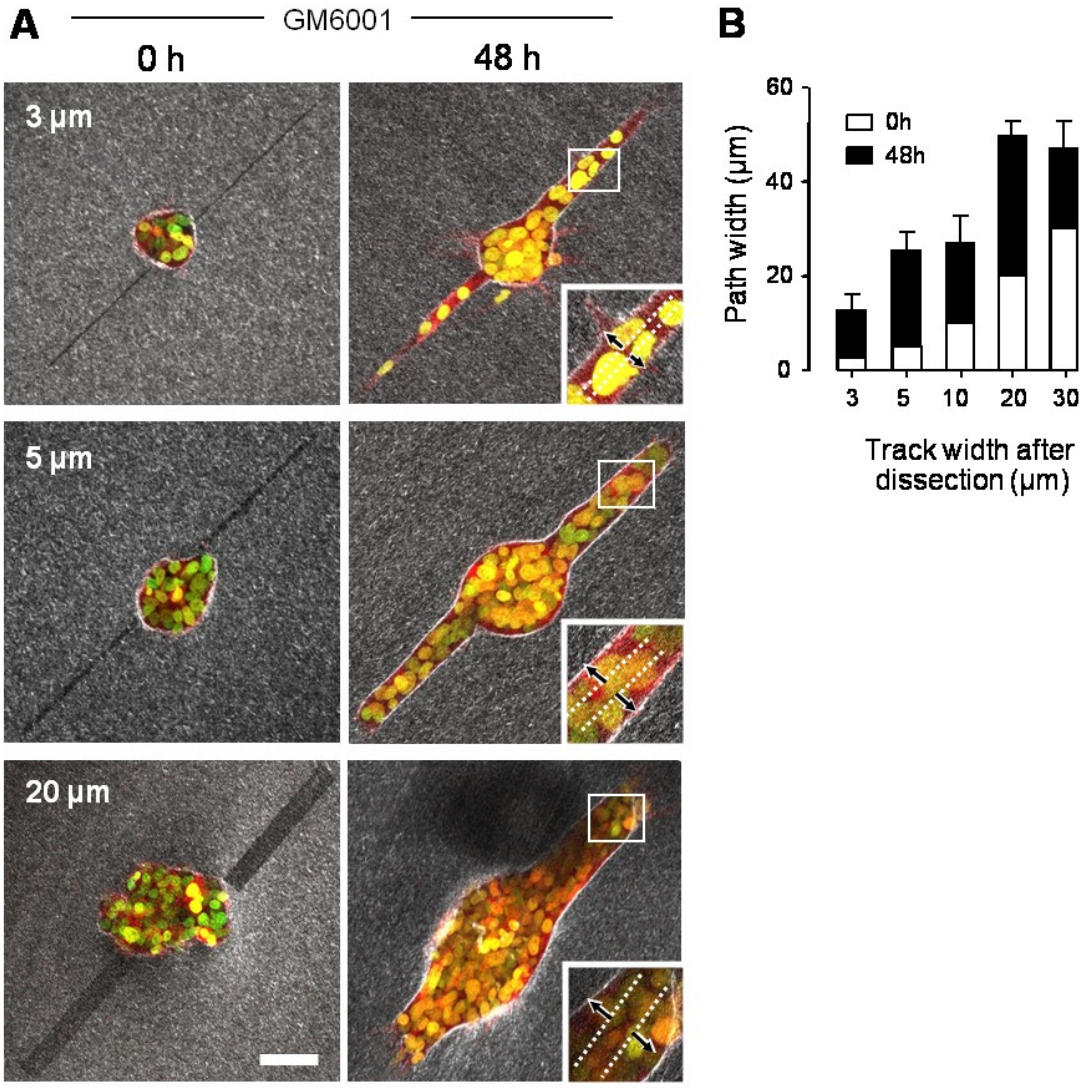


**Figure 3: Collective migration MMP independent in different size microtracks**

## DISCUSSION

Two-photon laser dissection allows to generate micro- or macro-patterned matrices of defined dimensions to study matrix guiding mechanisms of cell invasion in a physiological substrate, here 3D fibrillar collagen. Established 3D collagen-based models to study mechanisms cell invasion in vitro provide cells with physiological substrate for attachment and migration and recapitulate randomly or partially aligned matrix organization (Wolf *et al.*, 2009), yet fail to recapitulate aligned clefts and gaps of different calibre present in many connective tissues (Alexander et al., 2008; Friedl and Wolf, 2009a; Provenzano et al., 2008a). Substantial recent progress has provided micropatterned surfaces to for directing cell migration along biomolecules gradients (DeLong *et al.*, 2005; Lee *et al.*, 2008; Luo and Shoichet, 2004), pre-defined microtracks (Falconnet *et al.*, 2006; Sarig-Nadir *et al.*, 2009) , or artificial 3D substrates, i.e. polyethylene glycol (PEG) hydrogels as substrate (Bott *et al.*, 2010). Although these studies demonstrate spatial control of cell migration and implicate ECM structures in guiding cell directionality, but they do not fully recapitulate guidance principles by microtracks and trails that surround the cells three-dimensionally. Micropatterned collagen gels using microscale cavities (Nelson *et al.*, 2008; Raghavan *et al.*, 2010) are suited to construct 3D cavities with defined geometry into which cells are positioned, yet they do not generate cell-free tracks inside the matrix that the cells can use for individual and/or collective migration. The use of two-photon laser ablation of fibrillar type I collagen, which is a physiological in vivo-like substrate for cell attachment, is suited to position collagen-free tracks of defined geometry directly adjacent to cells and cell spheroids to be readily used for cell migration and secondary remodeling. The excitation wavelength of 830 nm at 400 mW focal power using a 20x 0.95 NA objective allows to ablate collagen fibres precisely with minimum of remaining debris down to a smallest caliber 3 µm in lateral and vertical directions. As down-side, the resulting tracks exceed the technical resolution of the system (approx. 500 nm lateral and 1.5 µm vertical resolution) and indicates heat-induced destruction of collagen fibers beyond the focal volume of the laser by factor 2 to 4. To further reduce the track caliber, an objective lens with higher numerical aperture combined with an excitation wave length in the visible range and/or altered laser pulse duration might be useful. The laser ablation approach may be amenable to other 3D fibrillar tissue scaffolds, such as fibrin or polyethylen glycol lattices and further

may be used to generate more complex track structures of varying width, direction and bifurcations for studying tissue-guided biophysics of cell migration. Several secreted MMPs, including MMP-1, MMP-2 and MMP-13, are effective collagenases, however for invasive cell migration through native fibrillar collagen, MT1-MMP is a rate-limiting protease the inhibition of which is not compensated by other proteases (Sabeh *et al.*, 2004). MT1-MMP has a key function in the generation of micro- and macrotracks generated by cancer cells themselves (Wolf *et al.*, 2007) or stromal cells (Gaggioli *et al.*, 2007) which are permissive for the formation of collective invasion strands through these tunnel-like trails (Friedl and Wolf, 2008). Consistent with MMP-dependent collagen remodelling, spontaneous invasion of MMT cells into dense 3D collagen matrices with laser-generated macrotracks consisted of two components, (i) the invasion into the preformed trails which were completely filled within few hours, and (ii) the secondary penetration of matrix within cell-derived tracks. Whereas the cell-derived track generation was abrogated by broad-spectrum MMP inhibition, migration into preformed microtracks persisted, which provides direct evidence that collective invasion is dependent on sufficient space available in the tissue matrix to accommodate the volume of the cell strand (Friedl and Wolf, 2008). In vivo, different ECM regions provide gaps and trails similar to those generated here by laser ablation. Matrix MMP-independent collective migration could occur in physiological clefts between tightly packed collagen bundles or along pro-invasive structure, such as blood or lymphatic vessels and muscle strands (Alexander *et al.*, 2008) which may represent preferential tracks of least resistance. The mechanisms supporting non-proteolytic migration into laser-ablated tracks comprise two synergistic processes, (i) contact guidance supporting cell alignment and movement along the edge of the track (Condeelis and Segall, 2003b; Gauvreau and Laroche, 2005; Jiang et al., 2005) and (ii) nonproteolytic movement of the cell-matrix interface resulting in secondary track widening, presumably by a pushing mechanism against an elastic fibrillar ECM network. Both, micro- and macrotracks which range below or exceed the respective cell diameter underwent secondary diameter widening by factor 2 to 3, suggesting an adaptive pressure-driven process to adjust to geometry of ECM as far as matrix elasticity permits. Besides widening the space to support cell migration, cell-derived compression of fibrillar tissue may lead to scaffold condensation, increase ECM tension and density, and further act as diffusion barrier (Davies Cde *et al.*, 2002). Although the current setting did not permit to directly measure the pressure forces exerted by the cells for

secondary track enlargement, cell-induced tissue pressure may contribute to increased hydrostatic tissue pressure in tumors caused by defective blood vessels (Fukumura et al., 2010; Fukumura and Jain, 2007; Vakoc et al., 2009) and ECM stiffness caused by proteolytic long-term remodelling and condensation of the ECM structure (Egeblad et al., 2010; Provenzano et al., 2006; Provenzano et al., 2008a; Provenzano et al., 2008b). It is unclear to which extent the tissue elasticity in vivo allows such cell-pressure induced tissue deformation, yet the histological sections of concentrically growing primary tumors and metastases suggest a high degree of tumor-induced pressure on the interstitial ECM structure (Pluen *et al.*, 2001). In conclusion, the 3D microtrack model allows to generate defined trails of least resistance to provide new insight into the physical principles of single-cell and collective cell migration.

## BIBLIOGRAPHY


Adams, J. (2001). Cell-matrix contact structures. Cell Mol Life Sci *58*, 371-392.

Affolter, M., and Weijer, C. (2005). Signaling to cytoskeletal dynamics during chemotaxis. Dev Cell *9*, 19-34.

Alexander, S., Koehl, G.E., Hirschberg, M., Geissler, E.K., and Friedl, P. (2008). Dynamic imaging of cancer growth and invasion: a modified skin-fold chamber model. Histochem Cell Biol *130*, 1147-1154.

Andresen, V., Alexander, S., Heupel, W.M., Hirschberg, M., Hoffman, R.M., and Friedl, P. (2009). Infrared multiphoton microscopy: subcellular-resolved deep tissue imaging. Curr Opin Biotechnol *20*, 54-62.

Arnaout, M., Goodman, S., and Xiong, J. (2007). Structure and mechanics of integrin-based cell adhesion. Curr Opin Cell Biol *19*, 495-507.

Association, A.D. (2003). Peripheral arterial disease in people with diabetes. Diabetes Care *26*, 3333-3341.

Baggiolini, M., and Loetscher, P. (2000). Chemokines in inflammation and immunity. Immunol Today *21*, 418-420.

Baggiolini, M., Walz, A., and Kunkel, S. (1989). Neutrophil-activating peptide-1/interleukin 8, a novel cytokine that activates neutrophils. J Clin Invest *84*, 1045-1049.

Balough, K., McCubbin, M., Weinberger, M., Smits, W., Ahrens, R., and Fick, R. (1995). The relationship between infection and inflammation in the early stages of lung disease from cystic fibrosis. Pediatr Pulmonol *20*, 63-70.

Bals, R., Weiner, D., and Wilson, J. (1999). The innate immune system in cystic fibrosis lung disease. J Clin Invest *103*, 303-307.

Bamburg, J., McGough, A., and Ono, S. (1999). Putting a new twist on actin: ADF/cofilins modulate actin dynamics. Trends Cell Biol *9*, 364-370.

Baum, C., and Arpey, C. (2005). Normal cutaneous wound healing: clinical correlation with cellular and molecular events. Dermatol Surg *31*, 674-686; discussion 686.

Bear, J., Loureiro, J., Libova, I., Fässler, R., Wehland, J., and Gertler, F. (2000). Negative regulation of fibroblast motility by Ena/VASP proteins. Cell *101*, 717-728.

Bear, J., Svitkina, T., Krause, M., Schafer, D., Loureiro, J., Strasser, G., Maly, I., Chaga, O., Cooper, J., Borisy, G.*, et al.* (2002). Antagonism between Ena/VASP proteins and actin filament capping regulates fibroblast motility. Cell *109*, 509-521.

Bonfield, T., Panuska, J., Konstan, M., Hilliard, K., Hilliard, J., Ghnaim, H., and Berger, M. (1995). Inflammatory cytokines in cystic fibrosis lungs. Am J Respir Crit Care Med *152*, 2111-2118.

Bott, K., Upton, Z., Schrobback, K., Ehrbar, M., Hubbell, J.A., Lutolf, M.P., and Rizzi, S.C. (2010). The effect of matrix characteristics on fibroblast proliferation in 3D gels. Biomaterials.

BOYDEN, S. (1962). The chemotactic effect of mixtures of antibody and antigen on polymorphonuclear leucocytes. J Exp Med *115*, 453-466.

Braiman-Wiksman, L., Solomonik, I., Spira, R., and Tennenbaum, T. (2007). Novel insights into wound healing sequence of events. Toxicol Pathol *35*, 767-779.

Bretscher, M. (1996). Getting membrane flow and the cytoskeleton to cooperate in moving cells. Cell *87*, 601-606.

Brown, E., McKee, T., diTomaso, E., Pluen, A., Seed, B., Boucher, Y., and Jain, R.K. (2003). Dynamic imaging of collagen and its modulation in tumors in vivo using second-harmonic generation. Nat Med *9*, 796-800.

Böttcher, R., and Niehrs, C. (2005). Fibroblast growth factor signaling during early vertebrate development. Endocr Rev *26*, 63-77.

Campbell, D., Kim, C., and Butcher, E. (2003). Chemokines in the systemic organization of immunity. Immunol Rev *195*, 58-71.

Carragher, N., Levkau, B., Ross, R., and Raines, E. (1999). Degraded collagen fragments promote rapid disassembly of smooth muscle focal adhesions that correlates with cleavage of pp125(FAK), paxillin, and talin. J Cell Biol *147*, 619-630.

Chou, F., Hill, J., Hsieh, J., Pouyssegur, J., Brunet, A., Glading, A., Uberall, F., Ramos, J., Werner, M., and Ginsberg, M. (2003). PEA-15 binding to ERK1/2 MAPKs is required for its modulation of integrin activation. J Biol Chem *278*, 52587-52597.

Condeelis, J., and Segall, J. (2003a). Intravital imaging of cell movement in tumours. Nat Rev Cancer *3*, 921-930.

Condorelli, G., Trencia, A., Vigliotta, G., Perfetti, A., Goglia, U., Cassese, A., Musti, A., Miele, C., Santopietro, S., Formisano, P.*, et al.* (2002). Multiple members of the mitogen-activated

protein kinase family are necessary for PED/PEA-15 anti-apoptotic function. J Biol Chem *277*, 11013-11018.

Condorelli, G., Vigliotta, G., Iavarone, C., Caruso, M., Tocchetti, C., Andreozzi, F., Cafieri, A., Tecce, M., Formisano, P., Beguinot, L*., et al.* (1998a). PED/PEA-15 gene controls glucose transport and is overexpressed in type 2 diabetes mellitus. EMBO J *17*, 3858-3866.

Condorelli, G., Vigliotta, G., Trencia, A., Maitan, M., Caruso, M., Miele, C., Oriente, F., Santopietro, S., Formisano, P., and Beguinot, F. (2001). Protein kinase C (PKC)-alpha activation inhibits PKC-zeta and mediates the action of PED/PEA-15 on glucose transport in the L6 skeletal muscle cells. Diabetes *50*, 1244-1252.

Cooper, J., and Schafer, D. (2000). Control of actin assembly and disassembly at filament ends. Curr Opin Cell Biol *12*, 97-103.

Dallon, J.C., Sherratt, J.A., and Maini, P.K. (1999). Mathematical Modelling of Extracellular Matrix Dynamics using Discrete Cells: Fiber Orientation and Tissue Regeneration. Journal of Theoretical Biology *199*, 449-471.

Davies Cde, L., Berk, D.A., Pluen, A., and Jain, R.K. (2002). Comparison of IgG diffusion and extracellular matrix composition in rhabdomyosarcomas grown in mice versus in vitro as spheroids reveals the role of host stromal cells. Br J Cancer *86*, 1639-1644.

Daynes, R., and Jones, D. (2002). Emerging roles of PPARs in inflammation and immunity. Nat Rev Immunol *2*, 748-759.

De La Cruz, E., Mandinova, A., Steinmetz, M., Stoffler, D., Aebi, U., and Pollard, T. (2000). Polymerization and structure of nucleotide-free actin filaments. J Mol Biol *295*, 517-526.

Dean, T., Dai, Y., Shute, J., Church, M., and Warner, J. (1993). Interleukin-8 concentrations are elevated in bronchoalveolar lavage, sputum, and sera of children with cystic fibrosis. Pediatr Res *34*, 159-161.

DeLong, S.A., Moon, J.J., and West, J.L. (2005). Covalently immobilized gradients of bFGF on hydrogel scaffolds for directed cell migration. Biomaterials *26*, 3227-3234.

Dickinson, R., Guido, S., and Tranquillo, R. (1994). Biased cell migration of fibroblasts exhibiting contact guidance in oriented collagen gels. Ann Biomed Eng *22*, 342-356.

Dickinson RB, T.R. (1993). Optimal estimation of cell movement indices from the statistical analysis of cell tracking data (AIChE Journal), pp. 1995-2010.

Du, X., Edelstein, D., Obici, S., Higham, N., Zou, M., and Brownlee, M. (2006). Insulin resistance reduces arterial prostacyclin synthase and eNOS activities by increasing endothelial fatty acid oxidation. J Clin Invest *116*, 1071-1080.

Eccles, S. (2004). Parallels in invasion and angiogenesis provide pivotal points for therapeutic intervention. Int J Dev Biol *48*, 583-598.

Eckert, A., Böck, B., Tagscherer, K., Haas, T., Grund, K., Sykora, J., Herold-Mende, C., Ehemann, V., Hollstein, M., Chneiweiss, H.*, et al.* (2008). The PEA-15/PED protein protects glioblastoma cells from glucose deprivation-induced apoptosis via the ERK/MAP kinase pathway. Oncogene *27*, 1155-1166.

Edmonds, M. (2004). The diabetic foot, 2003. Diabetes Metab Res Rev *20 Suppl 1*, S9-S12.

Egeblad, M., Nakasone, E.S., and Werb, Z. (2010). Tumors as organs: complex tissues that interface with the entire organism. Dev Cell *18*, 884-901.

Egeblad M, R.M.a.W.V. (in press). Dynamic interplay between the collagen scaffold and tumor evolution Curr Opin Cell Biol.

Erler, J.T., and Weaver, V.M. (2009). Three-dimensional context regulation of metastasis. Clin Exp Metastasis *26*, 35-49.

Estellés, A., Yokoyama, M., Nothias, F., Vincent, J.D., Glowinski, J., Vernier, P., and Chneiweiss, H. (1996). The major astrocytic phosphoprotein PEA-15 is encoded by two mRNAs conserved on their full length in mouse and human. J Biol Chem *271*, 14800-14806.

Eyles, J., Roberts, A., Metcalf, D., and Wicks, I. (2006). Granulocyte colony-stimulating factor and neutrophils--forgotten mediators of inflammatory disease. Nat Clin Pract Rheumatol *2*, 500-510.

Falanga, V. (2005). Wound healing and its impairment in the diabetic foot. Lancet *366*, 1736-1743.

Falconnet, D., Csucs, G., Grandin, H.M., and Textor, M. (2006). Surface engineering approaches to micropattern surfaces for cell-based assays. Biomaterials *27*, 3044-3063.

Fiory, F., Formisano, P., Perruolo, G., and Beguinot, F. (2009). Frontiers: PED/PEA-15, a multifunctional protein controlling cell survival and glucose metabolism. Am J Physiol Endocrinol Metab *297*, E592-601.

Formstecher, E., Ramos, J., Fauquet, M., Calderwood, D., Hsieh, J., Canton, B., Nguyen, X., Barnier, J., Camonis, J., Ginsberg, M.*, et al.* (2001). PEA-15 mediates cytoplasmic sequestration of ERK MAP kinase. Dev Cell *1*, 239-250.

Frevert, C., Huang, S., Danaee, H., Paulauskis, J., and Kobzik, L. (1995). Functional characterization of the rat chemokine KC and its importance in neutrophil recruitment in a rat model of pulmonary inflammation. J Immunol *154*, 335-344.

Friedl, P., and Brocker, E.B. (2000). The biology of cell locomotion within three-dimensional extracellular matrix. Cellular and Molecular Life Sciences *57*, 41-64.

Friedl, P., and Wolf, K. (2003a). Proteolytic and non-proteolytic migration of tumour cells and leucocytes. Biochem Soc Symp, 277-285.

Friedl, P., and Wolf, K. (2003b). Tumour-cell invasion and migration: diversity and escape mechanisms. Nat Rev Cancer *3*, 362-374.

Friedl, P., and Wolf, K. (2008). Tube travel: the role of proteases in individual and collective cancer cell invasion. Cancer Res *68*, 7247-7249.

Friedl, P., and Wolf, K. (2009a). Proteolytic interstitial cell migration: a five-step process. Cancer Metastasis Rev *28*, 129-135.

Friedl, P., and Wolf, K. (2009b). Proteolytic interstitial cell migration: a five-step process. Cancer Metastasis Rev *28*, 129-135.

Friedl, P., and Wolf, K. (2010). Plasticity of cell migration: a multiscale tuning model. J Cell Biol *188*, 11-19.

Friedl, P., Wolf, K., von Andrian, U.H., and Harms, G. (2007). Biological second and third harmonic generation microscopy. Curr Protoc Cell Biol *Chapter 4*, Unit 4 15.

Fukumura, D., Duda, D.G., Munn, L.L., and Jain, R.K. (2010). Tumor microvasculature and microenvironment: novel insights through intravital imaging in pre-clinical models. Microcirculation *17*, 206-225.

Fukumura, D., and Jain, R.K. (2007). Tumor microenvironment abnormalities: causes, consequences, and strategies to normalize. J Cell Biochem *101*, 937-949.

Fésüs, L., and Szondy, Z. (2005). Transglutaminase 2 in the balance of cell death and survival. FEBS Lett *579*, 3297-3302.

Gaggioli, C., Hooper, S., Hidalgo-Carcedo, C., Grosse, R., Marshall, J.F., Harrington, K., and Sahai, E. (2007). Fibroblast-led collective invasion of carcinoma cells with differing roles for RhoGTPases in leading and following cells. Nat Cell Biol *9*, 1392-1400.

Galkowska, H., Wojewodzka, U., and Olszewski, W. (2006). Chemokines, cytokines, and growth factors in keratinocytes and dermal endothelial cells in the margin of chronic diabetic foot ulcers. Wound Repair Regen *14*, 558-565.

Gary Sibbald, R., and Woo, K. (2008). The biology of chronic foot ulcers in persons with diabetes. Diabetes Metab Res Rev *24 Suppl 1*, S25-30.

Gauvreau, V., and Laroche, G. (2005). Micropattern printing of adhesion, spreading, and migration peptides on poly(tetrafluoroethylene) films to promote endothelialization. Bioconjug Chem *16*, 1088-1097.

Geiger, B., Bershadsky, A., Pankov, R., and Yamada, K. (2001). Transmembrane crosstalk between the extracellular matrix--cytoskeleton crosstalk. Nat Rev Mol Cell Biol *2*, 793-805.

Geiss-Friedlander, R., and Melchior, F. (2007). Concepts in sumoylation: a decade on. Nat Rev Mol Cell Biol *8*, 947-956.

Gelman, M., and Kopito, R. (2003). Cystic fibrosis: premature degradation of mutant proteins as a molecular disease mechanism. Methods Mol Biol *232*, 27-37.

Ghajar, C.M., Chen, X., Harris, J.W., Suresh, V., Hughes, C.C., Jeon, N.L., Putnam, A.J., and George, S.C. (2008). The effect of matrix density on the regulation of 3-D capillary morphogenesis. Biophys J *94*, 1930-1941.

Giacco, F., Perruolo, G., D'Agostino, E., Fratellanza, G., Perna, E., Misso, S., Saldalamacchia, G., Oriente, F., Fiory, F., Miele, C*., et al.* (2006). Thrombin-activated platelets induce proliferation of human skin fibroblasts by stimulating autocrine production of insulin-like growth factor-1. FASEB J *20*, 2402-2404.

Glading, A., Koziol, J., Krueger, J., and Ginsberg, M. (2007). PEA-15 inhibits tumor cell invasion by binding to extracellular signal-regulated kinase 1/2. Cancer Res *67*, 1536-1544.

Goode, B., Drubin, D., and Barnes, G. (2000). Functional cooperation between the microtubule and actin cytoskeletons. Curr Opin Cell Biol *12*, 63-71.

Griffin, M., Casadio, R., and Bergamini, C. (2002). Transglutaminases: nature's biological glues. Biochem J *368*, 377-396.

Guido, S., and Tranquillo, R. (1993). A methodology for the systematic and quantitative study of cell contact guidance in oriented collagen gels. Correlation of fibroblast orientation and gel birefringence. J Cell Sci *105 ( Pt 2)*, 317-331.

Harada, A., Sekido, N., Akahoshi, T., Wada, T., Mukaida, N., and Matsushima, K. (1994). Essential involvement of interleukin-8 (IL-8) in acute inflammation. J Leukoc Biol *56*, 559-564.

Harley, B.A., Kim, H.D., Zaman, M.H., Yannas, I.V., Lauffenburger, D.A., and Gibson, L.J. (2008). Microarchitecture of three-dimensional scaffolds influences cell migration behavior via junction interactions. Biophys J *95*, 4013-4024.

Haroon, Z., Hettasch, J., Lai, T., Dewhirst, M., and Greenberg, C. (1999). Tissue transglutaminase is expressed, active, and directly involved in rat dermal wound healing and angiogenesis. FASEB J *13*, 1787-1795.

Hood, J., and Cheresh, D. (2002). Role of integrins in cell invasion and migration. Nat Rev Cancer *2*, 91-100.

Horwitz, A., and Parsons, J. (1999). Cell migration--movin' on. Science *286*, 1102-1103.

Hotary, K.B., Allen, E.D., Brooks, P.C., Datta, N.S., Long, M.W., and Weiss, S.J. (2003). Membrane type I matrix metalloproteinase usurps tumor growth control imposed by the three-dimensional extracellular matrix. Cell *114*, 33-45.

Hubeau, C., Puchelle, E., and Gaillard, D. (2001). Distinct pattern of immune cell population in the lung of human fetuses with cystic fibrosis. J Allergy Clin Immunol *108*, 524-529.

Huttenlocher, A., Palecek, S., Lu, Q., Zhang, W., Mellgren, R., Lauffenburger, D., Ginsberg, M., and Horwitz, A. (1997). Regulation of cell migration by the calcium-dependent protease calpain. J Biol Chem *272*, 32719-32722.

Huveneers, S., and Danen, E. (2009). Adhesion signaling - crosstalk between integrins, Src and Rho. J Cell Sci *122*, 1059-1069.

Ilić, D., Furuta, Y., Kanazawa, S., Takeda, N., Sobue, K., Nakatsuji, N., Nomura, S., Fujimoto, J., Okada, M., and Yamamoto, T. (1995). Reduced cell motility and enhanced focal adhesion contact formation in cells from FAK-deficient mice. Nature *377*, 539-544.

Jiang, X., Bruzewicz, D.A., Wong, A.P., Piel, M., and Whitesides, G.M. (2005). Directing cell migration with asymmetric micropatterns. Proc Natl Acad Sci U S A *102*, 975-978.

Junn, E., Ronchetti, R., Quezado, M., Kim, S., and Mouradian, M. (2003). Tissue transglutaminase-induced aggregation of alpha-synuclein: Implications for Lewy body formation in Parkinson's disease and dementia with Lewy bodies. Proc Natl Acad Sci U S A *100*, 2047-2052.

Karpuj, M., Becher, M., Springer, J., Chabas, D., Youssef, S., Pedotti, R., Mitchell, D., and Steinman, L. (2002). Prolonged survival and decreased abnormal movements in transgenic model of Huntington disease, with administration of the transglutaminase inhibitor cystamine. Nat Med *8*, 143-149.

Kedrin, D., Gligorijevic, B., Wyckoff, J., Verkhusha, V.V., Condeelis, J., Segall, J.E., and van Rheenen, J. (2008). Intravital imaging of metastatic behavior through a mammary imaging window. Nat Methods *5*, 1019-1021.

Keller, R. (2002). Shaping the vertebrate body plan by polarized embryonic cell movements. Science *298*, 1950-1954.

Kim, D., Park, S., Nam, B., Kim, I., and Kim, S. (2006). Reversal of drug resistance in breast cancer cells by transglutaminase 2 inhibition and nuclear factor-kappaB inactivation. Cancer Res *66*, 10936-10943.

Kirschner, M. (1980). Implications of treadmilling for the stability and polarity of actin and tubulin polymers in vivo. J Cell Biol *86*, 330-334.

Klinghoffer, R., Sachsenmaier, C., Cooper, J., and Soriano, P. (1999). Src family kinases are required for integrin but not PDGFR signal transduction. EMBO J *18*, 2459-2471.

Kopito, R. (1999). Biosynthesis and degradation of CFTR. Physiol Rev *79*, S167-173.

Korff, T., and Augustin, H.G. (1998). Integration of endothelial cells in multicellular spheroids prevents apoptosis and induces differentiation. J Cell Biol *143*, 1341-1352.

Kunwar, P., Siekhaus, D., and Lehmann, R. (2006). In vivo migration: a germ cell perspective. Annu Rev Cell Dev Biol *22*, 237-265.

Köhidai, L. (1995). Method for determination of chemoattraction in Tetrahymena pyriformis. Curr Microbiol *30*, 251-253.

Lauffenburger, D.A., and Horwitz, A.F. (1996). Cell Migration: A Physically Integrated Molecular Process. Cell *84*, 359-369.

Lee, S.H., Moon, J.J., and West, J.L. (2008). Three-dimensional micropatterning of bioactive hydrogels via two-photon laser scanning photolithography for guided 3D cell migration. Biomaterials *29*, 2962-2968.

Legssyer, R., Huaux, F., Lebacq, J., Delos, M., Marbaix, E., Lebecque, P., Lison, D., Scholte, B., Wallemacq, P., and Leal, T. (2006). Azithromycin reduces spontaneous and induced inflammation in DeltaF508 cystic fibrosis mice. Respir Res *7*, 134.

Lerman, O., Galiano, R., Armour, M., Levine, J., and Gurtner, G. (2003). Cellular dysfunction in the diabetic fibroblast: impairment in migration, vascular endothelial growth factor production, and response to hypoxia. Am J Pathol *162*, 303-312.

Lock, J.G., Wehrle-Haller, B., and Strömblad, S. (2008). Cell-matrix adhesion complexes: Master control machinery of cell migration. Seminars in Cancer Biology *18*, 65-76.

Lorand, L., and Graham, R. (2003). Transglutaminases: crosslinking enzymes with pleiotropic functions. Nat Rev Mol Cell Biol *4*, 140-156.

Luo, Y., and Shoichet, M.S. (2004). A photolabile hydrogel for guided three-dimensional cell growth and migration. Nat Mater *3*, 249-253.

Mabb, A., Wuerzberger-Davis, S., and Miyamoto, S. (2006). PIASy mediates NEMO sumoylation and NF-kappaB activation in response to genotoxic stress. Nat Cell Biol *8*, 986-993.

Machesky, L., Atkinson, S., Ampe, C., Vandekerckhove, J., and Pollard, T. (1994). Purification of a cortical complex containing two unconventional actins from Acanthamoeba by affinity chromatography on profilin-agarose. J Cell Biol *127*, 107-115.

Maiuri, L., Luciani, A., Giardino, I., Raia, V., Villella, V., D'Apolito, M., Pettoello-Mantovani, M., Guido, S., Ciacci, C., Cimmino, M.*, et al.* (2008). Tissue transglutaminase activation modulates inflammation in cystic fibrosis via PPARgamma down-regulation. J Immunol *180*, 7697-7705.

Malorni, W., Farrace, M., Rodolfo, C., and Piacentini, M. (2008). Type 2 transglutaminase in neurodegenerative diseases: the mitochondrial connection. Curr Pharm Des *14*, 278-288.

Martin, P., and Parkhurst, S. (2004). Parallels between tissue repair and embryo morphogenesis. Development *131*, 3021-3034.

Matthes, T., and Gruler, H. (1988). Analysis of cell locomotion. Contact guidance of human polymorphonuclear leukocytes. Eur Biophys J *15*, 343-357.

Meulmeester, E., and Melchior, F. (2008). Cell biology: SUMO. Nature *452*, 709-711.

Miele, C., Raciti, G., Cassese, A., Romano, C., Giacco, F., Oriente, F., Paturzo, F., Andreozzi, F., Zabatta, A., Troncone, G.*, et al.* (2007). PED/PEA-15 regulates glucose-induced insulin secretion by restraining potassium channel expression in pancreatic beta-cells. Diabetes *56*, 622-633.

Moghe, P.V., Nelson, R.D., and Tranquillo, R.T. (1995). CYTOKINE-STIMULATED CHEMOTAXIS OF HUMAN NEUTROPHILS IN A 3-D CONJOINED FIBRIN GEL ASSAY. Journal of Immunological Methods *180*, 193-211.

Moser, B., Wolf, M., Walz, A., and Loetscher, P. (2004). Chemokines: multiple levels of leukocyte migration control. Trends Immunol *25*, 75-84.

Moss, M., and Lambert, M. (2002). Shedding of membrane proteins by ADAM family proteases. Essays Biochem *38*, 141-153.

Mostafavi-Pour, Z., Askari, J., Parkinson, S., Parker, P., Ng, T., and Humphries, M. (2003). Integrin-specific signaling pathways controlling focal adhesion formation and cell migration. J Cell Biol *161*, 155-167.

Nelson, C.M., Inman, J.L., and Bissell, M.J. (2008). Three-dimensional lithographically defined organotypic tissue arrays for quantitative analysis of morphogenesis and neoplastic progression. Nat Protoc *3*, 674-678.

Nicklas, W., Baneux, P., Boot, R., Decelle, T., Deeny, A., Fumanelli, M., Illgen-Wilcke, B., and Colonies), F.F.o.E.L.A.S.A.W.G.o.H.M.o.R.a.R. (2002). Recommendations for the health monitoring of rodent and rabbit colonies in breeding and experimental units. Lab Anim *36*, 20-42.

Nobes, C., and Hall, A. (1999). Rho GTPases control polarity, protrusion, and adhesion during cell movement. J Cell Biol *144*, 1235-1244.

Olson, T., and Ley, K. (2002). Chemokines and chemokine receptors in leukocyte trafficking. Am J Physiol Regul Integr Comp Physiol *283*, R7-28.

Osika, E., Cavaillon, J., Chadelat, K., Boule, M., Fitting, C., Tournier, G., and Clement, A. (1999). Distinct sputum cytokine profiles in cystic fibrosis and other chronic inflammatory airway disease. Eur Respir J *14*, 339-346.

Pascual, G., Fong, A., Ogawa, S., Gamliel, A., Li, A., Perissi, V., Rose, D., Willson, T., Rosenfeld, M., and Glass, C. (2005). A SUMOylation-dependent pathway mediates transrepression of inflammatory response genes by PPAR-gamma. Nature *437*, 759-763.

Peppa, M., Stavroulakis, P., and Raptis, S. (2009). Advanced glycoxidation products and impaired diabetic wound healing. Wound Repair Regen *17*, 461-472.

Pluen, A., Boucher, Y., Ramanujan, S., McKee, T.D., Gohongi, T., di Tomaso, E., Brown, E.B., Izumi, Y., Campbell, R.B., Berk, D.A.*, et al.* (2001). Role of tumor-host interactions in interstitial diffusion of macromolecules: cranial vs. subcutaneous tumors. Proc Natl Acad Sci U S A *98*, 4628-4633.

Pollard, T., Blanchoin, L., and Mullins, R. (2000). Molecular mechanisms controlling actin filament dynamics in nonmuscle cells. Annu Rev Biophys Biomol Struct *29*, 545-576.

Provenzano, P.P., Eliceiri, K.W., Campbell, J.M., Inman, D.R., White, J.G., and Keely, P.J. (2006). Collagen reorganization at the tumor-stromal interface facilitates local invasion. BMC Med *4*, 38.

Provenzano, P.P., Inman, D.R., Eliceiri, K.W., Knittel, J.G., Yan, L., Rueden, C.T., White, J.G., and Keely, P.J. (2008a). Collagen density promotes mammary tumor initiation and progression. BMC Med *6*, 11.

Provenzano, P.P., Inman, D.R., Eliceiri, K.W., Trier, S.M., and Keely, P.J. (2008b). Contact guidance mediated three-dimensional cell migration is regulated by Rho/ROCK-dependent matrix reorganization. Biophys J *95*, 5374-5384.

Raftopoulou, M., and Hall, A. (2004). Cell migration: Rho GTPases lead the way. Dev Biol *265*, 23-32.

Raghavan, S., Nelson, C.M., Baranski, J.D., Lim, E., and Chen, C.S. (2010). Geometrically controlled endothelial tubulogenesis in micropatterned gels. Tissue Eng Part A *16*, 2255-2263.

Rao, R., Yang, L., Garcia-Cardena, G., and Luscinskas, F. (2007). Endothelial-dependent mechanisms of leukocyte recruitment to the vascular wall. Circ Res *101*, 234-247.

Ratjen, F., and Döring, G. (2003). Cystic fibrosis. Lancet *361*, 681-689.

Reddy, M., Quinton, P., Haws, C., Wine, J., Grygorczyk, R., Tabcharani, J., Hanrahan, J., Gunderson, K., and Kopito, R. (1996). Failure of the cystic fibrosis transmembrane conductance regulator to conduct ATP. Science *271*, 1876-1879.

Regen, C., and Horwitz, A. (1992). Dynamics of beta 1 integrin-mediated adhesive contacts in motile fibroblasts. J Cell Biol *119*, 1347-1359.

Renault-Mihara, F., Beuvon, F., Iturrioz, X., Canton, B., De Bouard, S., Léonard, N., Mouhamad, S., Sharif, A., Ramos, J., Junier, M.*, et al.* (2006). Phosphoprotein enriched in astrocytes-15 kDa expression inhibits astrocyte migration by a protein kinase C delta-dependent mechanism. Mol Biol Cell *17*, 5141-5152.

Ridley, A., Schwartz, M., Burridge, K., Firtel, R., Ginsberg, M., Borisy, G., Parsons, J., and Horwitz, A. (2003). Cell migration: integrating signals from front to back. Science *302*, 1704-1709.

Roth, W., Eckert, A., Böck, B., Schirmacher, P., and Wiestler, O. (2007). [The PEA-15 protein induces resistance against glucose deprivation-induced cell death via the ERK/MAP kinase pathway]. Verh Dtsch Ges Pathol *91*, 343-350.

Ruiter, D., Bogenrieder, T., Elder, D., and Herlyn, M. (2002). Melanoma-stroma interactions: structural and functional aspects. Lancet Oncol *3*, 35-43.

Sabeh, F., Ota, I., Holmbeck, K., Birkedal-Hansen, H., Soloway, P., Balbin, M., Lopez-Otin, C., Shapiro, S., Inada, M., Krane, S.*, et al.* (2004). Tumor cell traffic through the extracellular matrix is controlled by the membrane-anchored collagenase MT1-MMP. J Cell Biol *167*, 769-781.

Sarig-Nadir, O., Livnat, N., Zajdman, R., Shoham, S., and Seliktar, D. (2009). Laser photoablation of guidance microchannels into hydrogels directs cell growth in three dimensions. Biophys J *96*, 4743-4752.

Sasaki, A., and Firtel, R. (2006). Regulation of chemotaxis by the orchestrated activation of Ras, PI3K, and TOR. Eur J Cell Biol *85*, 873-895.

Scheid, P., Kempster, L., Griesenbach, U., Davies, J., Dewar, A., Weber, P., Colledge, W., Evans, M., Geddes, D., and Alton, E. (2001). Inflammation in cystic fibrosis airways: relationship to increased bacterial adherence. Eur Respir J *17*, 27-35.

Schneider, I., and Haugh, J. (2006). Mechanisms of gradient sensing and chemotaxis: conserved pathways, diverse regulation. Cell Cycle *5*, 1130-1134.

Schultz, G., and Wysocki, A. (2009). Interactions between extracellular matrix and growth factors in wound healing. Wound Repair Regen *17*, 153-162.

Sieg, D., Hauck, C., and Schlaepfer, D. (1999). Required role of focal adhesion kinase (FAK) for integrin-stimulated cell migration. J Cell Sci *112 ( Pt 16)*, 2677-2691.

Siqueira, M., Li, J., Chehab, L., Desta, T., Chino, T., Krothpali, N., Behl, Y., Alikhani, M., Yang, J., Braasch, C.*, et al.* (2010). Impaired wound healing in mouse models of diabetes is mediated by TNF-alpha dysregulation and associated with enhanced activation of forkhead box O1 (FOXO1). Diabetologia *53*, 378-388.

Small, J., Geiger, B., Kaverina, I., and Bershadsky, A. (2002). How do microtubules guide migrating cells? Nat Rev Mol Cell Biol *3*, 957-964.

Small, J., and Kaverina, I. (2003). Microtubules meet substrate adhesions to arrange cell polarity. Curr Opin Cell Biol *15*, 40-47.

Smith, J., Travis, S., Greenberg, E., and Welsh, M. (1996). Cystic fibrosis airway epithelia fail to kill bacteria because of abnormal airway surface fluid. Cell *85*, 229-236.

Steffan, J., Agrawal, N., Pallos, J., Rockabrand, E., Trotman, L., Slepko, N., Illes, K., Lukacsovich, T., Zhu, Y., Cattaneo, E.*, et al.* (2004). SUMO modification of Huntingtin and Huntington's disease pathology. Science *304*, 100-104.

Su, W., Liao, Y., and Chu, I. (2007). Observation of fibroblast motility on a micro-grooved hydrophobic elastomer substrate with different geometric characteristics. Micron *38*, 278-285.

Tempé, D., Piechaczyk, M., and Bossis, G. (2008). SUMO under stress. Biochem Soc Trans *36*, 874-878.

Terranova, A. (1991). The effects of diabetes mellitus on wound healing. Plast Surg Nurs *11*, 20-25.

Thelin, W., and Boucher, R. (2007). The epithelium as a target for therapy in cystic fibrosis. Curr Opin Pharmacol *7*, 290-295.

Tirouvanziam, R., de Bentzmann, S., Hubeau, C., Hinnrasky, J., Jacquot, J., Péault, B., and Puchelle, E. (2000). Inflammation and infection in naive human cystic fibrosis airway grafts. Am J Respir Cell Mol Biol *23*, 121-127.

Totsukawa, G., Wu, Y., Sasaki, Y., Hartshorne, D., Yamakita, Y., Yamashiro, S., and Matsumura, F. (2004). Distinct roles of MLCK and ROCK in the regulation of membrane protrusions and focal adhesion dynamics during cell migration of fibroblasts. J Cell Biol *164*, 427-439.

Trousdale, R., Jacobs, S., Simhaee, D., Wu, J., and Lustbader, J. (2009). Wound closure and metabolic parameter variability in a db/db mouse model for diabetic ulcers. J Surg Res *151*, 100-107.

Tsai, W., Strieter, R., Mehrad, B., Newstead, M., Zeng, X., and Standiford, T. (2000). CXC chemokine receptor CXCR2 is essential for protective innate host response in murine Pseudomonas aeruginosa pneumonia. Infect Immun *68*, 4289-4296.

Tsuji, K., Yamauchi, K., Yang, M., Jiang, P., Bouvet, M., Endo, H., Kanai, Y., Yamashita, K., Moossa, A.R., and Hoffman, R.M. (2006). Dual-color imaging of nuclear-cytoplasmic dynamics, viability, and proliferation of cancer cells in the portal vein area. Cancer Res *66*, 303-306.

Vaidyanathan, H., and Ramos, J. (2003). RSK2 activity is regulated by its interaction with PEA-15. J Biol Chem *278*, 32367-32372.

Vakoc, B.J., Lanning, R.M., Tyrrell, J.A., Padera, T.P., Bartlett, L.A., Stylianopoulos, T., Munn, L.L., Tearney, G.J., Fukumura, D., Jain, R.K.*, et al.* (2009). Three-dimensional microscopy of the tumor microenvironment in vivo using optical frequency domain imaging. Nat Med *15*, 1219-1223.

Valentino, R., Lupoli, G., Raciti, G., Oriente, F., Farinaro, E., Della Valle, E., Salomone, M., Riccardi, G., Vaccaro, O., Donnarumma, G.*, et al.* (2006). The PEA15 gene is overexpressed and related to insulin resistance in healthy first-degree relatives of patients with type 2 diabetes. Diabetologia *49*, 3058-3066.

Velander, P., Theopold, C., Hirsch, T., Bleiziffer, O., Zuhaili, B., Fossum, M., Hoeller, D., Gheerardyn, R., Chen, M., Visovatti, S.*, et al.* (2008). Impaired wound healing in an acute diabetic pig model and the effects of local hyperglycemia. Wound Repair Regen *16*, 288-293.

Vigliotta, G., Miele, C., Santopietro, S., Portella, G., Perfetti, A., Maitan, M., Cassese, A., Oriente, F., Trencia, A., Fiory, F.*, et al.* (2004). Overexpression of the ped/pea-15 gene causes diabetes by impairing glucose-stimulated insulin secretion in addition to insulin action. Mol Cell Biol *24*, 5005-5015.

Wall, I., Moseley, R., Baird, D., Kipling, D., Giles, P., Laffafian, I., Price, P., Thomas, D., and Stephens, P. (2008). Fibroblast dysfunction is a key factor in the non-healing of chronic venous leg ulcers. J Invest Dermatol *128*, 2526-2540.

Wang, C.J., Li, X., Lin, B., Shim, S., Ming, G.L., and Levchenko, A. (2008). A microfluidics-based turning assay reveals complex growth cone responses to integrated gradients of substrate-bound ECM molecules and diffusible guidance cues. Lab on a Chip *8*, 227-237.

Wang, W., Goswami, S., Sahai, E., Wyckoff, J., Segall, J., and Condeelis, J. (2005). Tumor cells caught in the act of invading: their strategy for enhanced cell motility. Trends Cell Biol *15*, 138-145.

Ward, C., Omura, S., and Kopito, R. (1995). Degradation of CFTR by the ubiquitin-proteasome pathway. Cell *83*, 121-127.

Wear, M., Schafer, D., and Cooper, J. (2000). Actin dynamics: assembly and disassembly of actin networks. Curr Biol *10*, R891-895.

Webb, D., Parsons, J., and Horwitz, A. (2002). Adhesion assembly, disassembly and turnover in migrating cells -- over and over and over again. Nat Cell Biol *4*, E97-100.

Welch, M., and Mullins, R. (2002). Cellular control of actin nucleation. Annu Rev Cell Dev Biol *18*, 247-288.

Wittmann, T., and Waterman-Storer, C. (2001). Cell motility: can Rho GTPases and microtubules point the way? J Cell Sci *114*, 3795-3803.

Wolf, K., Alexander, S., Schacht, V., Coussens, L.M., von Andrian, U.H., van Rheenen, J., Deryugina, E., and Friedl, P. (2009). Collagen-based cell migration models in vitro and in vivo. Semin Cell Dev Biol *20*, 931-941.

Wolf, K., Mazo, I., Leung, H., Engelke, K., von Andrian, U.H., Deryugina, E.I., Strongin, A.Y., Brocker, E.B., and Friedl, P. (2003). Compensation mechanism in tumor cell migration: mesenchymal-amoeboid transition after blocking of pericellular proteolysis. J Cell Biol *160*, 267-277.

Wolf, K., Wu, Y.I., Liu, Y., Geiger, J., Tam, E., Overall, C., Stack, M.S., and Friedl, P. (2007). Multi-step pericellular proteolysis controls the transition from individual to collective cancer cell invasion. Nat Cell Biol *9*, 893-904.

Woolhouse, I., Bayley, D., and Stockley, R. (2002). Sputum chemotactic activity in chronic obstructive pulmonary disease: effect of alpha(1)-antitrypsin deficiency and the role of leukotriene B(4) and interleukin 8. Thorax *57*, 709-714.

Wyckoff, J.B., Pinner, S.E., Gschmeissner, S., Condeelis, J.S., and Sahai, E. (2006). ROCK- and myosin-dependent matrix deformation enables protease-independent tumor-cell invasion in vivo. Curr Biol *16*, 1515-1523.

Yang, J., and Weinberg, R.A. (2008). Epithelial-Mesenchymal Transition: At the Crossroads of Development and Tumor Metastasis. Developmental Cell *14*, 818-829.

Zhang, Y., Redina, O., Altshuller, Y., Yamazaki, M., Ramos, J., Chneiweiss, H., Kanaho, Y., and Frohman, M. (2000). Regulation of expression of phospholipase D1 and D2 by PEA-15, a novel protein that interacts with them. J Biol Chem *275*, 35224-35232.

Zicha, D., Dunn, G., and Brown, A. (1991). A new direct-viewing chemotaxis chamber. J Cell Sci *99 ( Pt 4)*, 769-775.

Zigmond, S., and Hirsch, J. (1973). Leukocyte locomotion and chemotaxis. New methods for evaluation, and demonstration of a cell-derived chemotactic factor. J Exp Med *137*, 387-410.

Zlotnik, A., and Yoshie, O. (2000). Chemokines: a new classification system and their role in immunity. Immunity *12*, 121-127.

# APPENDIX

## *Publications*

- Luciani A, Villella VR, **Vasaturo A**, Giardino I, Pettoello Mantovani M, Guido S, Cexus ON, Peake N, Londei M, Quaratino S, Maiuri L. "*Lysosomal accumulation of gliadin p31-43 peptide induces oxidative stress and Tissue Transglutaminase mediated PPAR{gamma} downregulation in intestinal epithelial cells and coeliac mucosa*". GUT December 2009

- Luciani A, Villella VR, **Vasaturo A**, Giardino I, Raia V, Pettoello-Mantovani M, D'Apolito M, Guido S, Leal T, Quaratino S, Maiuri L. "*SUMOylation of tissue transglutaminase as link between oxidative stress and inflammation*". J Immunol. August 2009

## *Scientific publications under consideration:*

Ferdinando Giacco, Roberta Buonomo, **Angela Vasaturo**, Stefano Guido, Corrado Garbi, Valentina Pagliara, Gelsomina Mansueto, Claudio Bellevicine, Giuseppe Perruolo, Francesco Oriente, Claudia Miele, Francesco Beguinot, Pietro Formisano.

*"Phosphoprotein enriched in diabetes/phosphoprotein enriched in astrocytes-15 controls fibroblast migration and wound closure by an extracellular signal-regulated kinase 1/2-dependent mechanism"*

Paper under consideration by reviewers of Journal of Cellular Phisiology

Olga Ilina, Gert-Jan Bakker, **Angela Vasaturo**, Robert M. Hoffman, Peter Friedl.

*"Two-photon laser-generated microtracks in 3D collagen lattices to dissect MMP-dependent and -independent collective cancer cell invasion"*

Paper under consideration by reviewers of Physical Biology

## *Conferences*

- A. Vasaturo, V. Preziosi, V. Villella, L. Sabetta, S.Caserta, S. Guido "A novel chemotaxis assay in 3-D collagen gels by time-lapse video microscopy" Invadopodia, Podosomes and Focal Adhesions in Tissue Invasion 26-30 September 2009 Hyeres- South of France.

- A. Vasaturo, V. Preziosi, V. Villella, L. Sabetta, S.Caserta, S. Guido "Sviluppo di un sistema di microscopia time-lapse per lo studio della motilità cellulare in vitro" Convegno GR.I.C.U. 2008 Ingegneria Chimica: le nuove frontiere- Le Castella (KR) 14-17 September 2008. **Young Scientists Award**

## *Experiences in foreign laboratories*

Radboud University Nijmegen Medical Center- Nijmegen Center for Molecular Life sciences (NCMLS), Department of Cell Biology, Nijmegen, Netherlands. **Multiphoton Microscopy for Intravital Imaging Applications** under the supervision of Prof. P. Friedl and in collaboration with Prof. S. Guido of the University of Naples (13 May 10 – 5 Dec 10).

## ACKNOWLEDGEMENTS

*I'd like to thank:*

*My supervisor Prof. Stefano Guido for giving me the opportunity to work in his lab and believing in me day by day. His expertise, understanding and patience has enriched considerably my laboratory experience. Moreover, I thank him for the moral and technical support he has provided at all levels of my research project and for the pleasant atmosphere that he is able to create even during the worst moments of this work.*

*Prof. Pietro Formisano for teaching me humility, willingness and devotion to work. He is the one professor who truly made a difference in my life. My passion for research started when I met him on my way. His trust strengthens me. Besides being a professor, he is for me a mentor and a friend.*

*Prof. Luigi Maiuri for his ability to stimulate my mind and for a decisive role in saving me from leaving research. His motivation and encouragement have been instrumental in getting me to pursue doctoral study.*

*Prof. Peter Friedl for his availability and for giving me the opportunity to work in his laboratory, for his helpfulness and professionalism.*

*Ing. Sergio Caserta for all the time he spent teaching me the basic principles of the chemical engineering , discussing data with me, and for the technical support and the constructive suggestions essential to this work.*

*Ing. Giovanna Tomaiuolo, Ing. Valentina Preziosi, Dott.ssa Valeria Villella, Dr. Alessandro Luciani, Ing. Luca Lanotte and Ing. Angelo Pomella for all the joyful moments spent together, for the sustained support and for the esteem that you always showed to me.*

*Ing. Luca Micoli, Ing. Mariano Sirignano and Ing. Antonio Picarelli for introducing me to the Reynolds number: your explanations were so clear that I still don't know what it is! Everyone of you, one way or another, gave me something special and I'll never forget it.*

*All the people from Peter Friedl's group: thanks for your warm welcome and for making me look forward to become your colleague. Special thanks to Olga Ilina and Bettina Weigelin for patiently teaching me advanced microscopy techniques. I am proud that I had the opportunity to work with an exceptionally experienced scientist like them.*

*My lovely friends Antoine Khalil, Ganesh Manjeri, Claire Monge and Cindy Dieteren who took care of me during my time in Nijmegen. Your hugs, your words made me feel at home. Your friendship is a 'heaven's gift'. Even if you are in a different Country, I will never forget the funny moments spent together!*

*Giuseppe, Sergio, Elisa, Anchel, Mauro, Laura, Marco, Irene, Martin, Samuel, Robert, Federica, Olga, Pavel, Bettina, and all my friends in Nijmegen for making my first experience abroad unforgettable!*

*Last but not least, special thanks go to my family: always with me, when there is the sun, when there is the storm, when we are far or close. There are no words to express how important and how essential was your unconditional love and support to reach this goal. Thank you for supporting me and all my decisions and for having taught me to love life and to believe in its values.*